Tampereen yliopisto

KIM KUNTZE

SYNTHESIS AND CHARACTERIZATION OF ORGANIC PHOTOSWITCHES FOR FUNCTIONAL LIQUID CRYSTALLINE MATERIALS

Master of Science Thesis

Examiner: Prof. Arri Priimägi
Examiner and topic approved on 20th December 2018

ABSTRACT

KIM KUNTZE: Synthesis and characterization of organic photoswitches for functional liquid crystalline materials
Tampere University
Master of Science Thesis, 73 pages, 20 Appendix pages
January 2019
Master's Degree Programme in Chemistry
Major: Chemistry (honors)
Examiners: Prof. Arri Priimägi, Dr. Zafar Ahmed

Keywords: photoswitch, azobenzene, diarylethene, indigo, DASA, synthesis

Control over the properties and functionality of catalysts, pharmaceuticals, and materials is an essential objective for contemporary chemists. Light is a particularly attractive remote stimulus due to its clean and highly controllable nature. Thus, organic molecules whose properties can be controlled with light – photoswitches – are widely studied for such purposes. In the case of functional light-responsive materials, photoactuators in particular, liquid crystalline polymers with covalently bound or doped photoswitches are often exploited. The design of new photoswitches is imperative in order to acquire materials with the desired properties. In addition to photochemical properties, it is important to design the materials to be compatible with the liquid crystalline polymer matrix.

In this thesis, four previously unreported photoswitchable molecules were designed and successfully synthesized: azobenzene, diarylethene and indigo crosslinkers, and a donor-acceptor Stenhouse adduct (DASA) dopant. Regarding the azobenzene and diarylethene crosslinkers, the design was derived from already published molecules, the main motivation stemming from the need for truly bistable photoswitches with excellent thermal stability in light-driven robotics applications. Indigo crosslinkers had not been reported previously, so acquiring the crosslinker and exploring its functionality was the main objective; similarly, DASAs have not been utilized in the context of liquid crystals earlier, so the structure was primarily designed to have the best possible liquid crystal compatibility.

The photochemical properties of the photoswitches were studied in solution. Molar absorption coefficients, photoisomerization efficiency and quantum yield, and thermal stability of the more energetic isomer were determined. All molecules showed fast, reversible and efficient photoisomerization with quantum yields similar to published values of related compounds in literature. The azobenzene and diarylethene crosslinkers were found to be thermally stable at room temperature, whereas the indigo crosslinker and the DASA dopant had thermal lifetimes of several minutes. In general, the measured properties matched the aims of the molecular design targeted for.

The azobenzene and diarylethene molecules synthesized in this thesis enable the fabrication of novel bistable photoactuators. The indigo crosslinker and DASA dopant are novel, previously unexplored molecules whose incorporation into suitable liquid crystalline materials can now be studied. Regarding the indigo and DASA switches, the research should be continued with more synthetic studies in order to optimize the reaction conditions. The study on the indigo crosslinker should be further extended to other crosslinkers in order to acquire information on the relationship between the molecular structure and the photoresponsive behavior in an LC material.

TIIVISTELMÄ

KIM KUNTZE: Orgaanisten valokytkinten synteesi ja karakterisointi toiminnallisia nestekidemateriaaleja varten
Tampereen yliopisto
Diplomityö, 73 sivua, 20 liitesivua
Tammikuu 2019
Luonnontieteiden ja tekniikan diplomi-insinöörin tutkinto-ohjelma
Pääaine: Kemia (laaja)
Tarkastajat: Prof. Arri Priimägi, Dr. Zafar Ahmed

Avainsanat: valokytkin, atsobentseeni, diaryylieteeni, indigo, DASA, synteesi

Katalyyttien, lääkeaineiden ja materiaalien ominaisuuksien ja toiminnallisuuden kontrollointi on yksi nykykemistien olennaisista tavoitteista. Valo soveltuu kontrollointiin erityisen hyvin, koska se on helposti hallittavissa eikä tuota jätettä. Tästä johtuen valokytkimiä eli orgaanisia molekyylejä, joiden ominaisuuksia voidaan hallita valon avulla, tutkitaan laajasti. Toiminnallisiin materiaaleihin ja erityisesti valoaktuaattoreihin käytetään usein valokytkimiä sisältäviä nestekidepolymeerejä. Uusien valokytkinten luominen on välttämätöntä haluttuja ominaisuuksia omaavien materiaalien valmistamiseksi. Valokemiallisten ominaisuuksien lisäksi kytkimet on suunniteltava niin, että ne ovat yhteensopivia nestekiteisten materiaalien kanssa.

Tässä työssä suunniteltiin ja syntetisoitiin neljä aiemmin julkaisematonta valokytkintä: atsobentseeni-, diaryylieteeni- ja indigosilloittimet sekä donori-akseptori-Stenhouse-adduktiväriaine (DASA). Atsobentseeni- ja diaryylieteenisilloittimien rakenne suunniteltiin aiemmin julkaistujen molekyylien pohjalta mahdollisimman hyvän termisen stabiiliuden saavuttamiseksi. Ainuttakaan indigosilloitinta ei ole julkaistu, joten tavoitteena oli valmistaa potentiaalisesti valoaktuaattoriin soveltuva silloitin. Myöskään DASA-kytkimiä ei ole käytetty nestekiteissä, joten rakenne suunniteltiin yksinkertaisesti mahdollisimman hyvin nestekideyhteensopivaksi.

Molekyylien valokemiallisia ominaisuuksia tutkittiin liuoksessa, ja niille määritettiin molaariset absorptiokertoimet, valoisomerisaation tehokkuus ja kvanttisaanto sekä terminen stabiilius. Kaikki molekyylit isomeroituivat nopeasti ja tehokkaasti valon vaikutuksesta, ja kvanttisaannot olivat samankaltaisia kuin kirjallisuudessa julkaistut arvot vertailuyhdisteille. Atsobentseeni- ja diaryylieteenisilloittimet olivat termisesti stabiileja huoneen lämpötilassa, kun taas indigosilloittimen ja DASA-väriaineen termiset elinajat olivat minuuttien aikaskaalassa. Kaikkiaan yhdisteiden ominaisuudet olivat hyvin lähellä alkuperäistä suunnitelmaa.

Tässä työssä syntetisoidut atsobentseeni- ja diaryylieteenimolekyylit mahdollistavat uusien, bistabiilien valoaktuaattorien valmistamisen. Indigosilloitin ja DASA-väriaine ovat aiemmin tutkimattomia kytkimiä, joiden lisäämistä nestekidemateriaaleihin voidaan nyt tutkia. Reaktioita on edelleen optimoitava indigo- ja DASA-molekyylien osalta parempien saantojen saamiseksi. Indigotutkimuksen laajentaminen erilaisiin indigosilloittimiin tuottaisi informaatiota silloittimen molekyylirakenteen ja sitä sisältävän nestekidemateriaalin valoherätteisten ominaisuuksien välisistä riippuvuussuhteista.

PREFACE

This Master of Science thesis was done in the Smart Photonic Materials group located in the Faculty of Engineering and Natural Sciences at Tampere University. The experimental work was mostly carried out at Tampere University and partly at Humboldt University of Berlin. The work was funded by the European Research Council (Starting Grant Project PHOTOTUNE, Decision number 679646).

I thank my supervisor, Prof. Arri Priimägi, for enabling this interesting study and for all the support and encouragement I have received during the years. I am also deeply grateful to Dr. Zafar Ahmed for the help with synthesis and molecular characterization, and to Dr. Matti Virkki for helping with photochemical measurements. In particular, I would like to thank both Arri and Prof. Stefan Hecht for the research visit at Humboldt University, as the experience I acquired there is valuable beyond measure. In addition, thanks to Dr. Chung-Yang Huang from Humboldt University of Berlin for the help with indigos and to Prof. Javier Read de Alaniz from University of California, Santa Barbara for helping with DASAs.

The working days in the lab would be long indeed without continuous peer support from coworkers. Thank you Tatu, Suvi, Rafael, Markus, Antti, Jagadish, Benedicta and Vesa, and the whole SPM group; and from Berlin, special thanks to Svante, Jan and Ellen for teaching me the ways of the laboratory.

Finally, this thesis could never have been accomplished without my family and friends. Meri, thank you for your kindness, supportiveness and patience – I do not know how I would cope without you.

Tampere, 30th January 2019

Kim Kuntze

CONTENTS

LIST OF SYMBOLS AND ABBREVIATIONS

Φ	quantum yield
τ	thermal lifetime
ε	molar extinction coefficient
Al-	alkyl
Ar-	aryl
Bu-	butyl
Cy-	cyclohexyl
DAE	diarylethene
DASA	donor-acceptor Stenhouse adduct
dba	dibenzylideneacetone
DBU	1,8-diazabicyclo[5.4.0]undec-9-ene
DCM	dichloromethane
DMAP	4-dimethylaminopyridine
DMF	*N*,*N*-dimethylformamide
DMSO	dimethylsulfoxide
Et-	ethyl
i-Pr-	isopropyl
LCE	liquid crystal elastomer
LCN	liquid crystal polymer network
Me-	methyl
MeCN	acetonitrile
NBS	*N*-bromosuccinimide
pin	pinacolato ligand
Ph-	phenyl
RT	room temperature
TEA	triethylamine
THF	tetrahydrofuran
UV	ultraviolet

1. INTRODUCTION

Advances in synthetic chemistry in recent decades have led to countless achievements in medicinal chemistry, materials science, and nanotechnology. However, almost all contemporary catalysts, materials, and pharmaceuticals are static in their nature: their functionality cannot be controlled after it is initially created. For the next generation of functional chemicals and materials, control over their chemical and physical properties is essential. This can be accomplished with *molecular switches*, molecules whose qualities can be controlled reversibly with external stimuli such as light [1], electricity [2], or chemical interactions [3]. Light is a particularly attractive stimulus due to its non-invasive and clean nature, excellent spatial and temporal resolution, and high controllability.

By definition, photochromic molecular switches (photoswitches) exhibit a change in their absorption spectrum when changing from the thermally stable to more energetic form, which is visualized by coloration or decoloration for positive and negative photochromes, respectively [1]. This is accompanied by changes in properties such as geometry, dipole moment, refractive index, conductivity, magnetic properties, acidity, or coordination [4]. Reversibility of the isomerization reaction differentiates molecular switches from molecular gates, the reverse reaction occurring thermally (T-type chromophore) or upon photoexcitation (P-type chromophore) [1].

The light-induced changes in the chemical and physical properties of the molecule can be exploited in catalysis, enabling external control over the reaction. Even simultaneous control of several processes is possible with orthogonal systems, i.e., catalysts that can be activated independently using different wavelengths or by utilizing some other stimuli together with light. This opens doors to novel one-pot reactions unobtainable with conventional catalysts [5]. In pharmacy, the ability to activate or deactivate a pharmaceutical molecule with a safe stimulus such as light enhances the selectivity of medicines, thus reducing side effects, environmental harm and development of drug resistance, and allowing the utilization of more efficient drugs [6]. The field of molecular machines also relies heavily on photoswitches [7].

When a photoswitch is integrated into a solid material or onto its surface, control over the properties of the material can be obtained. This way, photoswitches can be utilized in materials applications such as memories [8, 9], organic electronics [10], biomaterials [11], soft robotics [12], and optical-to-mechanical-energy conversion [13]. In many applications photoswitches are incorporated into polymer matrices either as dopants or covalently as crosslinks or side chains. The geometrical and other changes occurring in the molecule upon light irradiation can then be translated into macroscopic changes of materials properties. For example, liquid crystal elastomers (LCEs) are often used, the liquid

crystalline structure amplifying the molecular-level changes of the photoresponsive units into macroscopic [14, 15].

The preferences for the nature of the photoinduced physical changes vary depending on the application, so the photoswitch family should be chosen accordingly. In addition, the properties within a photoswitch family can be tuned with slight modifications in the molecular structure, providing the means to the optimization of absorption range and molar extinction, photoconversion efficiency, thermal stability, isomerization quantum yields, and fatigue resistance. Often, yet not exclusively, bistable P-type molecules – whose thermal relaxation to the energetically more favorable form is very slow – are preferred over faster-relaxing T-type molecules [16]. Absorption at visible or near-infrared wavelengths is favored over ultraviolet due to the damaging nature and short material and tissue penetration depth of the latter [17].

The most widespread photoswitch families are azobenzenes [18], diarylethenes [19], and spiropyrans [20], all of which have been studied extensively since late 20th century. Other conventional photoswitches include fulgides, chromenes, quinones, and hemithioindigos [1]. In addition, some new families such as indigo derivatives [21], donor-acceptor Stenhouse adducts (DASAs) [22], and hydrazones [23, 24] show great prospects. Of these, azobenzenes, diarylethenes, spiropyrans, indigos and DASAs are covered in this work, each having different advantages in applications. Azobenzenes show very fast isomerization with great geometrical changes and practically no photodegradation, and are easy to synthesize; diarylethenes exhibit supreme bistability and good fatigue resistance; indigos can be switched with visible light and the geometrical changes upon irradiation are even greater than for azobenzenes; DASAs are negative photochromes that can be operated with near-IR light. The properties and synthetic methods of these photoswitches are presented in Chapters 2 and 4, respectively. The spiropyran family is also introduced because of its versatility in photochromic materials. Applications of photochromic compounds in the fields of catalysis, medicine, and soft materials are reviewed in Chapter 3.

In the experimental part, four different types of new photochromic molecular switches are synthesized and characterized: azobenzene and diarylethene crosslinkers with very long thermal lifetimes; an indigo crosslinker; and a DASA dopant with good LC-compatibility. The photochemical properties of the switches are then studied and compared with reference compounds in literature. The results are given in Chapter 5 and summarized in Chapter 6, while the experimental methods are described in Chapter 7.

2. PHOTOCHROMIC MOLECULAR SWITCHES

The four photoswitch families studied experimentally in this thesis (azobenzenes, diarylethenes, indigos, and DASAs) as well as the widespread spiropyrans are introduced in chapters 2.1–2.5. Other photochromic families are not addressed in this work. Special attention is given to the properties of all families, especially relative to each other.

The most important qualities of photoswitches in terms of comparing different photochromic compounds with similar photoinduced physical changes are (i) absorption region, molar extinction and spectral shape, (ii) efficiency of photoconversion, (iii) thermal lifetime of the less stable form, (iv) fatigue resistance, and (v) quantum yield of photoswitching [8, 21, 25]. As noted above, absorption at long wavelengths is a preferred quality, and high molar absorption decreases the need for high-intensity irradiation for efficient isomerization. Photoconversion efficiency follows from the spectral separation of the two forms, which also allows for driving the equilibrium to either side with distinct wavelengths.

Terms thermal *lifetime* and thermal *half-life* are used concurrently. Half-life $t_{1/2}$ is the time in which half of the photoinduced change in absorbance is canceled in dark [1] and lifetime τ is the time in which the absorbance change decreases to e^{-1}. Usually, compounds with either very long or extremely short lifetimes are beneficial for applications as they give rise to bistable and dynamic photoswitches, respectively. [26]

Although photoswitching is theoretically non-destructive, irradiation always causes a small amount of side reactions, most notably oxidation, that with time reduce the photochromic qualities of the compound. Most typically, this is seen as photobleaching. Resistance to photodegradation, or fatigue, is measured either as the number of cycles a system can undergo with the desired properties, or as cyclability, i.e., the number of cycles needed for the absorption to drop by half. [1]

Quantum yield Φ, in photochemical context, is the amount of reactant consumed or product formed divided by the amount of absorbed photons. For most reactions, the quantum yield value is between 0 and 1, exceeding the upper limit only for certain chain reactions [27]. High or moderate quantum yields are generally required in all applications utilizing photochromic molecular switches [28].

2.1 Azobenzenes

Azobenzenes are a class of diazene molecules in which two benzene rings are bridged by an azo linkage [18]. Because of their absorption in UV-Visible range due to the conjugated system, many compounds have been used as industrial dyes since the late 19th century, but it is their use as photoswitches in recent decades that has lifted them back into

the frontier of science. The photoresponsivity is based on the efficient and reversible *cis–trans* (*E–Z*) isomerization at the azo bond: with UV or near-UV irradiation, the thermally stable *trans*-form is isomerized into *cis*, for which the reversed *cis–trans* relaxation can occur thermally or by irradiation with visible light (**Fig. 1**). The compounds are extremely robust, their fatigue resistance generally exceeding 10^5 isomerization cycles. Isomerization changes the size and form of the molecule significantly, with the length of the molecule decreasing from 1.0 to 0.59 nm and dipole moment increasing from 0 to 3.0 Debye for unsubstituted azobenzene [18]. The absorption spectrum and dynamics of isomerization depend on the substitution pattern in the phenyl rings, creating a way for chemists to tune the properties of azobenzenes and materials in which they are incorporated. Another interesting property of azobenzenes is that due to their rod-like structure, many azobenzenes exhibit liquid crystalline properties as such, as part of a supramolecular system, or at least show good compatibility with liquid crystalline systems [29].

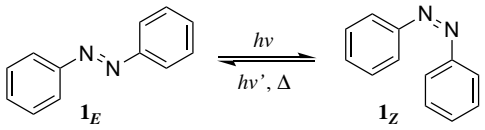

Figure 1. *The structure and trans–cis (E–Z) isomerization of azobenzene.*

The classification of azobenzenes is based on their spectroscopic properties and particularly the relative energies of the π–π* and n–π* absorption bands in relaxed state. Azobenzene-type molecules have a strong symmetry-allowed π–π* absorption band in the ultraviolet region and a notably smaller symmetry-forbidden n–π* band at ca. 440 nm. The π–π* band is red-shifted to approximately 400 nm for aminoazobenzene-type molecules, and to 500 nm for pseudostilbene-type molecules, for which the π–π* transition has the lowest energy, thus overshadowing the n–π* transition totally. This is attributed to the push-pull character of these molecules, having electron-donating and electron-withdrawing substituents in the opposite ends of the molecules and thus inducing a strong charge separation into the system. Absorption spectra of azobenzene-, aminoazobenzene-, and pseudostilbene-type molecules are shown in **Fig. 2**. It should be noted that the terms azobenzene, aminoazobenzene and pseudostilbene are based purely on spectral properties, and thus, for example, aminoazobenzenes are not restricted to azobenzenes containing an amino moiety, as seen in **Fig. 2**. Moreover, pseudostilbene is a somewhat misleading, although established term, seeing that stilbenes have an ethylene bridge in the place of the azo linkage in azobenzenes. [14, 18]

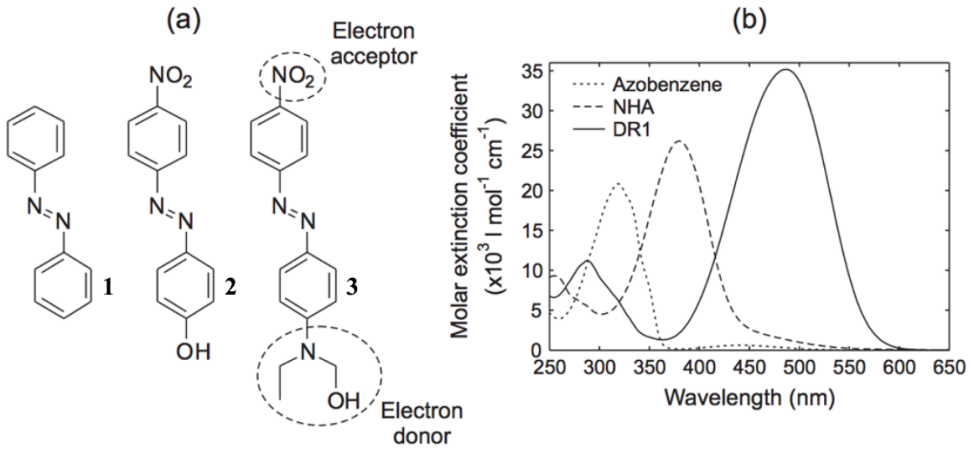

Figure 2. *a) Azobenzene-type (azobenzene,* ***1****), aminoazobenzene-type (4-nitro-4'-hydroxyazobenzene,* ***2****), and pseudostilbene-type (Disperse Red 1,* ***3****) azobenzenes and b) their absorption spectra in 20 μM THF solutions. Adapted from* [29].

Azobenzene-type molecules have a tendency for longer lifetimes than aminoazobenzenes and, especially, pseudostilbenes [14]. Thus, pseudostilbene-type azobenzenes show potential in ultrafast on/off-type switches, while in the search of bistable azobenzene materials, azobenzene-type compounds are preferred. In particular, *ortho*-fluorination with respect to the azo moiety increases the *cis*-lifetime significantly, being up to two years at room temperature for tetra- and hexafluorinated species **4** and **5** (**Fig. 3**) as found out by Blegér *et al.* [30, 31].

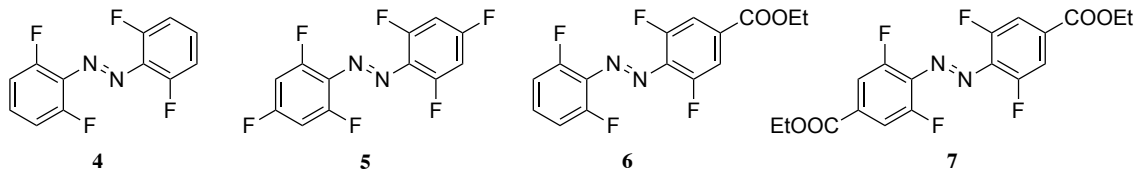

Figure 3. *The structures of four ortho-tetrafluorinated azobenzenes of which* ***4*** *and* ***5*** *have longest cis-lifetimes, and* ***6*** *shows the best combination of photoconversion efficiency and thermal stability of the cis-isomer.*

As a highly electronegative element, fluorine stabilizes the *cis*-isomer by more than 25 kJ mol^{-1} compared to the *trans* isomer through a negative inductive effect that reduces the electronic repulsion in HOMO. Simultaneously, the n–π* absorption bands of *cis* and *trans* isomers are separated, enabling *trans–cis* and *cis–trans* isomerization with visible light through a more efficient route than the π–π* transition. The separation is further strengthened by the introduction of electron-withdrawing substituents such as ester moieties in the *para* position. However, this also decreases the *cis*-lifetime due to positive mesomeric effect that leads to stabilization of the transition state in the isomerization reaction. Bléger *et al*. found out that the best compromise was an *ortho*-tetrafluorinated monoester **6** (**Fig. 3**), having a lifetime of more than half a year in room temperature combined with over 95 % photoconversion in both directions [31]. The absorption spectra of a corresponding diester **7** is portrayed in **Fig. 4**, showing the resolution between the n–π* bands in *cis* and *trans*.

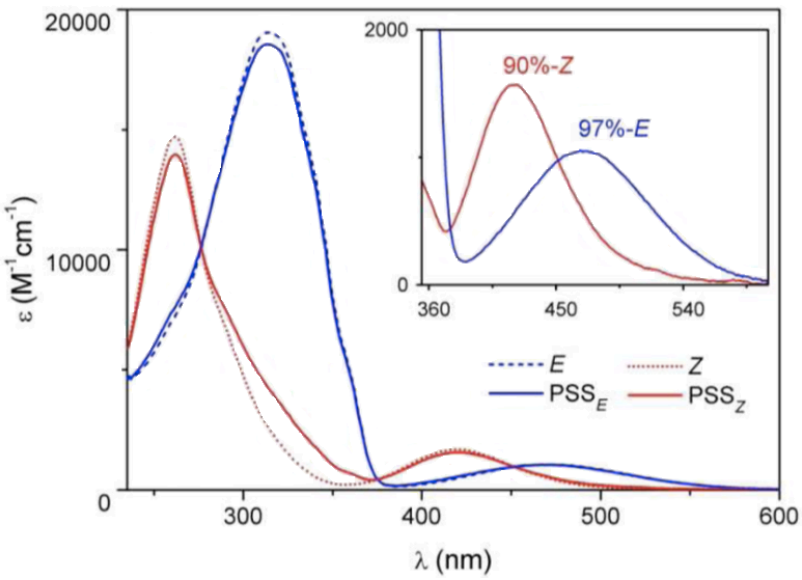

Figure 4. *Absorption spectra of pure cis- (Z) and trans-isomers (E) and the photostationary state mixtures (PSS) of ortho-tetrafluorinated azobenzene diester* ***7****. Adapted from* [30].

Despite these excellent qualities, the drawback of the *ortho*-fluorinated azobenzene photoswitches is the relatively low absorption of the n–π* band. With molar extinction coefficients below 2000 M^{-1} cm^{-1}, high-intensity irradiation must be used for efficient isomerization. By substituting one of the fluorines with an amine such as the five-ring pyrrolidine, the absorption of the n–π* band may be increased while maintaining relatively long *cis*-lifetimes, as recently reported by Ahmed *et al.* [26].

2.2 Diarylethenes

Diarylethenes are 1,2-aryldisubstituted ethene derivatives. The simplest example is stilbene or 1,2-diphenylethene, a UV-absorbing photoswitch **8** whose functionality arises from *cis–trans* isomerization of $\mathbf{8}_E$ at the ethylenic double bond and the subsequent conrotatory 6π ring-closing reaction of $\mathbf{8}_o$, producing a colorful dihydrophenanthrene molecule $\mathbf{8}_c$ (**Fig. 5**). Under air, the reaction will advance via hydrogen elimination to form phenanthrene **9**, but in deaerated conditions the isomerization is reversible [8]. Hydrogen elimination may be avoided by methylation at *ortho* positions of the phenyl rings, although the thermal lifetime of this switch (**10**) is only 1.5 minutes at room temperature [32].

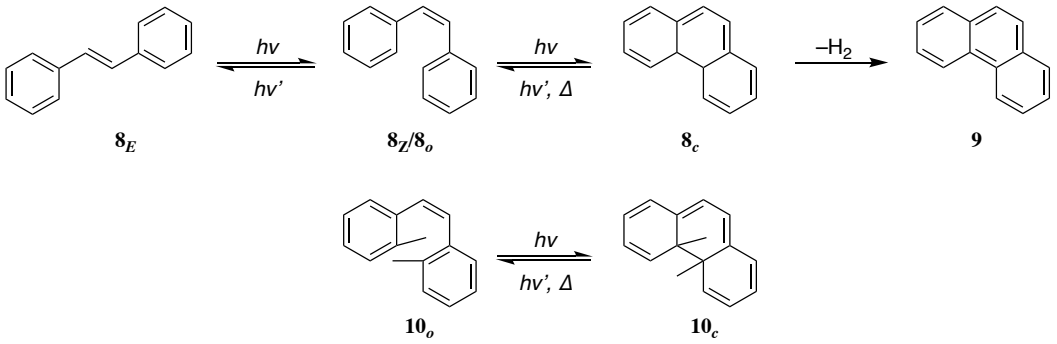

Figure 5. *The isomerization of stilbene (**8**$_E$ and **8**$_Z$/**8**$_o$), ring-closing to form **8**$_c$, and dehydrogenation to form phenanthrene **9**; and the ring-closing reaction of ortho-methylated stilbene **10**$_o$ to form **10**$_c$.*

To prolong the lifetime, the phenyl moieties must be substituted with heteroaromatic substituents. Kellogg *et al.* [33] studied the photocyclization of thiophene- and furan-disubstituted ethenes and found out that thiophene substitution prolonged the closed-cycle-lifetimes. Encouraged by this, Irie and Mohri [32] built similar thiophene systems in search for bistable P-type photoswitches and added electron-withdrawing groups to the ethylene moiety in order to cause a red-shift in the absorption of the closed-ring isomer of **11** and **12** (**Fig. 6**). In addition, enclosing the ethylene moiety in a cyclic structure of **11** prevents *cis–trans* isomerization of the open-ring isomer that might compete with the cyclization reaction. These molecules were found to be truly bistable photoswitches between colorless (open-ring, abbreviated o) and colored (closed-ring, abbreviated c) forms, thermal relaxation not occurring even after several months in elevated temperatures. In addition to the coloration, photocyclization induces changes in the conformational flexibility and electronic properties of the molecule.

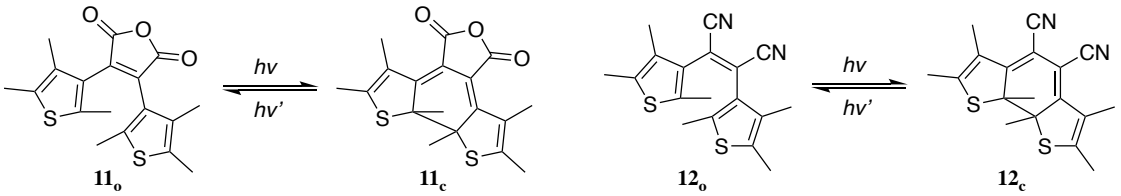

Figure 6. *Structures of two bistable dithienylethene-based photoswitches.*

Shortly afterwards, it was found that the best results in terms of closed-ring lifetimes are acquired using a perfluorinated cyclopentene ring (e.g., **13** in **Fig. 7**) as the ethylene equivalent [19] even though also the maleic anhydride [8] and maleimide [34] derivatives are commonly used [35]. In studies made with other cycle sizes it was discovered that both undesired twisting of the planarity and desired increase in the photocyclization quantum yield take place with increasing ring size, making cyclopentene the best compromise between four-, five- and six-ring systems [36]. In **Fig. 7** the absorption spectra of a perfluorinated dithienylcyclopentenyl derivative **13** in open and closed forms are shown.

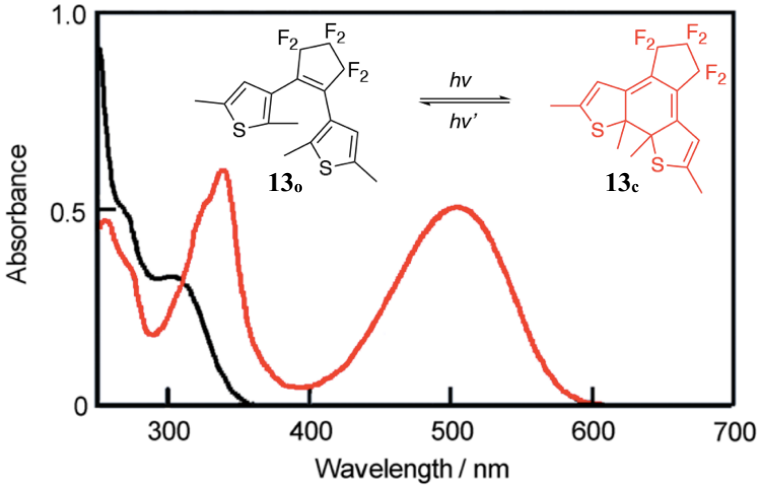

Figure 7. *UV-Vis absorption spectra of colorless 1,2-bis(2,5-dimethylthiophen-3-yl)-3,4,5-hexafluorocyclopent-1-ene* ***13o*** *(dark) and its colored closed-ring isomer* ***13c*** *(red). Adapted from* [16].

The properties of some perfluorinated diarylethenes are superior for bistable P-type switches: (i) the thermal lifetimes of both isomers may exceed 400,000 years in room temperature, (ii) quantum yields may rise to practically 100 %, (iii) molecules are fatigue-resistant up to at least 10,000 isomerization cycles, and (iv) both isomerization reactions take place in a picosecond scale. In addition, the absorption band of the colored isomer can easily be shifted, and the photoswitching is also effective in crystalline state as exemplified in **Fig. 8** [16].

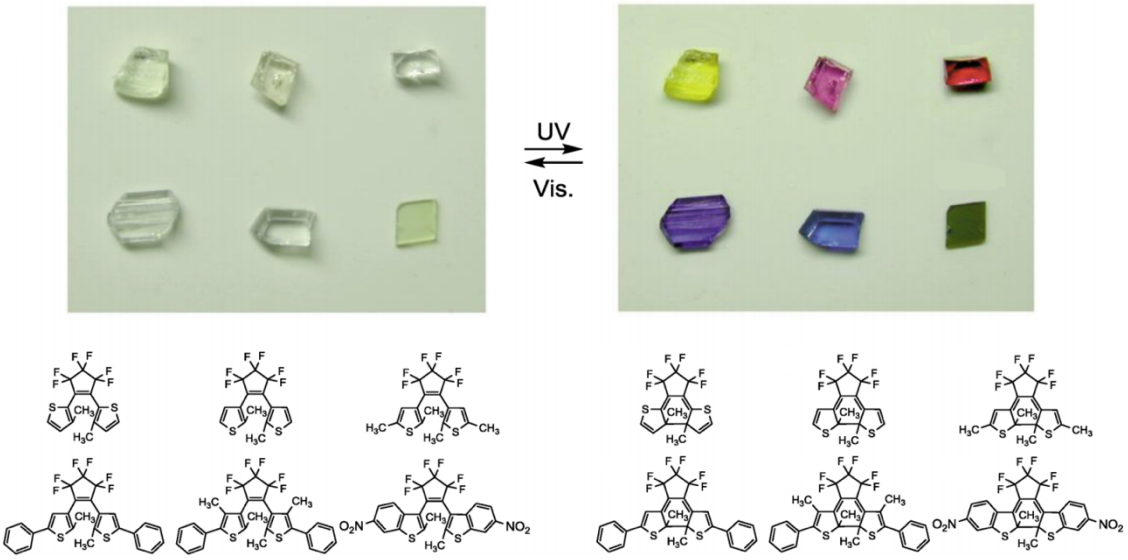

Figure 8. *Switching between colorless and colored isomers of six perfluorinated dithienylcyclopentene derivatives in crystalline state. Adapted from* [16].

2.3 Indigo derivatives

Indigo is an aromatic, deeply conjugated molecule **14** with a characteristic blue color (**Fig. 9**). It has been used for dyeing purposes for millennia, extracted from certain plant species. In modern textile industry, synthetic indigo is the primary dyeing agent for denim cloth. As such, it is an inexpensive chromophore whose absorption is extremely red-shifted compared to, for example, typical azobenzenes, with absorption maximum above 600 nm [21]. This property makes the use of indigos in medical and biological applications advantageous as the tissue-penetration is strongest with red light [37] in addition to avoiding the use of UV irradiation, which is hazardous in biological environments. Unsubstituted indigo does not undergo isomerization upon photoexcitation due to fast intramolecular proton exchange [38], but *N*,*N*-disubstituted derivatives can be switched from thermally stable *trans*-isomer into *cis*, which relaxes thermally back to *trans* [21]. This brings about changes to the properties of the molecule similar to those observed during azobenzene isomerization.

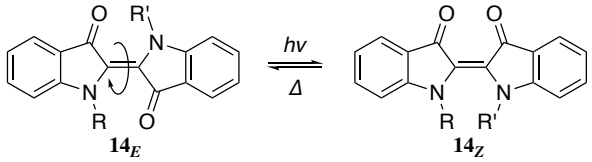

Figure 9. *Structure of indigo derivatives (for unsubstituted indigo, R = R' = H) and their photoisomerization between the E and Z isomers.*

For such a well-known parent molecule, the studies regarding photoswitching abilities of indigo derivatives are surprisingly scarce, with only methyl- [39], acyl- [40], Boc- [41], and some aryldisubstituted [42] derivatives reported earlier. In a recent study Huang *et al.* investigated the effects of *N*-substitution with a vast library of indigo derivatives [21]. Their main finding was that aryl substituents prolonged the thermal lifetime of the *cis*-isomer, probably due to π–π interactions between the aryl moieties. Moreover, electron-poor substituents such as *para*-nitrated or *para*-trifluoromethylated phenyls increased the thermal stability the most, with the former (**15**) yielding a *cis*-lifetime of 408 min at room temperature. It also showed the best photoconversion of all the compounds studied, from 12 % *cis* in dark to 82 % in photostationary state upon irradiation with 660 nm light, owing to one of the largest differences between the absorption maxima of *cis*- and *trans*-isomers, 43 nm. The structure and absorption spectra in dark and upon irradiation are shown in **Fig. 10**.

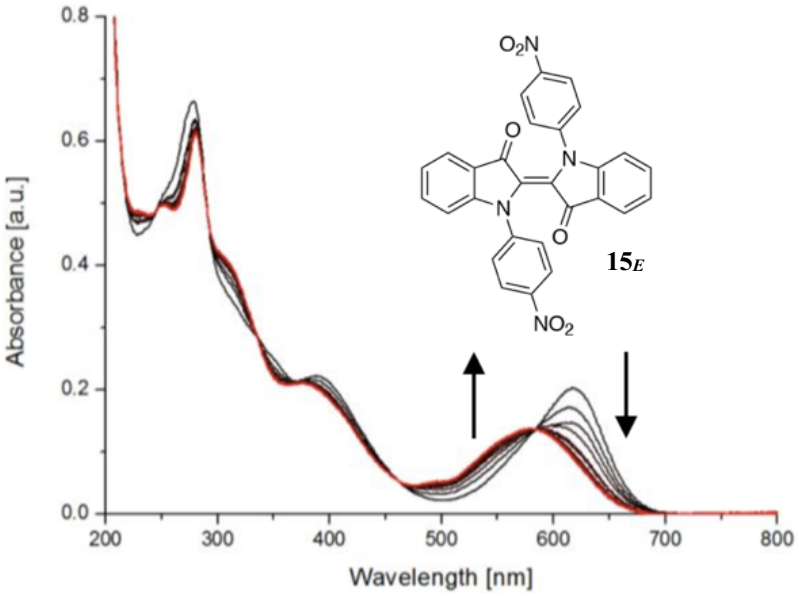

Figure 10. *The structure of para-nitrophenyl-disubstituted indigo and its UV-Vis spectrum in dark (black line furthest from red) and upon irradiation with 660 nm light (red line). Black arrows indicate the spectral changes upon trans–cis-isomerization. Adapted from* [21].

2.4 Donor-acceptor Stenhouse adducts

Donor-acceptor Stenhouse adducts (DASA), named after the similar Stenhouse salts discovered by John Stenhouse in the mid-19th century [43], are a new photoswitch family, introduced in 2014 by de Alaniz *et al.* [22] although the photoswitching ability of Stenhouse salts was known already 30 years earlier [44]. DASA photoswitches (e.g., **16** and **17**) display many interesting qualities: negative photochromism, visible light absorption, and formidable changes in the physical properties of the molecules, including geometry [22]. The photohromic properties are based on the reversible cyclization reaction mechanistically similar to Piancatelli rearrangement [45, 46], in which a deeply conjugated triene moiety in the thermally stable form is converted into an unconjugated five-membered ring (**Fig. 11**).

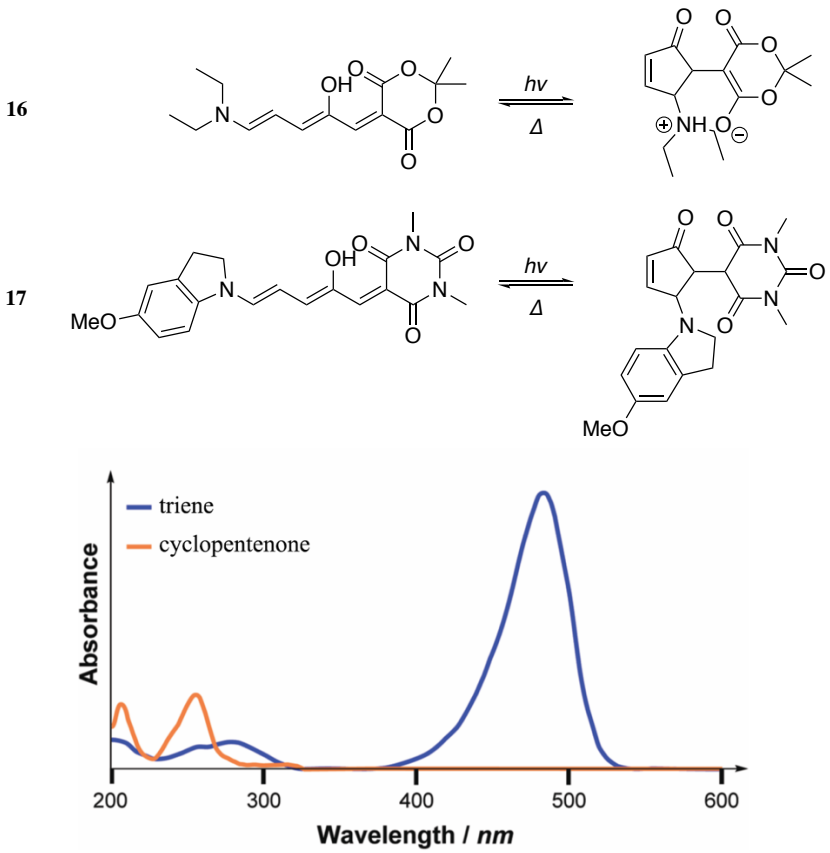

Figure 11. *Triene and cyclopentenone isomers of 1st and 2nd generation DASAs* ***16*** *and* ***17****, respectively, derived from Meldrum's and barbituric acid, respectively, and the absorption spectra of the former. Adapted from* [28].

The topmost structures in **Fig. 11** describe the general photochromic behavior of DASAs synthesized from Meldrum's acid and 1,3-dimethyl barbituric acid. The acid-derived part is an electron acceptor, while the amine in the other end is an electron donor, creating a push-pull effect [22]. In the caption, the notations 1st and 2nd generation refer to the original DASA molecules and the new compounds published two years later [47], respectively. In the 2nd generation DASAs an aromatic amine has been used, extending the conjugation and, subsequently, red-shifting the π–π* absorption maximum. While the tunability of 1st generation compounds is limited to 570 nm for barbituric acid derivatives and even less for Meldrum's acid derivatives, 2nd generation DASAs absorb at up to 750 nm (**Fig. 12**).

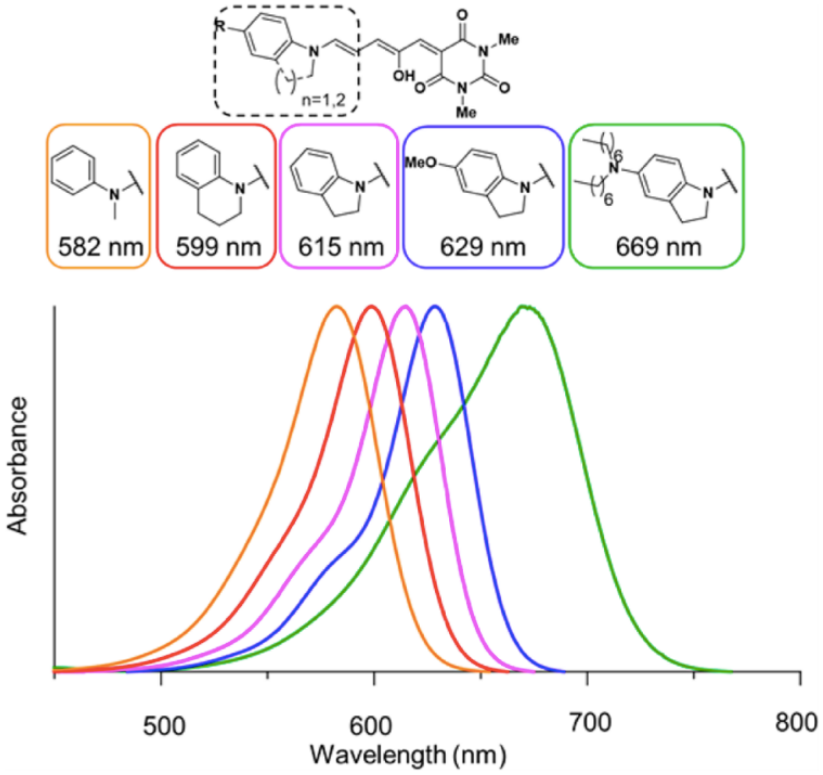

Figure 12. *Relaxed state absorption of selected 2nd generation DASA photoswitches. Adapted from* [47].

In addition to absorbing higher wavelengths, 2nd generation DASAs are better applicable in various solvents and polymer matrices than 1st generation switches whose solubility and functionality as reversible switches suffer from their zwitterionic cyclic form (**16** in **Fig. 11**). Thus, in the development of polymerizable or polymer-doped DASA photoswitches, 2nd generation switches are preferential [47]. Extensive photodynamic studies of the thermal lifetimes have not been carried out, but solvent effects on the kinetics are greater for the 1st than for the 2nd generation DASAs. For a single 2nd generation molecule, the *para*-methoxyindoline-substituted **17** in **Fig. 11**, thermal lifetime was in the range of a few minutes. Fatigue was also measured by repeating photocyclization cycles for the same compound. The absorbance maximum decreased by 20 % after 100 cycles and by 40 % after 200 cycles [47], so fatigue resistance of DASAs is not as formidable as in the case of azobenzenes and diarylethenes [14, 16]. Also, it should be noted that photochemical switching back to the triene form is not possible unless deep UV is used (**Fig. 11**).

2.5 Spiropyrans and analogues

Spiropyrans were first introduced to the chemical society by Decker and Fellenberg in early 20th century [48] and their photochromism was discovered nearly 50 years later by Fischer and Hirshberg, following the discovery of their thermochromism [49]. Nowadays, spiropyrans are the most widespread photochromic family [20] due to the fact that they can be activated not only by light but by half a dozen other stimuli such as acids and bases, solvents, and metal ions [50]. The structure of a spiropyran molecule in its closed

(spiro) and open (merocyanine) forms are presented in **Fig. 13**. Spiropyran constitutes of indoline and chromene parts, left and right side of the spiro center in **18$_{SP}$**, respectively.

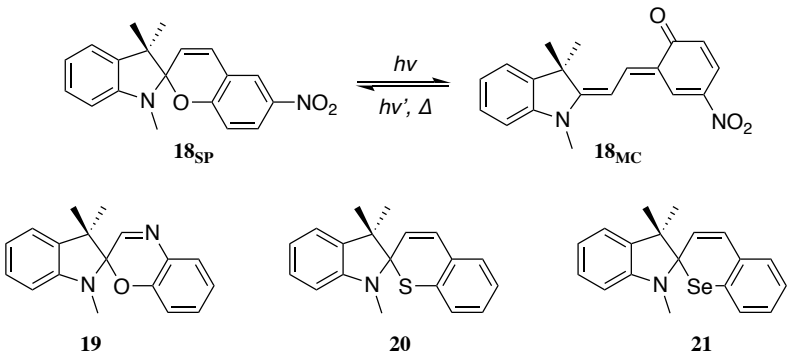

Figure 13. *Structures of nitrated spiropyran **18$_{SP}$** and its merocyanine form **18$_{MC}$**, spirooxazine **19**, spirothiapyran **20**, and spiroselenapyran **21**.*

In addition to the original spiropyran and its derivatives, similar heteroanalogues such as spirooxazines **19**, spirothiapyrans **20**, and spiroselenapyrans **21** have been investigated. The spirocyclic form of spiropyrans and related analogues is colorless and major changes into the absorption spectrum cannot be induced with the derivatization of either aromatic parts of the molecule. However, the spectrum of the colored merocyanine form can be modified with substitutions. More precisely, it has been established that electron-withdrawing π acceptors such as nitro groups introduced to the chromene part of the spiropyran molecule (**18**) red-shift the spectrum. Also the substitution of oxygen for sulfur or selenium brings about a bathochromic shift. [20]

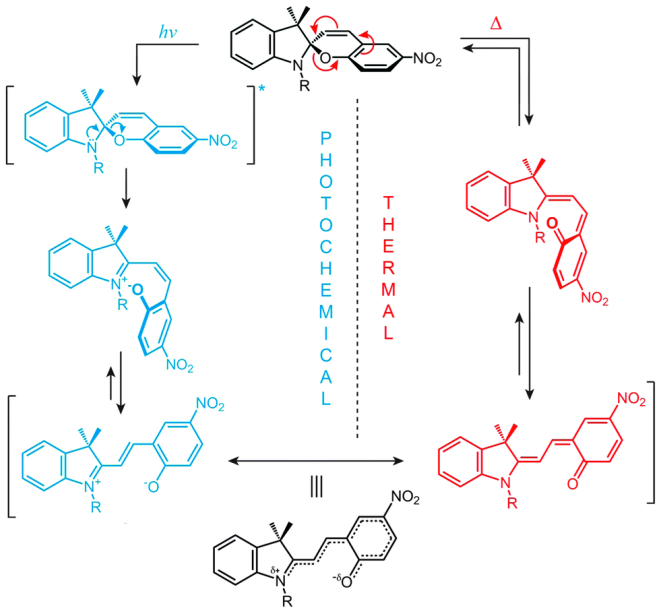

Figure 14. *The mechanism of photochemical and thermal isomerization between the spiro and merocyanine forms* [50].

The isomerization of spiropyran is proposed to follow the routes presented in **Fig. 14**, starting with either heterolytic cleavage of the C_{spiro}–O bond that is weakened and elongated due to orbital interactions between the antibonding orbital of the bond and the free electron pair of the indoline nitrogen, or a 6π electrocyclic ring opening [51]. In addition to the obvious color change between transparent and blue (**Fig. 15**), physical properties of spiropyrans and their analogues change drastically upon ring-opening and cyclization. Most interestingly, the dipole moment increases from ca. 5 to 15 Debye upon ring-opening. Also, the merocyanine form is considerably more basic and readily protonated to form another species with a distinct spectral shape (**Fig. 15**), and also emits at 650 nm while the spirocyclic form exhibits virtually no emission. A geometric change takes place as well, although not as pronounced as for azobenzenes, indigos, and DASAs. [50]

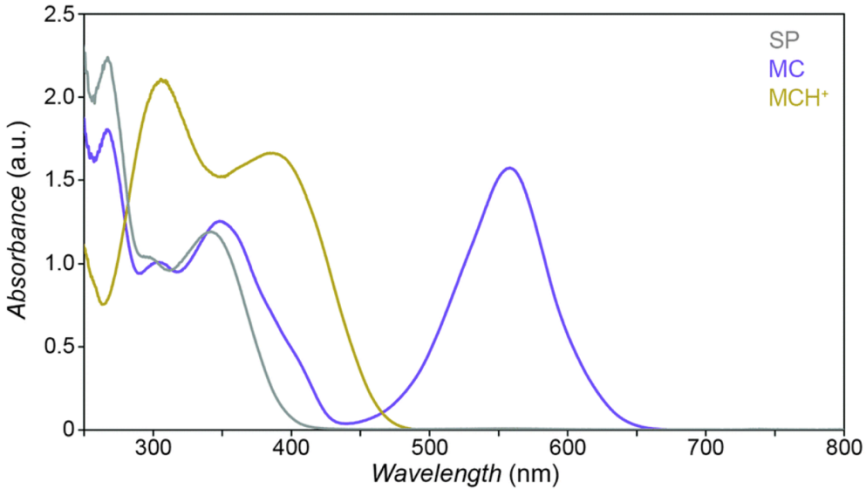

Figure 15. *The absorption spectrum of spiropyran in its spirocyclic (SP), merocyanine (MC), and protonated merocyanine (MCH^+) forms. Adapted from* [50].

3. PHOTOSWITCH APPLICATIONS

There is a general consensus among scientists that the next generation catalysts, medicinal compounds, and materials need to be controllable by an external stimulus such as electric or magnetic field, moisture, or light [4–6, 15]. Although practical use remains elusive, a range of prospective designs for these photoswitchable systems have been designed. Herein, the basics regarding photoswitch applications in catalysis, pharmacy, photomechanics, and memories are introduced, along with representative examples of each.

3.1 Catalysis and pharmacy

Three types of catalysts whose catalytic activity can be controlled with light exist: photocatalysts that are active in their photoexcited form; photoactivated "gated" catalysts whose catalysis can be initiated with light; and photoswitchable catalysts whose activity can reversibly be turned on and off [5, 52], as depicted in **Fig. 16**.

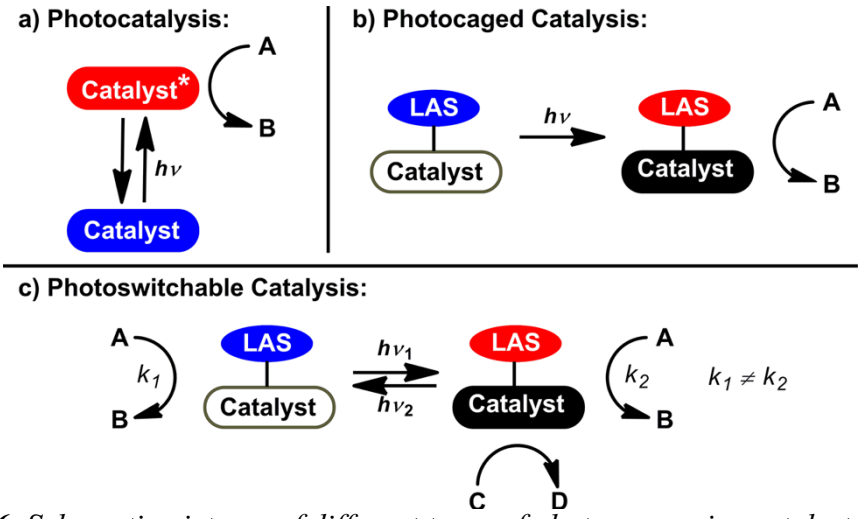

Figure 16. *Schematic pictures of different types of photoresponsive catalysts carrying light-absorbing species (LAS). Red and black color refer to the active LAS and catalyst species, respectively, while inactive LAS and catalyst are colored blue and white.* [5]

Several examples of photoswitchable heterogeneous catalysts have been presented [5], but organic chromophores are typically utilized in homogeneous catalysis. The activity of a photoswitchable catalyst is determined as the ratio of the rate constants of the catalytically active (on) and inactive (off) forms, as shown in Eq. (1). Good catalysts show high k_{rel} values, i.e., high catalytic activity in the on-form and low activity in the off-form [52]:

$$k_{rel} = \frac{k_{on}}{k_{off}} \tag{1}$$

Applying P- and T-type photoswitches brings about two ways to control the catalytic activity. With P-type photoswitches, switching between the active and inactive forms is performed by irradiating with two wavelengths. With T-type, the thermal relaxation can take place instantly (for very short τ) or over time, in which case the relaxation can be controlled with the reaction temperature, adding another external stimulus with which to control the catalysis [52]. Activation with visible light is preferential to ultraviolet, as high-frequency irradiation may cause unwanted side reactions in the substrate.

There are two mechanisms through which the catalytic activity is controlled: steric effects and preorganization. Steric effects are typically utilized with *cis–trans*-isomerization, most often using azobenzene derivatives [5]. The catalytic site is open for reagents only in one of the forms, usually the *cis* isomer, and sterically blocked in the other. Thus, the catalyst is active only upon irradiation with proper wavelength. For instance, general-base catalysts can be activated and deactivated by revealing or shielding a basic nitrogen atom in the structure, respectively [53].

Some catalytic processes require two or more catalytic sites to be located in a specific way with respect to one another in order for the reaction to proceed. This preorganization is the driving force of many enzymatic processes and bifunctional catalysis, leading to a high effective concentration of the reagents, the reaction thus resembling an intramolecular process. In photoswitchable catalysts, the preorganization effect is induced via *cis–trans*-isomerization, typically so that the catalytic sites are brought near one another in *cis* form, thus initiating the catalysis. One of the first examples was introduced already in 1981 by Ueno *et al.* who attached an azobenzene unit to β-cyclodextrin and were able to control the hydrolysis rate of an aromatic ester with light [54].

Also photoinduced changes in chelation and electronic properties have been taken advantage of in catalysis: by changing the geometry of the molecule, chelating properties can be altered, and the degree of conjugation leads to changes in electronic properties. These both effects have been investigated with diarylethenes. Branda *et al.* were able to utilize the photocyclization in the catalysis of cyclopropanation, switching between enantioselective and non-selective catalysis in open and closed form, respectively, due to diminished chelation in the latter because of reduced conformational flexibility [55]. The same group also exploited the change in electronic effects of a dithienylhexafluorocyclopentene switch upon photocyclization in mimicking the catalytic properties of vitamin B_6 in the racemization of L-alanine. They found out that the catalyst was active only in the closed form in which electronic connectivity exists between the two ends of the molecule [56].

Pharmacological photoswitch applications are based on similar principles: the bioactive functionality is incorporated into a photoswitchable unit, most typically azobenzene or diarylethene, and the activity of the drug can be controlled with light, utilizing the same

steric effects and preorganization as in photoswitchable catalysis [6]. Efficient photoconversion, high k_{rel} values, and absorption in the visible or even near-infrared part of the spectrum are essential for well-performing photoswitchable pharmaceuticals.

Photopharmacology was pioneered already in 1969 by Erlanger and Nachmansohn who used azobenzenes to control acetylcholinesterase inhibition [57, 58]. However, only recent advances in the field have brought photoswitchable pharmaceuticals near realization in practical medicine. As maybe the most intriguing example of all, Velema *et al.* [59] designed a photoswitchable antibiotic by introducing the functionalities of quinolones, broad spectrum antibiotics, into an azobenzene core. The molecule was activated by *trans–cis*-isomerization upon UV irradiation, leading to notably higher antibacterial activity which decreased in time due to thermal *cis–trans* relaxation. They concluded that the photodynamics of the antibiotic compound could be optimized so that the bioactivity is lost before the drug leaves the body, thus preventing the emergence of resistant bacterial populations.

3.2 Materials chemistry

The numerous potential materials applications of photoswitches range from an all-optical computer [4] to biomimetic microrobotics [12]. Herein, due to the scope of the experimental part of this work, the focus will be on materials whose mechanical properties and motion can be controlled optically. In addition, photoswitchable systems that can be utilized in organic electronics and memories are briefly introduced.

For efficient control over the mechanical properties of a material, the photoswitches need to be incorporated into a bulk material. The "material" can be of different types, e.g., molecular crystal or glass, or gel-based, but photoresponsive polymer-based materials are perhaps the most versatile and widely used. The photoswitches can be doped into the polymer matrix or covalently attached to it. In both cases, only a relatively small amount of the photoresponsive molecules is needed for efficient modification of macroscopic materials properties [60].

In the case of photomechanics (production of macroscopic mechanical movements triggered by light) [14], liquid crystalline (LC) polymer networks are often utilized. Liquid crystals combine the mobility of liquids with the orientational and/or positional order of crystals [61]. Among different classes of liquid crystals, thermotropic liquid crystals exhibit a liquid crystalline phase between the crystalline and isotropic phases upon warming or cooling. Most commonly, these are calamitic molecules that have a rigid rod-like structure with polar and non-polar terminal groups, thus aligning unidirectionally due to supramolecular interactions such as van der Waals forces and π-stacking. Due to their unique combination of properties usually associated with crystalline and liquid states as well as effective self-assembly, liquid crystals are utilized in various materials. When doping LCs with photoswitchable molecules, one can use light to induce isothermal order–disorder transitions (**Fig. 17a**) [62]. In the solid state, light-triggered control over the

molecular order of liquid crystal elastomers (LCEs) and polymer networks (LCNs) is the key for efficient photomechanical motions [63]. LCEs and LCNs differ by the degree of crosslinking, LCEs being less crosslinked and thus softer than the glassy LCNs. The most convenient fabrication technique for LCEs and LCNs is photopolymerization, incorporating the photoswitchable compounds as crosslinks into the network.

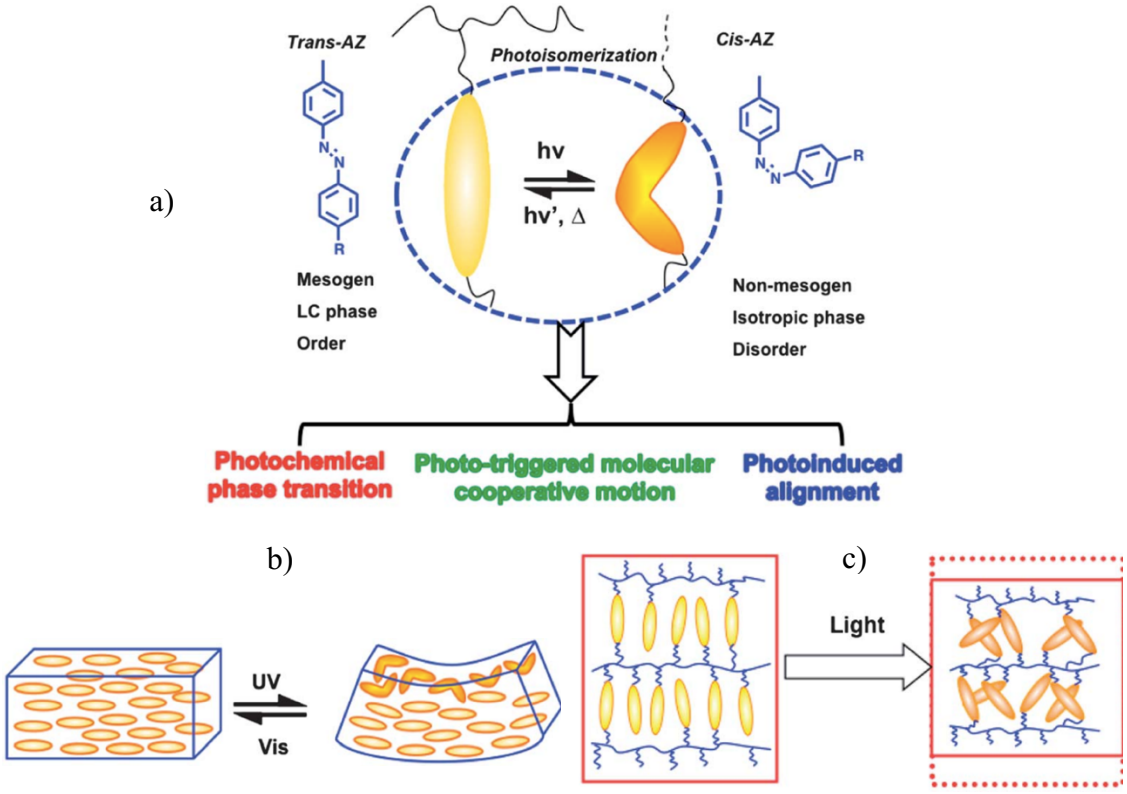

Figure 17. *a) Photoisomerization of azobenzene in an LC disrupts the order. Thus, phase transition, molecular motion and molecular alignment can be controlled with light. Examples in the field of photomechanics include b) photoinduced bending of a material containing azobenzene units due to photochemical effect, and c) photoinduced shape change of an LCE containing crosslinked azobenzene units. Adapted from* [62].

There are two phenomena through which the molecular changes in the photoswitch can be translated into macroscopic scale: photothermal and photochemical effects. The former attributes to temperature increase in the material due to photothermal heat released from the photoswitches upon light absorption. Due to heat-induced isotropization, the order in the LCE/LCN decreases and – if the material is properly designed – the material deforms. This effect requires no covalent crosslinking but is also efficient when doping the photoactive compounds into the network [63]. Photochemical effect, on the other hand, stems from the spatial changes in the molecular conformation upon photoisomerization, translated into macroscopic motion of the material. Photochemical effect is only effective for covalently bound photoswitchable crosslinkers, and even in that case, pho-

tothermal effect is always present and separating the two effects from one another is difficult. Photothermal effect typically leads to faster photomechanical motions than photochemical effect(s), and lower concentration of the photoswitch is required for efficient deformation. The working principle of photochemically triggered actuation in the case of azobenzene-containing LCEs/LCNs is shown in **Fig. 17b**. [63]

A number of ways can be utilized to bind the actuator covalently into the polymer matrix. The most used strategy is to add a vinyl-containing substituent such as acrylate **22**, methacrylate **23** or styrene **24** (**Fig. 18**) into one end (side-chain) or both ends (crosslinker) of the photoswitch, after which it can be incorporated into the matrix via chain polymerization. Acrylates and methacrylates are most commonly used and show similar behavior in polymerization, only differing in their polymerization rates [64]. Thus, it is usually preferred that acrylates and methacrylates are not used concurrently in the bulk monomer and actuator unless the difference in their reactivity is specifically exploited in building phase-separated polymer networks [65].

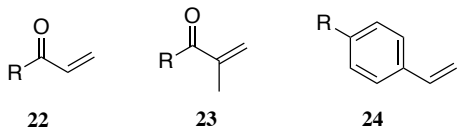

Figure 18. *Acrylate, methacrylate, and styrene linkers.*

Other reactions are also used in incorporating the photoswitches into the polymer material. One method takes advantage of thiol-ene click reaction [66] between a terminal alkene **25** and a thiol **26** depicted in **Fig. 19**. The reaction is highly stereoselective and proceeds without solvent or catalyst, giving the anti-Markovnikov product **27** in quantitative yield. It is also possible to utilize esterification, amidification, and other substitution reactions in step-growth polymerization.

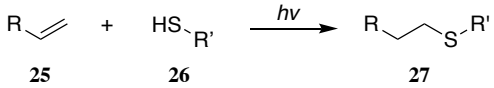

Figure 19. *The reaction scheme of the thiol-ene reaction.*

The photoswitch of choice in photomechanics has conventionally been azobenzene and its derivatives due to its robustness and, most importantly, the large shape-change upon isomerization [14]. However, recently, some studies have also been carried out with diarylethene crosslinkers; while the shape-change related to the photocyclization reaction is relatively small, the bistability of such crosslinkers is superior in comparison with azobenzenes [67]. Indigos and DASAs have not yet been incorporated into LCEs.

In addition to photoinduced mechanical motion, photoswitches incorporated into bulk materials have potential applications in other branches of materials chemistry. Memories are one of the most important field in current research. Photochromic optical memories are based on photochemical recording that has several advantages over the traditional thermal recording such as better resolution and faster recording speed [16]. While studies

have been made with azobenzenes, most famously by Ikeda and Tsutsumi [9] and by Rafal Klajn *et al.* [68] who controlled nanoparticle aggregation via azobenzene isomerization, diarylethenes are more commonly applied in memory systems due to their excellent qualities in terms of thermal stability, fatigue resistance, and response time [8, 16]. Non-destructive readout of diarylethene-based memories can be achieved with, e.g., IR [69] or Raman spectroscopy [70]. Also more novel modes of data recording and storage have been pursued; examples include 3D memories, holographic memories, and multi-wavelength recording [16]. Holographic memories are based on photoalignment, as extensively studied with azobenzenes during last decades [71].

4. SYNTHESIS OF PHOTOSWITCHES

Due to the diversity of organic photoswitches, there are thousands of synthesis routes to produce photochromic molecular switches. However, the syntheses of molecules inside a given photoswitch family usually follow the same few routes. Herein, general synthesis routes for azobenzenes, diarylethenes, photochromic indigo compounds, and DASA compounds are presented. In addition, special attention is paid to the synthetic routes to photochromic crosslinkers similar to those produced in the experimental section of this work.

4.1 Azobenzenes

Due to the long-lasting interest in azobenzene derivatives both in academic and industrial fields, numerous methods for synthesis of both symmetrical and unsymmetrical azobenzenes have been developed [72]. The three most conventional reactions, azo coupling, Mills reaction, and Wallach reaction all date back to the 19th century [73–75]. Azo coupling, a reaction between an aromatic primary amine and an electron-rich arene proceeding via a diazonium intermediate, remains the first choice for the synthesis of unsymmetrical azobenzenes. Typically, the amine is first treated with sodium nitrite and concentrated hydrochloric acid in water or a mixture of water and a water-soluble organic solvent at 0 °C or lower temperature, followed by the addition of the electron-rich arene in a cold basic aqueous solution. The synthetic scheme for 4-hydroxyazobenzene from aniline **28** and phenol and the mechanism for it [76] are depicted in **Fig. 20**. The upper row in the mechanism constitutes the diazotization reaction in which aniline first attacks the nitrosium ion generated *in situ* from nitrite and hydrochloric acid, followed by protonation and elimination of water to create the diazonium compound. It is then attacked by the phenol in an electronic aromatic substitution reaction, releasing hydrochloric acid that is neutralized by the carbonate in the solution. The azo product is isolated as a yellow or red compound **29**.

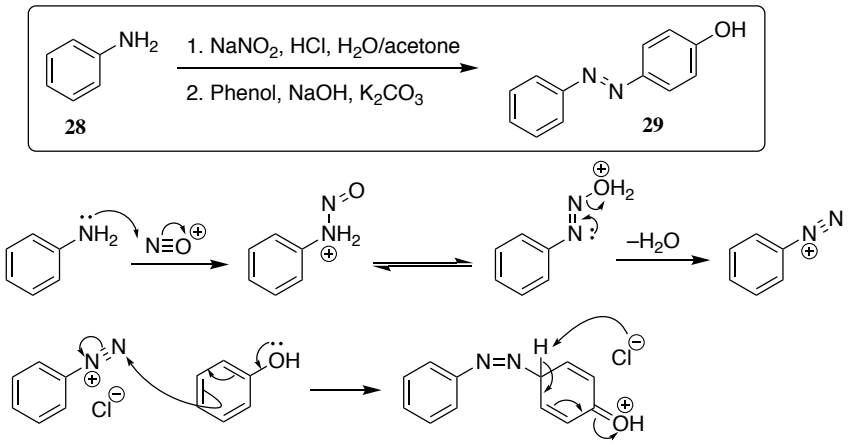

Figure 20. *Reaction scheme and mechanism of the azo coupling reaction between aniline and phenol to produce 4-hydroxyazobenzene* ***29****.*

The one-pot, two-step reaction typically gives good yields, and some diazonium compounds are available commercially as tetrafluoroborate salts. However, the reaction temperature must be kept low to stabilize the potentially explosive diazonium compound, and the reaction works tenuously for electron-poor arenes that lack the activating electron-donating group needed to attack the weakly electrophilic diazonium compound. For the synthesis of unsymmetrical azobenzenes **31** inaccessible with azo coupling, Mills reaction is often the most reasonable choice. The reaction takes place between an aromatic nitroso compound **30** and a primary aromatic amine, typically in glacial acetic acid (**Fig. 21**). The nitroso compound can be oxidized from the corresponding aniline, and the simplest derivatives are also available commercially. In addition to the traditional method shown below, modern adaptions with more complex reagents are numerous [72].

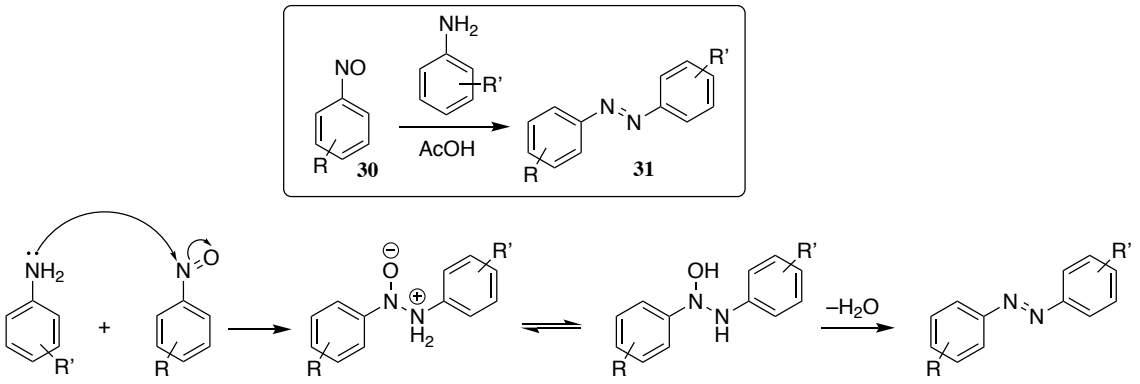

Figure 21. *Reaction scheme and mechanism for a Mills reaction between a nitroso compound and an aniline derivative.*

Wallach reaction is an alternative method for building hydroxyazobenzenes. It proceeds through an azoxybenzene intermediate, reduced from an aromatic nitro compound with, e.g., alcoholic sodium hydroxide/acetaldehyde [77], or oxidized from an aromatic primary amine with, e.g., potassium permanganate [78]. In a strongly acidic medium a Wallach rearrangement takes place, resulting in an isomeric mixture of 4- and 2-hydroxysubstituted products as shown in **Fig. 22** for 4,4'-dinitroazoxyazobenzene **32** [79].

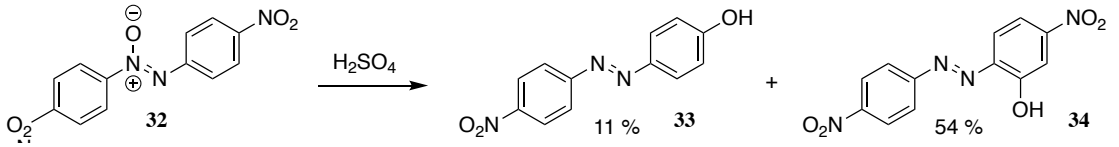

Figure 22. *Reaction scheme for a Wallach rearrangement from 4,4'-dinitroazoxybenzene into 4-hydroxy-4'-nitroazobenzene and 2-hydroxy-4,4'-dinitroazobenzene.*

Other, more novel procedures for making unsymmetrical azobenzenes have also been introduced, for instance, palladium-catalyzed coupling between *N*-Boc-arylhydrazines and aryl halides, yielding *N*-Boc-diarylhydrazines that are ultimately oxidized into the corresponding azobenzene [80]. In addition, a number of one-step reactions based on oxidation of aromatic amines or reduction of aromatic nitro compounds have been developed for the synthesis of symmetrical azobenzenes [72]. Of these, the oxidation of anilines with potassium permanganate and iron sulfate heptahydrate [31] has gained most popularity among azobenzene synthesizers.

4.2 Diarylethenes

Three distinct synthetic routes to symmetric perfluorinated diarylethenes exist. Of these, most common is the two-step reaction in which a thiophene halide **35** is first lithiated with *n*-butyllithium in ether or tetrahydrofuran at low temperature and the intermediate **36** then reacted with octafluoropentene (0.5 equivalents) in a nucleophilic addition–elimination reaction [81], resulting in a perfluorinated dithienylcyclopentene **37** that can be further functionalized if the thiophene derivatives have chloro-, bromo- or iodosubstituents that can be used in organometal-catalyzed coupling or nucleophilic substitution [82]. As a representative sample, the reaction scheme for the synthesis of 1,2-bis(5-chloro-2-methylthiophen-3-yl)-hexafluorocyclopent-1-ene is presented in **Fig. 23**. The halogenated thiophene derivative can be prepared via electrophilic substitution reactions or purchased commercially.

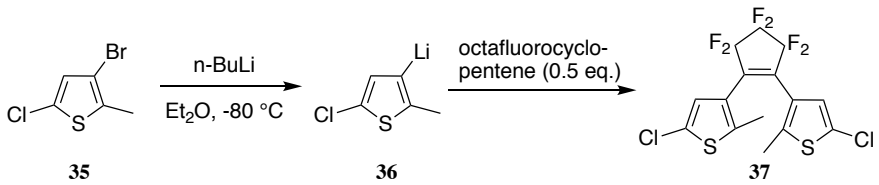

Figure 23. *Synthesis of a perfluorinated dithienylcyclopentene using lithiated thiophenyl species.*

This synthesis is relatively easy and enables the production of many functional dithienylethenes. However, yields are often relatively small, and the volatility of octafluoropentene (bp 27 °C) causes practical problems. [82] Another method, presented by Shinokubo *et al.* [83], takes advantage of Suzuki reaction in the coupling of the desired thienylboronic acid **38** and 1,2-dichloro-hexafluorocyclopentene, to yield the corresponding diarylethene product **39** (**Fig. 24**). During optimization of the reaction conditions,

they found the best choices for catalyst, ligand, and base to be tris(dibenzylideneacetone)dipalladium(0), tricyclohexylphosphine, and cesium fluoride, respectively. This route enables the direct synthesis of carbonyl- and cyanosubstituted dithienylethenes inaccessible when using organolithium reagents. However, halogenated dithienylethenes cannot be synthesized using Pd-mediated catalysis due to unwanted homocoupling reactions.

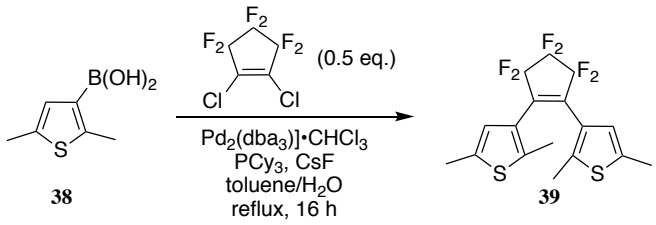

Figure 24. *Synthesis of a perfluorinated dithienylcyclopentene via Suzuki coupling.*

The third synthetic route utilizes an intramolecular McMurry reaction, a reductive coupling of two carbonyl compounds catalyzed by titanium chloride [84]. The synthesis of per- and non-fluorinated dithienylcyclopentenes by the routes depicted in **Fig. 25** was first introduced by Feringa *et al.* [35] and has been commonly used since [85]. There are two variations for the production of the diketone intermediate, first one utilizing Friedel-Crafts acylation of **40** and the second one nucleophilic acyl substitution of a corresponding diester with **35**. The diketone **41** or **43** is then reduced with zinc or some other reducing agent in the presence of titanium (III) chloride, typically in THF, to yield the product (**42** or **37**, respectively).

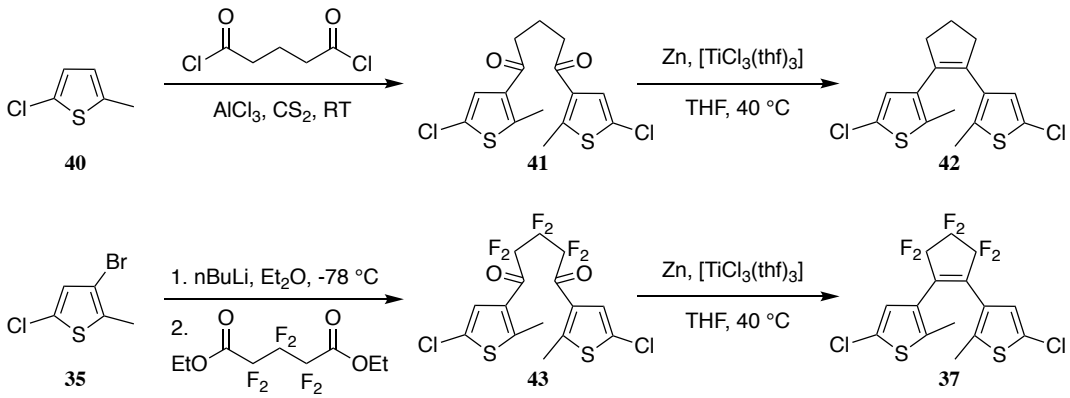

Figure 25. *Synthesis of per- and nonfluorinated dithienylcyclopentenes using an intramolecular McMurry reaction.*

Nonsymmetrical products may be synthesized with any of the methods presented above [82], but the organolithium pathway is most commonly applied (**Fig. 26**). In the first step, thienyl halide **A**X is lithiated and then treated with the cyclopentene fluoride, typically in excess (1–3 eq.). Another thienyl halide **B**X is then lithiated and let to react with the **A**-monosubstituted cyclopentene fluoride to yield the **A**,**B**-disubstituted product. Total yields for the two-step route typically lie in the range of 60–70 % [86, 87].

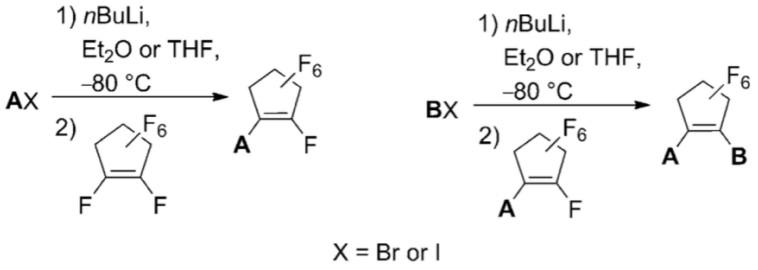

Figure 26. *General synthesis of nonsymmetrical dithienylcyclopentenes.* ***A*** *and* ***B*** *are thienyl bromides or iodides* [82].

4.3 Indigos

The synthesis of unsubstituted indigo was first achieved by Adolf Baeyer in the late 19th century [88]. However, it was Heumann, in 1890, and Pfleger, in 1901, who first developed practical methods for mass production of indigo starting from available aniline derivatives (**Fig. 27**), Pfleger's method being commercially viable and still used in industry with some modifications [89]. Both methods use alkaline melts in high temperatures, for which reason less toxic and more environmentally-friendly approaches have been tried with, for example, the enzymatic oxidation of indole [90].

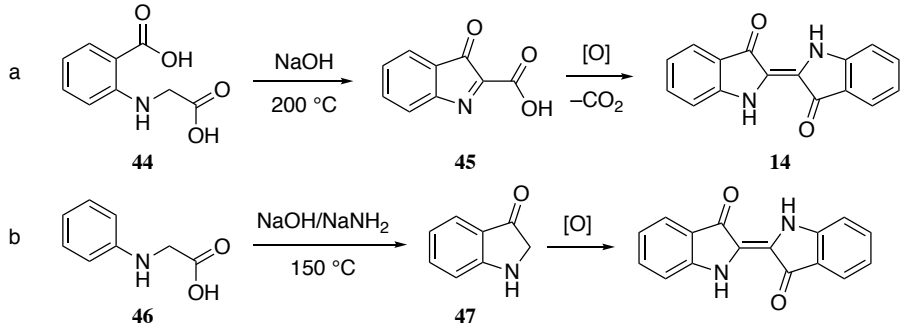

Figure 27. *a) Heumann's and b) Pfleger's method for the synthesis of indigo.*

In the synthesis of indigo photoswitches the parent indigo molecule is typically purchased from commercial sources. The fundamentals of indigo derivatization via *N*-alkylation, acylation and arylation have been introduced by Huang *et al.* [21] and are presented in **Fig. 28**. *N*-alkylation and acylation (latter not shown below) of secondary amines such as indigo are easily achieved via nucleophilic substitution reactions (S_N2 and S_N2Ac, respectively) of alkyl and acyl halides (method A). The reaction proceeds in room temperature with a mild base, cesium carbonate.

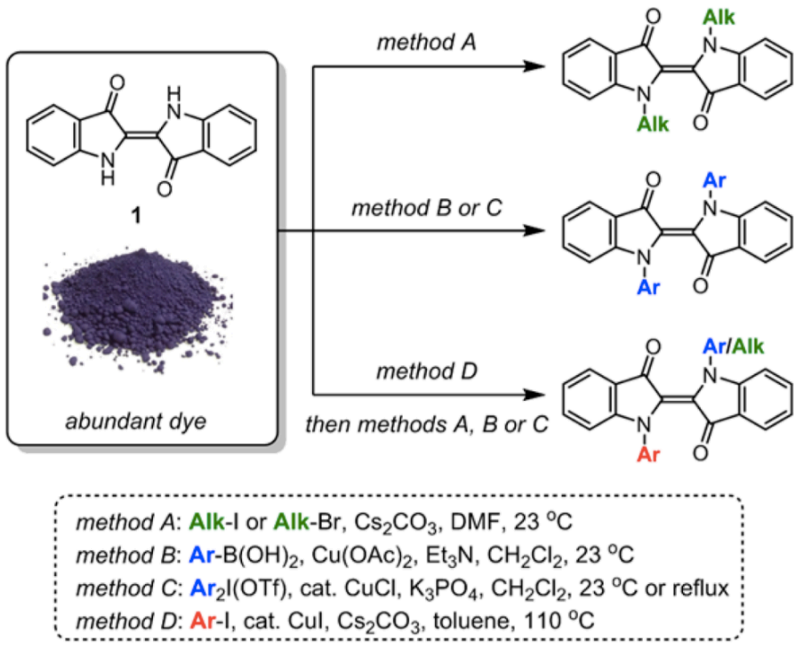

Figure 28. *Derivatization of indigo using four alkylation and arylation methods.* [21]

Two methods have been introduced for symmetric double arylation. Method B, Chan-Lam coupling [91], is applicable to electron-rich arenes. The reaction includes ligand exchange of one of the acetates in the copper catalyst with the indigo molecule, transmetalation with the arylboronic acid, reductive elimination of the product with a new nitrogen-carbon bond formed, and oxidation of copper. Triethylamine is used as a base for proton transfer during ligand exchange, and atmospheric air oxidizes the copper catalyst [92].

Chan-Lam coupling does not proceed with electron-deficient aryls such as nitrobenzene. For the synthesis of such indigo derivatives, copper-catalyzed coupling (method C) using diaryliodonium triflates [93] and potassium phosphate as a base has been utilized. Chan-Lam and diaryliodonium-mediated coupling are conducted in room temperature and mild conditions [21]. Both methods also avoid the use of expensive palladium catalysis that is applied in other aryl–amine couplings such as Buchwald-Hartwig amination [94].

Methods B and C provide the desired disubstituted products in good yields, with negligible amounts of monosubstituted byproducts. In the synthesis of unsymmetrical indigos, however, controlled monosubstitution is needed. The fourth method (D) takes advantage of Goldberg-Ullmann reaction [95] which requires harsher conditions in terms of temperature (110 °C) compared to the others. Monosubstituted products are acquired, after which the synthesis is completed by alkylating or arylating the remaining secondary amine moiety with one of the other three methods [21]. In an older study, diarylation of indigo was also accomplished with Goldberg-Ullmann coupling, although notable amounts of monosubstituted products were also retrieved [42].

4.4 Donor-acceptor Stenhouse adducts

Because DASAs were designed before first synthesized and were not found by accident, their synthesis has a unique modularity and easiness compared to other photoswitches [22]. In the standard method the switch is built of three modules: donor (the amine), acceptor (Meldrum's or barbituric acid), and furfural that will form the skeleton of the molecule. A synthetic route to DASAs is exemplified by the scheme in **Fig. 29**. In the first step, *N*,*N*-dimethylated barbituric acid undergoes a Knoevenagel condensation [96] with furfural **48** to yield **49**. Diethylamine then attacks the furfural ring, which, after several rearrangements similar to Piancatelli rearrangement [45], produces the target molecule **50** [22].

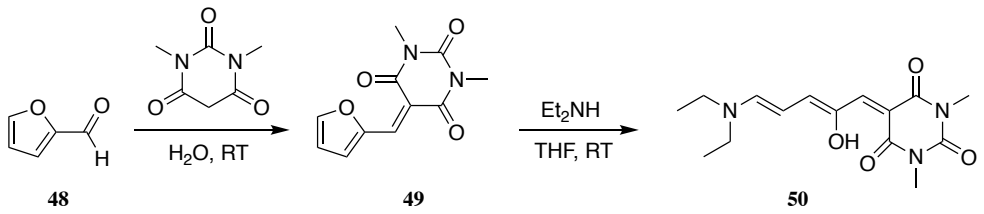

Figure 29. *Formation of a DASA product from furfural, N,N-dimethylbarbituric acid, and diethylamine.*

It is worth mentioning that (i) the synthesis proceeds with excellent yields (>85 % overall) without catalysts, and (ii) extremely mild conditions and easily available reagents are used throughout the synthesis. However, the 2nd generation DASAs [47] are not as trivial to make, since the amines used in the second step are aromatic and thus less nucleophilic than aliphatic amines used in the 1st generation switches. Also, purification on Silica may result in a loss in yield due to degradation in acidic conditions. [28]

5. RESULTS AND DISCUSSION

In the experimental part of this thesis, four types of photoswitches were synthesized for materials applications, mainly photomechanics. The aim was to produce two thermally stable switches (an azobenzene and a diarylethene) for the purpose of exploiting photochemical effect in multifunctional photoactuators [97]; an indigo crosslinker for inducing significant changes in the mechanical properties of an LCE material due to big conformational changes upon isomerization; and a DASA dopant for efficient order-disorder transitions in LC materials. In addition, the photochemical behavior of each photoswitch was characterized. The design and synthesis are presented in Chapter 5.1 and the photochemical properties in Chapter 5.2.

5.1 Molecular design and synthesis

5.1.1 *ortho*-Tetrafluorinated azobenzene crosslinker

The synthesis of an azobenzene crosslinker with four *ortho*-fluorines has been presented twice in literature, with different approaches to the attachment of the azobenzene unit to the acrylate or methacrylate chains (**Fig. 30**) by Iamsaard *et al.* [98] and Kumar *et al.* [65]. In **51**, the chains are attached via phenolic ether bonds, whereas in **52**, a benzoic ester linkage is used. Thus, the aliphatic chains function as electron donors and acceptors in **51** and **52**, respectively. According to Bleger *et al*., the separation of n–π* bands of *cis*- and *trans*-isomers is stronger for **52** due to its ester moiety, leading to better photoconversion [25, 30]. Thus, **52** can be converted to both directions with visible light, which is a particularly attractive feature in an azobenzene switch. Furthermore, the *E*–*Z* isomerization has a considerably larger quantum yield at the n–π* band, which increases the amount of photochemical effect compared to thermal. For these reasons, an ester linkage was chosen.

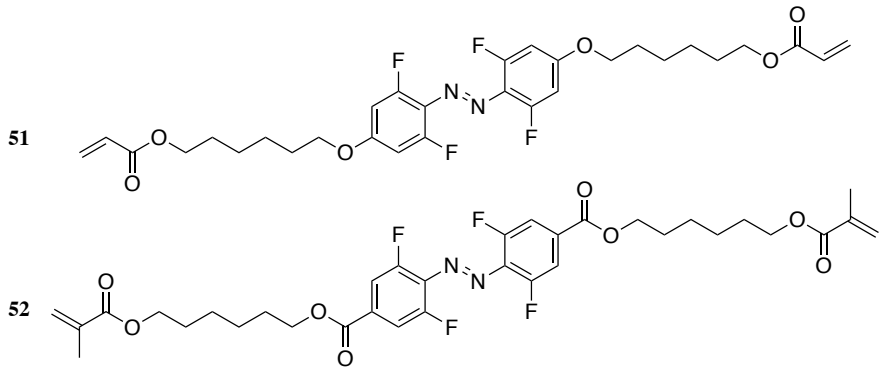

Figure 30. *The structures of two azobenzene diacrylates with four ortho-fluorines.*

In this thesis, the synthetic route by Kumar *et al.* was repeated to produce the azobenzene crosslinker **56**, modified from **52** by using acrylation instead of methacrylation in the last step (**Fig. 31**). The synthesis was started from the commercially available intermediate **53** to avoid unnecessary synthetic steps.

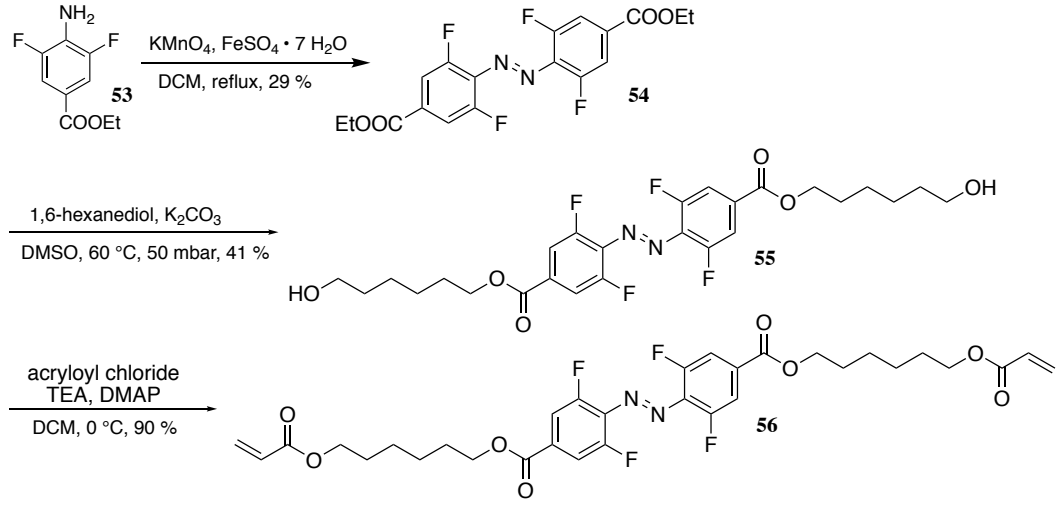

Figure 31. *Synthesis of a tetrafluorinated azobenzene crosslinker.*

In the first step, the aniline **53** was oxidized into the symmetrical azobenzene **54** with potassium permanganate and ferrous sulfate. Base-catalyzed transesterification with 1,6-hexanediol took place under reduced pressure, taking advantage of the evaporation of the forming ethanol, and finally the acquired diol **55** was acrylated with acryloyl chloride to yield the crosslinker **56**.

5.1.2 Diarylethene crosslinker

Three factors affected the design of a diarylethene crosslinker: absorption region of the closed form, LC compatibility of the molecular structure, and synthetic viability. These criteria were met in the molecule **57** whose structure and retrosynthetic approach are shown in **Fig. 32**. The chlorinated diarylethene core **58** can be accessed easily from commercial starting materials (see **Fig. 25** in Chapter 4.2) and is readily functionalized with palladium-catalyzed coupling reactions between **59** and itself. The arylation of **58** extends the π-system, thus red-shifting the absorption spectrum of the closed isomer. At the same time, the enhanced rigidity helps to improve the compatibility with LC monomers, as similar structures have successfully been utilized by Mamiya *et al*. [67]. Furthermore, *meta*-substitution was chosen to restrict the absorption band of the closed isomer from reaching above 600 nm in order to avoid overlapping with the absorption band of the dye Disperse Red 1 in the context of orthogonal use of photochemical and photothermal effects in actuators continuing the research outlined in [97].

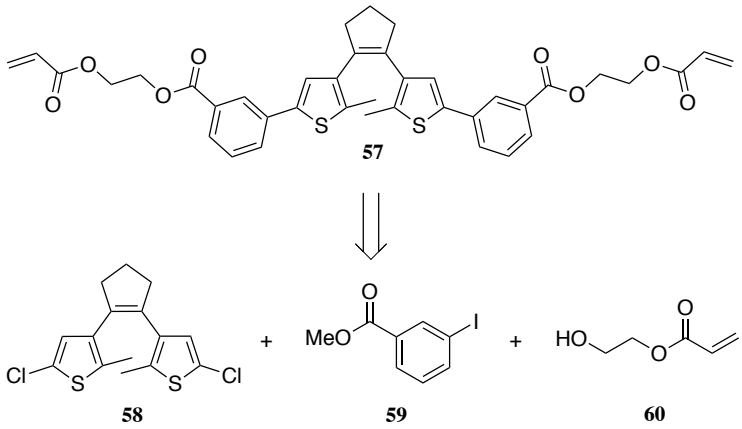

Figure 32. *The molecular structure and retrosynthesis of a diarylethene crosslinker.*

The crosslinker was built from the precursor **58** [99] by first adding aryl spacers and then acrylate moieties. The first approach included the formation of a boronic ester **61** from the commercially available **59** by Miayura borylation and then the Suzuki-Miayura coupling between **58** and **61** to produce **62** (**Fig. 33**). This reaction, however, did not proceed with four different catalyst–solvent combinations, presumably due to the poor reactivity of the thiophene chloride in the oxidative addition step of the coupling.

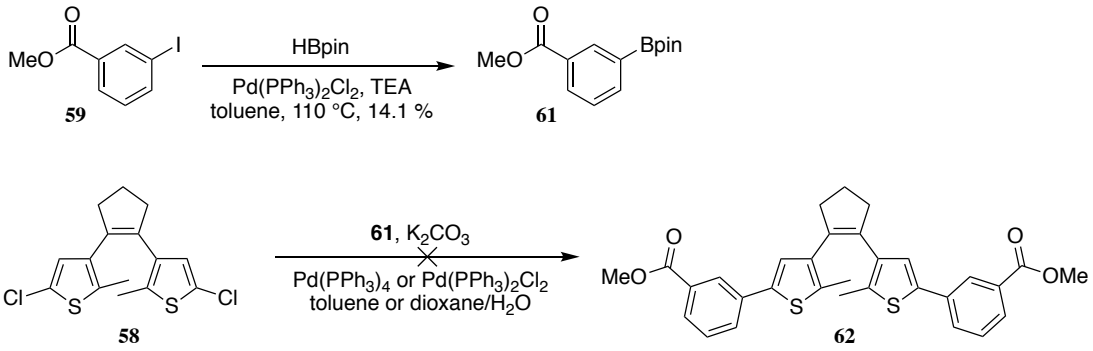

Figure 33. *Borylation and attempted Suzuki-Miayura coupling.*

Thus, an alternative route was adopted to obtain the desired product. By forming a boronate of **58** with sequential additions of *sec*-butyllithium and triisopropyl boronate before reacting it with **59**, the reaction produced the bis-substituted diarylethene **62** in a 49 % yield (**Fig. 34**). It should be noted that by using *n*-butyllithium, even in a four-fold molar excess, the reaction yielded mainly the monosubstituted product **63**.

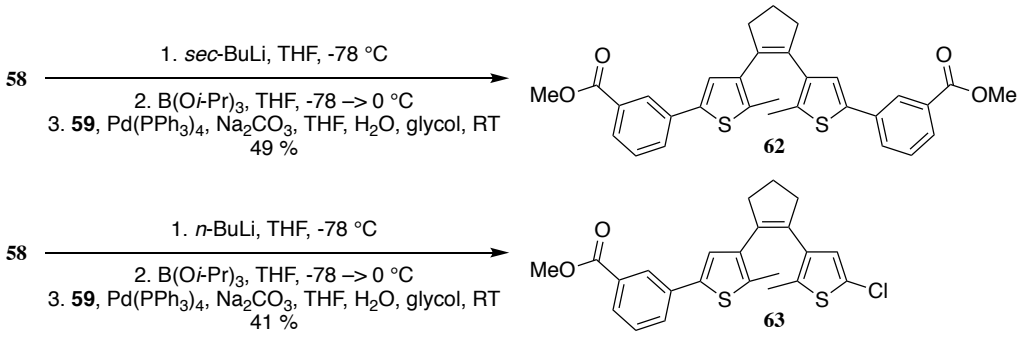

Figure 34. *Suzuki-Miayura reactions to form the bis- and monosubstituted DAEs.*

The bis-substituted compound **62** was then hydrolyzed to produce the diacid **64** which was further esterified by converting it *in situ* into the corresponding acyl chloride with oxalyl chloride and catalytic *N*,*N*-dimethylformamide, and then reacting with **60** in a nucleophilic acyl substitution reaction, producing the desired crosslinker **57** in good yield (**Fig. 35**).

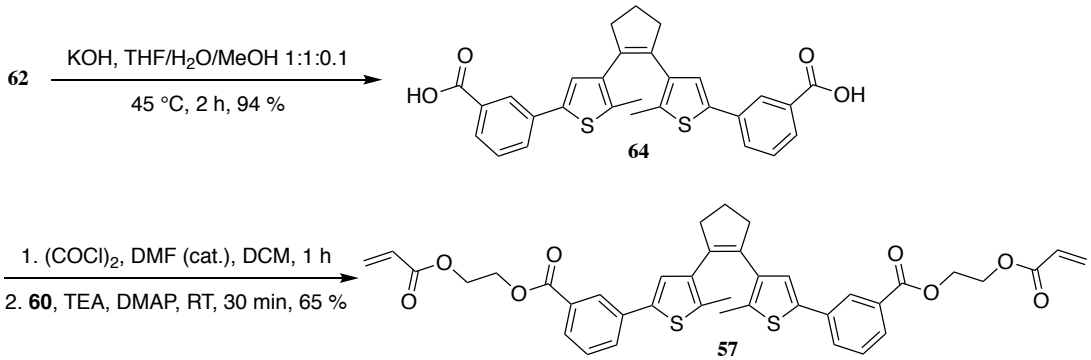

Figure 35. *The transesterification of the bis-substituted DAE to produce the crosslinker.*

5.1.3 Indigo crosslinker and side-chain

Indigo crosslinkers have not been published thus far. However, the synthetic routes established by Huang *et al.* [21] are applicable to the *N*-functionalization of indigo required in the synthesis of indigo crosslinkers and side-chains. In this thesis, a symmetrical crosslinker and an unsymmetrical side-chain were designed, aiming for a crosslinker with a relatively long *Z*-lifetime as well as a side-chain with a short *Z*-lifetime. The compounds **65** and **66** (**Fig. 36**) meet these criteria, as compounds of similar design were reported to have *Z*-lifetimes of 2.9 min and < 5 s [21].

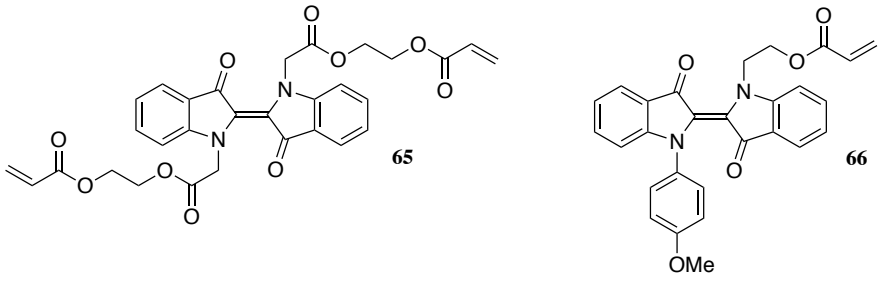

Figure 36. *Molecular structures of an indigo crosslinker and a side-chain.*

The initial route for the synthesis of the crosslinker is described in **Fig. 37**. In the first step, the nucleophilic acyl substitution reaction between hydroxyethyl acrylate **60** and 2-bromoacetyl bromide produced the *N*-substituent **67** in quantitative yield. The treatment of indigo with **67** did not yield the target molecule, perhaps due to unwanted reactivity or supramolecular interactions between the indigo nitrogens and **60**.

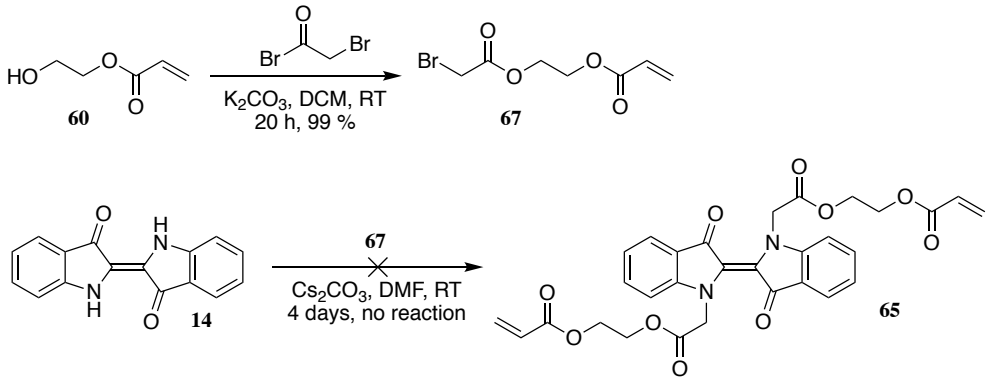

Figure 37. *Original synthetic route to an indigo crosslinker.*

In another approach, 3-bromopropanol **68** was reacted with bromoacetyl bromide to yield **69** which was further reacted with indigo to produce **70** in extremely low yield. Finally, the acrylation with methacrylic acid produced the crosslinker **71**, differing from the original target molecule **65** by one extra methylene carbon (**Fig. 38**). The indigo alkylation step should be studied more thoroughly to acquire the crosslinker in better overall yield.

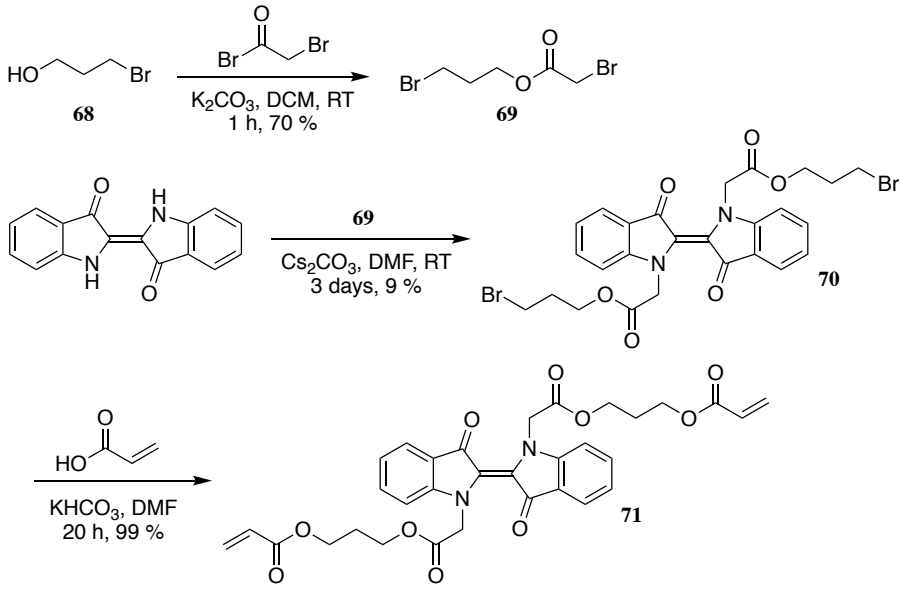

Figure 38. *Synthesis of an indigo crosslinker **71**.*

The structure of the indigo side-chain is unsymmetrical, so *N*-substitution was carried out in two parts (**Fig. 39**). First, indigo was monoarylated with copper-catalyzed Goldberg-Ullman coupling. The alkylation of the remaining nucleophilic nitrogen in **72** was attempted first with 1,2-diiodoethane, and then with 1,6-dibromohexane, to produce **73** and **74**, respectively. However, the first reaction suffered from poor yield, and no product could be isolated from either route. Finally, nucleophilic substitution of the bromide by acrylate was designed to have yielded the target molecule **75** (dashed arrow), but the synthesis was not accomplished.

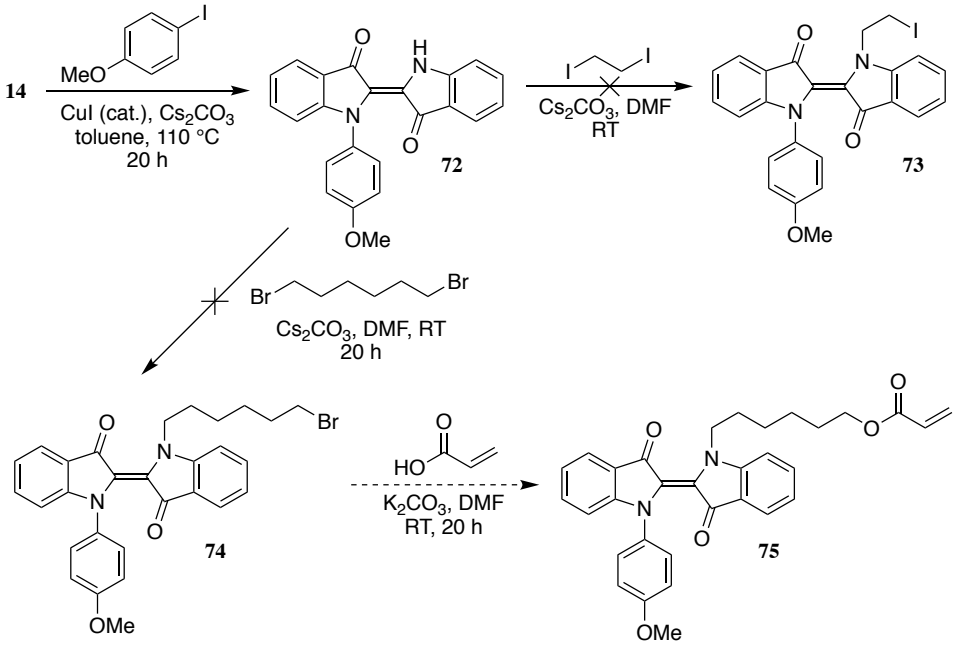

Figure 39. *Synthesis of an indigo side-chain.*

The bottleneck of the synthesis was the Goldberg-Ullman coupling which afforded the product in very low yields. It is possible that more detailed study of the step and optimization of the conditions would significantly increase the yield, making the next steps feasible. However, as noted in the literature [21], the *N*-substitution of indigo is notoriously difficult due to the poor nucleophilicity of the nitrogen atoms and the low solubility in organic solvents of the parent indigo.

5.1.4 Donor-acceptor Stenhouse adduct dopant

DASA switches have not been utilized in LC materials thus far. The 2nd generation general structure was tailored with a terminal alkyl chain to have optimal LC compatibility. Indolines are generally the best donor molecules for the synthesis of DASAs in terms of absorption range and product yields [47], but as no indolines were commercially available with alkyl tails, an alkylated aniline was chosen as the precursor instead.

The synthesis of the DASA photoswitch consisted of three reactions (**Fig. 40**). First of these was the reductive amination between 4-hexylaniline **76** and butyraldehyde to produce the monoalkylated aniline **77**; different conditions were screened, and zinc-chloride-catalyzed reaction in methanol gave the best yield. Knoevenagel condensation between furfural and *N*,*N*'-dimethyl barbituric acid yielded **49**. In final step, the addition reaction between **49** and **77** produced the desired DASA dopant **78** in extremely poor yield.

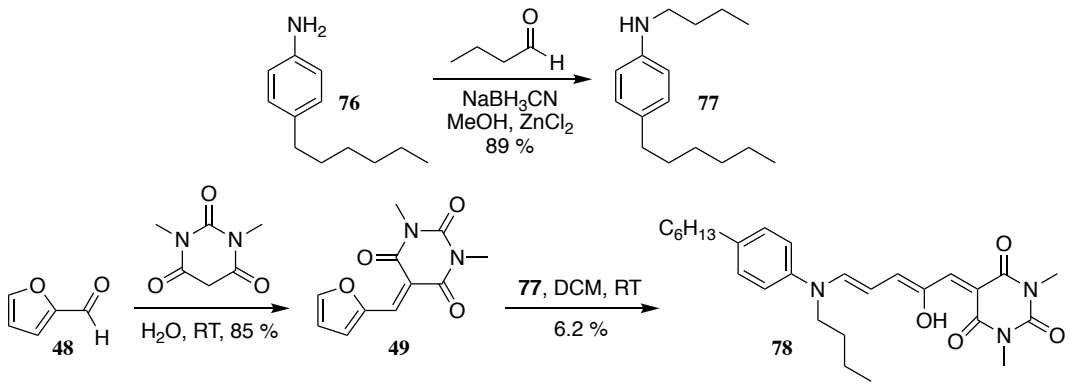

Figure 40. *The synthesis of a DASA dopant.*

The purification of the DASA switch proved to be difficult for three main reasons: i) the yield was very low, resulting in a large excess of starting materials; ii) attempts to isolate the product by means of solubility failed to dispose of **77** even though **49** could be filtered off; iii) the product was unstable on Silica; and iv) the product isomerized readily even in a completely dark environment. These problems were encountered by earlier DASA researchers, e.g., Hemmer *et al.* [47] but no universal solutions have been proposed so far. The reaction and purification conditions need to be further optimized to acquire the switch in reasonable amounts for further studies.

5.2 Photochemical properties

In this section, the photochemical theories and equations relevant for the determination of the key characteristics of photoswitches are discussed; these include molar extinction coefficients, isomerization efficiency and quantum yields, and thermal lifetime of the more energetic form. These equations are then utilized in characterizing the synthesized switches. The results are presented in this section, whereas the calculations are shown in Chapter 7. In graphs and tables, the azobenzene crosslinker is referred to as **Azo-F4** and the diarylethene crosslinker as **DAE**.

5.2.1 Molar extinction coefficients and isomerization efficiency

The transmittance T of light with certain wavelength λ inside an absorbing medium is defined as the ratio of the light intensities after and before the medium:

$$T(\lambda) = \frac{I_{out}(\lambda)}{I_{in}(\lambda)} \tag{2}$$

Transmittance can be measured with a spectrometer. Absorbance is calculated from transmittance as the negative of its decadic logarithm,

$$A(\lambda) = -\lg(T(\lambda)) = \lg\left(\frac{I_{in}(\lambda)}{I_{out}(\lambda)}\right), \tag{3}$$

and according to the Beer-Lambert law [100], it is proportional to the concentration of the absorbing species, c, and to the length of the light path in the medium, l:

$$A(\lambda) = \varepsilon(\lambda)\, c\, l \tag{4}$$

Here, $\varepsilon(\lambda)$ is the molar extinction coefficient at a given wavelength. Typically, c is expressed in mol dm^{-3} and l in cm, thus yielding $\varepsilon(\lambda)$ in $dm^3\ mol^{-1}\ cm^{-1}$ or $M^{-1}\ cm^{-1}$. The molar extinction coefficient values of practical organic dyes range from 10^4 to more than 10^5 $M^{-1}\ cm^{-1}$. For instance, the molar absorptivity of unsubstituted azobenzene is 2.387×10^4 $M^{-1}\ cm^{-1}$ at 319 nm [101].

The absorption spectra of the studied molecules are presented in **Fig. 41**. The compounds were studied in ca. 50 μM acetonitrile solutions at 25 °C unless stated otherwise.

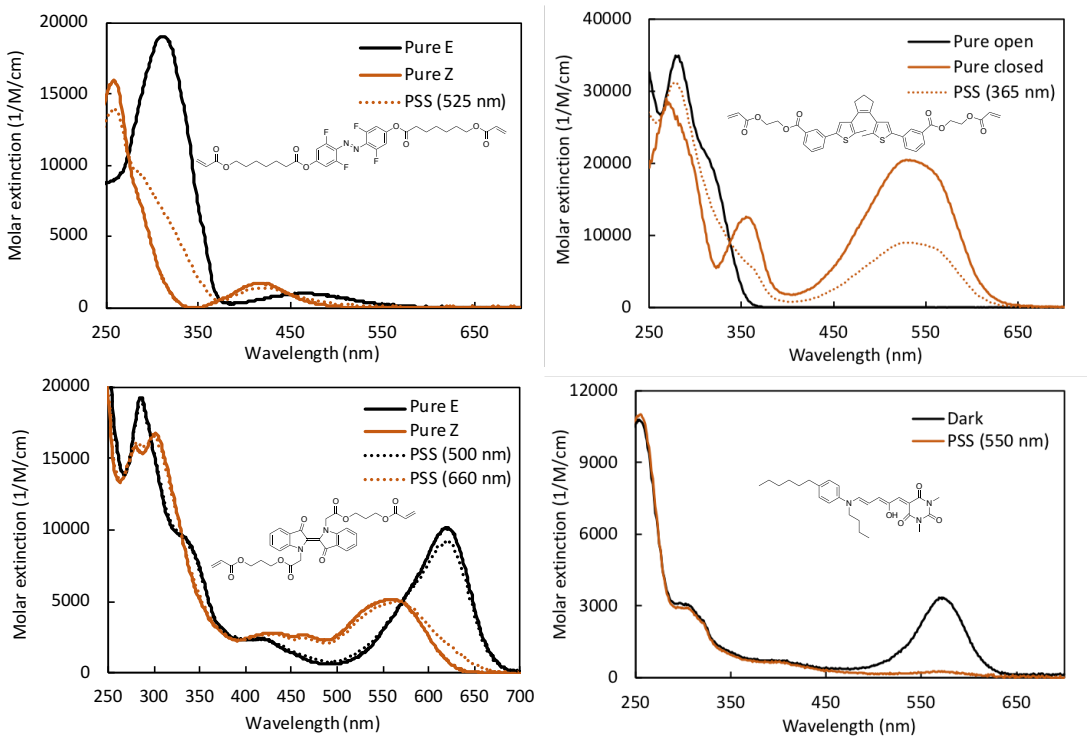

Figure 41. *Absorption spectra of azobenzene* ***56*** *(top left), DAE* ***57*** *(top right), indigo* ***71*** *(bottom left) and DASA* ***78*** *(bottom right) in 50 µM acetonitrile solutions.*

The molar extinction coefficients for the synthesized switches were calculated using Eq. (4). The extinction coefficients of absorption maxima are shown in **Table 1** along with the respective wavelengths. The absorption bands and molar absorptivities of the azobenzene crosslinker **56** were identical to those reported in literature for an F4-diester (later referred to as reference molecule) [25]. Similarly, the DAE switch **57** showed results similar to comparable diarylethenes: e.g., a simple phenyl-substituted version of **58** had an open-form absorption maximum of 34 500 M^{-1} cm^{-1} [102]. The indigo crosslinker **71** had absorption maxima at similar wavelengths as the reference compound (–CH_2COO*t*-Bu-substituted molecule in [21]) with differences of just a few nanometers. However, molar absorptivity was reported to be significantly higher (15 700 M^{-1} cm^{-1}) than acquired here.

No extinction coefficient was reported for the DASA molecule **78** due to degradation and isomerization in solution, rendering the absorbance values meaningless. In solution form, it was estimated that the DASA dopant had the greatest molar absorptivity of all studied molecules, so the visible range maximum shown in **Fig. 41** is undoubtedly too low by at least a factor of 10; moreover, in earlier studies, similar DASAs have been reported to have molar extinction coefficients reaching 10^6. The thermal isomerization into the colorless form has been reported earlier and can sometimes lead to an equilibrium strongly favoring the cyclic form [28, 47]. However, it was surprising to note that the phenomenon was so strong in acetonitrile, as earlier studies have found that it is a good solvent for avoiding the thermal equilibration. To further test the phenomenon, another sample was prepared in a non-polar solvent, *n*-hexane, for which the equilibrium was found to lie completely on the cyclic side (no visible color). When the solvent was evaporated, the

violet–blue color reappeared, stating that the cyclization is reversed upon increased concentration.

Table 1. *Molar extinction coefficients and the respective absorption maxima of the four studied molecules in 50 µM acetonitrile solutions.*

	$\boldsymbol{\varepsilon}$ **(M^{-1} cm^{-1})**	$\boldsymbol{\lambda_{max}}$ **(nm)**
Azo-F4 (*E*, π–π*)	19 000	310
Azo-F4 (*Z*, π–π*)	15 900	258
Azo-F4 (*E*, n–π*)	1 000	470
Azo-F4 (*Z*, n–π*)	1 700	418
DAE (open)	34 900	282
DAE (closed)	20 500	528
Indigo (*E*)	10 100	620
Indigo (*Z*)	5 200	565
DASA (triene)	-	573

Photoisomerization efficiency upon irradiation at certain wavelength can easily be calculated from the spectra if the pure spectrum of either isomer is available and if the spectral separation between the two forms is good enough. In the case of bistable switches, it is possible to take advantage of NMR spectroscopy to calculate the PSS compositions. The compositions upon irradiation with a given wavelength are shown in **Table 2**.

The azobenzene crosslinker showed very good conversion (97 %) to *E*-isomer upon irradiation with 405 nm, but the reverse isomerization could only be driven to 69 % *Z*-isomer with 525 nm although an earlier study of the reference compound reported a 90 % conversion [25]; this can perhaps be attributed to the broad irradiation spectra. For the DAE **57**, irradiation with shorter wavelength would have been needed to acquire a PSS with more closed form [102]; however, the c–o isomerization could be driven to completion, similarly as the DASA **78** could be driven completely to the cyclic form. For the indigo **71**, the PSS compositions are better than reported for the reference compound, although in the earlier study, the chosen irradiation wavelength was not as optimal for good conversion [21].

Table 2. *Isomer compositions at the photostationary state (PSS) upon irradiation with certain wavelength, measured in 50 µM acetonitrile solutions at 25 °C.*

	Azo-F4	**DAE**	**Indigo**	**DASA**
PSS (% *E* or % *o*)	31, 97	44, 100	13, 89	0
$\boldsymbol{\lambda_{irr}}$ **(nm)**	525, 405	365, 550	660, 500	550

5.2.2 Isomerization quantum yields

Combination of Eq. (3) and (4) yields the intensity after the absorbing medium as a function of the concentration of the absorbing species:

$$I_{out}(\lambda) = I_{in}(\lambda)\, 10^{-\varepsilon(\lambda)\, c\, l} \tag{5}$$

In this work, the photochemical behavior of photoswitches stems from the isomerization reaction $A \rightleftharpoons B$ that is either *E–Z* isomerization (azobenzene and indigo) or cyclization (DAE and DASA). Although the isomerization events differ to some extent and different analysis methods are therefore used for each switch, the fundamental equations remain the same for all. For the reaction $A \rightarrow B$, the quantum yield ϕ_{AB} is defined as a dimensionless value with the formula

$$\phi_{AB} = \frac{\frac{da(t)}{dt}}{I_{abs,A}} \tag{6}$$

in which *a(t)* is the concentration of *A* as a function of time and $I_{abs,A}$ is the amount of light intensity absorbed by *A* with respect to time and solution volume (mol dm^{-3} s^{-1}). If only one absorbing species is present at the wavelength in question, $I_{abs,A}$ is the difference between I_{in} and I_{out}, and from equation (5) we get

$$I_{abs,A} = I_{in}\left(1 - 10^{-\varepsilon(\lambda)\, c\, l}\right). \tag{7}$$

The equation (7) only holds when only one of the isomers absorbs at the given wavelength. When *A* and *B* are both absorbing at the irradiation wavelength, the amount of light absorbed by *A* with regard to the total absorbance A_{tot} must be taken into account:

$$I_{abs,A} = I_{in}\,(1 - 10^{-A_{tot}})\,\frac{\varepsilon_A(\lambda)\, a(t)\, l}{A_{tot}} \tag{8}$$

Combining equations (7) and (8), a relationship between the absorbance and quantum yield is acquired:

$$\frac{da(t)}{dt} = -I_{in}\,(1 - 10^{-A_{tot}})\,\frac{\varepsilon_A(\lambda) a(t) l}{A_{tot}}\,\phi_{AB} \tag{9}$$

Furthermore, the equation can be simplified by defining a photochemical factor

$$F(t) = \frac{1-10^{-A_{tot}}}{A_{tot}}, \tag{10}$$

Thus, Eq. (9) is reduced to

$$\frac{da(t)}{dt} = -I_{in}\, F(t)\, \varepsilon_A(\lambda)\, a(t)\, l\, \phi_{AB}\,. \tag{11}$$

Taking into account the reverse reaction $B \rightarrow A$, Eq. (11) is further derived to the form

$$\frac{da(t)}{dt} = I_{in}\, F(t)\, l\, \left(-\varepsilon_A(\lambda)\, \phi_{AB}\, a(t) + \varepsilon_B(\lambda)\, \phi_{BA}\, b(t)\right) \tag{12}$$

in which $\varepsilon_B(\lambda)$, $b(t)$ and ϕ_{BA} are the molar extinction coefficient and concentration of *B* and the quantum yield of the reaction $B \rightarrow A$, respectively. Similarly, for *B*, Eq. (12) takes the form

$$\frac{db(t)}{dt} = I_{in}\, F(t)\, l\, \left(\varepsilon_A(\lambda)\, \phi_{AB}\, a(t) - \varepsilon_B(\lambda)\, \phi_{BA}\, b(t)\right). \tag{13}$$

Equations (12) and (13) carry two major assumptions: (i) thermal relaxation is negligible in the timeframe of the photoisomerization, and (ii) no side-reactions occur. The equations cannot be integrated since the photokinetic factor is time-dependent, unless the absorption bands of *A* and *B* are completely separated or some approximative methods are utilized. This is possible in the case of the DAE crosslinker by using an approximative initial slope method for the cyclization reaction; for the reverse reaction, ring-opening, Eq. (12) can be integrated because the cyclized form has an absorption peak that does not overlap with the absorption spectrum open form.

In order to use Eq. (13) and its derivatives, the irradiation intensity I_{in} inside the cuvette must be determined. This is typically accomplished with actinometry, an experiment in which a photochemical reaction with known reaction quantum yield is monitored to calculate the irradiation intensity from the kinetic rate law. However, in this work, six different wavelengths were used for isomerization reactions, so the utilization of actinometry would have required several actinometers. Instead, the light intensity was measured with a power meter, keeping in mind its limitations in terms of accuracy.

Initial slope method

If only the beginning of the isomerization is considered, it can be approximated that the consumption of *A* is small and, consequently, the concentration of *B* is negligible, leading to the approximation that the absorbance at the irradiation wavelength stays the same (A_0):

$$A_{tot} \approx A_0 \tag{14}$$

$$\varepsilon_B(\lambda)\, \phi_{BA}\, b(t) \approx 0 \tag{15}$$

This leads to the approximation

$$\varepsilon_A(\lambda)\, a(t)\, l = A_{tot}, \tag{16}$$

and Eq. (13) is thus reduced to

$$\frac{da(t)}{dt} = -\, I_{in}\, \phi_{AB}\, (1 - 10^{-A_0}) \tag{17}$$

in which A_0 is the initial absorption at the irradiation wavelength.

The monitoring wavelength is best chosen to be the absorption peak of B (A_{obs}) which is well separated from the absorption region of A. Combining Eq. (4) and (17), we acquire

$$\frac{dA_{obs}(t)}{dt} = I_{in}\,\phi_{AB}\,(1-10^{-A_0})\,\varepsilon_{B,obs}\,l\,. \tag{18}$$

This can now be integrated to yield the final equation:

$$A_{obs}(t) = A_{obs,0} + I_{in}\,\phi_{AB}\,(1-10^{-A_0})\,\varepsilon_{B,obs}\,l\,t \tag{19}$$

The case of only one absorbing species

If only one of the isomers (here, B) absorbs in the irradiation region, Eq. (13) is simplified and can actually be integrated (here for the reaction $B \rightarrow A$):

$$\int_{A_0}^{A(t)} \frac{dA_{tot}}{1-10^{-A_{tot}}} = \int_o^t -I_{in}\,l\,\varepsilon_{B,obs}(\lambda)\,\phi_{BA}\;dt \tag{20}$$

This integral yields

$$\lg\left(10^{A(t)}-1\right) - \lg(10^{A_0}-1) = -I_{in}\,l\,\varepsilon_B(\lambda)\,\phi_{BA}\,t\;. \tag{21}$$

The determined quantum yields

The quantum yields for each isomerization reaction along with the used irradiation wavelengths are presented in **Table 3**. Each quantum yield was determined with one of the abovementioned methods (see Chapter 7 for details).

Table 3. *Isomerization quantum yields upon irradiation in 50 µM acetonitrile solutions.*

	Direction	ϕ	λ_{irr} (nm)
Azo-F4	*E–Z*	0.097	525
	Z–E	0.97	405
DAE	o–c	0.64	365
	c–o	0.0034	550
Indigo	*E–Z*	0.37	660
	Z–E	0.65	500
DASA	o–c	0.0010	550

There are several major sources of error for the quantum yields. Firstly, the irradiation intensity I_{in} was determined with an estimated error of ca. 20 % (see Chapter 7). Secondly, the irradiation was performed with LEDs that, especially in the visible region, have quite broad spectra (FWHM 9–28 nm) but were considered to be monochromatic. This should not be a major problem since the irradiation wavelength was chosen near the absorbance maximum where possible; in addition, the use of a bandpass filter for 405 nm

irradiation was not seen to make any difference to the results. Thirdly, the linear fit itself can be approximated to have an intrinsic error of 10 % [21, 102].

The *E*–*Z* isomerization of the azobenzene crosslinker has a quantum yield close to 0.1, and this is perfectly in line with the reported value of 0.11 for the reference compound [25]. However, the *Z*–*E* isomerization exhibited a quantum yield of nearly 1, and attempts to repeat the experiment with better defined irradiation parameters and lower intensity (slower and thus more easily monitored reaction) afforded the same result. Although the n–π* isomerization typically has quite high quantum yields, the reported values lie between 0.5 and 0.6. The reason for this anomaly is unknown and can only partly be explained by the large margin of error in the experiment.

The DAE showed quantum yield values very typical for similar switches; cyclization QYs typically lie between 0.001 and 0.01, and cycloreversion QYs may even reach close to unity [102]. For a compound otherwise identical to **62** but with esters in *para*-position, the corresponding quantum yields were 0.65 and 0.0021 [103]. Similarly, the DASA switch exhibited a cyclization quantum yield close to what was expected based on literature values [28]. The indigo crosslinker showed significantly higher *E*–*Z* QY as reported for the reference compound even as the *Z*–*E* value was almost identical [21]. It is possible that minor differences in, e.g., irradiation light source may lead to large variation in the calculated quantum yields.

5.3 Thermal stability

The thermal relaxation reaction of the photoswitches, in the absence of catalysts, is unimolecular. Thus, the reaction $B \rightarrow A$ follows a first-order rate law:

$$\frac{db(t)}{dt} = -k\, b(t) = k\, a(t) \tag{22}$$

in which *b(t)* and *a(t)* are the concentrations of *B* and *A*, respectively, and *k* is the rate constant. This can be integrated to yield the integrated rate law:

$$\int_{b_0}^{b(t)} \frac{db(t)}{b(t)} = -\int_0^t k\, dt \Longrightarrow b(t) = b_0\, e^{-kt} \tag{23}$$

If *B* has an absorption band that is absent from *A*, Eq. (23) can be combined with Eq. (4). Hence, the thermal isomerization rate can be monitored by

$$A_B(t) = A_{B,0}\, e^{-kt} = A_{B,0}\, e^{-t/\tau}\,, \tag{24}$$

where *A(t)* is the absorbance at a certain time *t*, A_0 is the absorption at the time $t = 0$, and $\tau = 1/k$ is the thermal lifetime. However, more typically, it is the increase in an absorption band of *A* that is easily monitored. Based on Eq. (24) and the fact that $a_0 + b_0 = a_\infty$ (the concentration of *A* when the reaction is complete), the integrated rate law can be modified to the form

$$a(t) = a_0 + b_0\,(1 - e^{-kt}) = a_\infty - (a_\infty - a_0)\,e^{-kt}. \quad (25)$$

This can further be converted into absorbance values:

$$A(t) = A_\infty - (A_\infty - A_0)\,e^{-kt} = A_\infty - (A_\infty - A_0)\,e^{-t/\tau}. \quad (26)$$

The equation can also be expressed in a logarithmic form for linear fitting as a function of time:

$$\ln\left(\frac{A(t) - A_\infty}{A_0 - A_\infty}\right) = -kt \quad (27)$$

In this work, the only molecule whose thermal relaxation could be calculated using Eq. (24) is the DAE. For all others, the lifetimes are most conveniently determined by using Eq. (26) and, in this work, the logarithmic form (27). The results are collected in **Table 4**. Of the studied molecules, the diarylethene is stable even at 60 °C, showing no thermal isomerization even upon prolonged heating. The azobenzene is also extremely long-lived, 38 hours at 60 °C, corresponding to weeks at 25 °C. The indigo and DASA are notably shorter-lived but still in the range of minutes, making them somewhat bistable switches in second-scale applications.

Table 4. *Thermal lifetimes of the less stable isomers in 50 µM acetonitrile solutions.*

	Azo-F4	**DAE**	**Indigo**	**DASA**
$\boldsymbol{\tau}$	38 h (60 °C)	stable (60 °C)	2.5 min (25 °C)	15.2 min (25 °C)

The azobenzene lifetime can be compared with that of a similar compound (tetrafluorinated azobenzene diester **7**) studied by Knie *et al.* [25]. They reported a thermal half-life of 15 h at 60 °C; the experimental result in this work is roughly double that value. This can be partly explained with the difference between half-life and lifetime, but the rest of the deviation must stem from small differences in experimental setup and solvent purity. It is also possible, although difficult to rationalize, that the substitution of ethyl with longer, terminally acrylated chain truly results in a longer lifetime even though the electronic structure in the azobenzene core should remain the same.

The diarylethene is thermally stable at 60 °C, as expected based on earlier studies performed on similar compounds [16, 102]. For instance, a molecule identical to **62** except lacking the ester functionalities was found to have a stable closed form even at 95 °C (butyronitrile as solvent). The ester moieties might have a destabilizing effect, as the introduction of electron-withdrawing units in *para* positions of the phenyl rings was found to decrease the lifetime; however, the effect was small (thermal half-life of 41 h at 95 °C) [102]. Thus, for any applications in room temperature, the diarylethene crosslinker may be considered to be a truly bistable switch.

The indigo switch had a lifetime almost identical to the reference compound in literature (2.8 min), as expected. The lifetime is short compared to the bistable systems of the azo

and DAE crosslinkers, so there will probably be a significant photothermal component in contrast to the other two crosslinkers. For this reason, another indigo crosslinker with a longer thermal lifetime would enable an interesting comparison of the photothermal and photochemical effects upon irradiation. Finally, the DASA switch showed a lifetime of more than 15 minutes, which is a typical value for 2nd generation DASAs [47]. It should be noted that the lifetimes in solution can differ significantly from those in solid state, which needs to be taken into consideration when incorporating the switches into LC materials.

6. CONCLUSIONS

In this work, carried out in the Smart Photonics Materials group at Tampere University, four new photoswitch molecules for the fabrication of photoresponsive materials were designed and successfully synthesized: a tetrafluorinated azobenzene crosslinker, a diarylethene (DAE) crosslinker, an indigo crosslinker, and a DASA dopant. Similar extremely bistable azobenzene and diarylethene crosslinkers had already been reported, and the aim was to adjust the reported structures to best suit the demand of bistable photoswitches for reconfigurable photoactuators. Indigo crosslinkers had not been reported previously, so the main motivation was to explore the functionality of LCE/LCN materials with such a crosslinker. The DASA dopant was designed to have good solubility to the liquid crystal matrix while maintaining the attractive properties of the 2nd generation DASAs.

The synthetic pathways consisted mainly of previously known elementary reactions. However, good and reproducible synthetic routes could only be found for the azobenzene and diarylethene crosslinkers for which every synthetic step produced either good or moderate yields. For the indigo crosslinker, one synthetic step reduced the total yield significantly, as reported in literature for similar indigo functionalization reactions, and further studies are needed to circumvent this problem. Likewise, the DASA adduct could only be acquired in low yield, and the purification of the product proved to be extremely difficult, again mirroring the contemporary research in the field. Further studies are needed to optimize the yields. Still, the synthetic results presented in this thesis pave the way for more efficient routes to these two photoswitches as well.

The photochemical properties of the switches were studied in dilute acetonitrile solutions. All four molecules were efficient photoswitches with distinct spectral differences between the isomers. Switching efficiencies from the less energetic to the more energetic isomer ranged from 56 (DAE) to 100 % (DASA). The poor efficiency of the DAE cyclization can be attributed to the lack of far-UV light sources, whereas the excellent efficiency of the DASA switch stems from the complete separation of the absorption bands. The reverse light-induced reaction showed efficiencies from 89 (indigo) to 100 % (DAE); for the DASA switch, the reverse reaction could not be driven with light. The efficiencies were all similar to those reported in literature. The DASA dopant showed a general problem of thermal isomerization and decomposition, due to which the molar absorptivity could not be determined accurately. For other switches, the molar extinction coefficients were identical or close to reference molecules.

Photoisomerization kinetics were also studied and quantum yields determined for each reaction. For all crosslinkers, the isomerization to one direction showed a high QY (> 0.5) and the reverse QY was notably lower. The findings were consistent with the trends reported for similar compounds in literature, and most values were extremely close to those

of reference molecules. There were two exceptions: the QYs for the *Z–E* isomerization of the azobenzene and the *E–Z* isomerization of the indigo were significantly higher than the QYs of the reference molecules in literature. The anomalies can be explained with possible errors in the concentrations, the inaccurate determination of the irradiation intensities, or the broad spectra of the LEDs used as irradiation sources.

Finally, thermal lifetimes in solution were determined for the switches. The azobenzene and diarylethene crosslinkers were found to be stable at room temperature and the latter even at elevated temperatures, whereas the lifetimes of the indigo and the DASA lay in a minute scale. The results were similar to expected based on literature values.

In conclusion, all the synthesized molecules are extremely attractive for incorporation into photoswitchable materials, combining effective isomerization, fast isomerization kinetics and excellent or moderate thermal stability. The efforts made in this thesis enable the utilization of new crosslinkers and dopants in photoresponsive liquid crystal elastomers for the fabrication of new functional materials. The next steps in this line of research should be: i) the optimization of the synthetic routes of the indigo crosslinker and DASA dopant; ii) the polymerization of the azobenzene, DAE and indigo crosslinkers into LCE matrices and the study of their isomerization in solid state; iii) the doping of the DASA switch into an LC material and the study of the DASA-induced order–disorder transitions; and iv) the synthesis of other indigo crosslinkers with different thermal half-lives and their incorporation into LCEs for systematic studies of structure–property relationships.

7. EXPERIMENTAL

General information on the experimental methods is given in Chapter 6.1. The synthetic routes are shown in Chapters 6.2–6.5, followed by the photochemical characterization procedures in Chapter 6.6.

7.1 General synthetic methods

Synthetic work was carried out in Tampere University and Humboldt University of Berlin. All reagents and solvents were commercial and purchased from Sigma Aldrich, TCI Europe, VWR or FluoroChem except for **92** which was previously synthesized at Humboldt University of Berlin [99]. When needed, dry solvents were acquired using Inert PureSolv and Innovative Technologies solvent purification systems. Reactions were monitored with either thin-layer chromatography (TLC) or ultra-performance liquid chromatogaphy coupled to mass spectrometry (UPLC-MS). TLC was performed on commercial Merck Silica 60 F_{254} TLC plates, and the developed plates were visualized with UV irradiation (254 nm) or with potassium permanganate and cerium ammonium permanganate stains. UPLC-MS was performed with a Waters Alliance system (a Waters Separations Module 2695, a Waters Diode Array Detector 2996, a Waters LCT Premier XE Mass Spectrometer, and a Waters Mass Detector ZQ 2000) equipped with Acquity UPLC columns and a water–acetone eluent system with gradient from 5 to 95 % acetonitrile. High-resolution mass spectra (HR-MS) were recorded either with the abovementioned system or a Waters ESI-TOF MS spectrometer.

Nuclear magnetic resonance spectra (NMR) were measured with a 500 MHz JEOL ECZR 500 (125 MHz for ^{13}C), a 500 MHz Bruker AVANCE II 500 (125 MHz for ^{13}C), a 300 MHz Bruker DPX 300 (75 MHz for ^{13}C), or a 300 MHz Varian Mercury (75 MHz for ^{13}C) at 25 °C. Chemical shifts are given in ppm and are referenced to solvent signals ($CHCl_3$: δ = 7.26 ppm (^1H), 77.16 ppm (^{13}C), DMSO: δ = 2.50 ppm (^1H), 39.52 ppm (^{13}C), MeOH: δ = 3.31 ppm (^1H), 49.00 ppm (^{13}C). Multiplicities are abbreviated as follows: singlet (s), doublet (d), triplet (t), quartet (q), pentet (p), and multiplet (m). Coupling constants (*J*) are given in Hz.

7.2 *ortho*-Tetrafluorinated azobenzene crosslinker

7.2.1 Diethyl 4,4'-(diazene-1,2-diyl)(*E*)-bis(3,5-difluorobenzoate) (54)

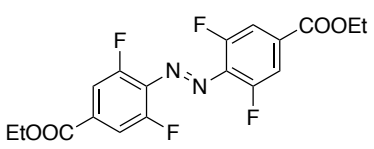

To a 100 ml round-bottom flask, **53** (1.2 g, 6.0 mmol, 1.0 eq.), potassium permanganate (3.0 g, 19.0 mmol, 3.2 eq.) and iron sulfate heptahydrate (3.0 g, 10.8 mmol, 1.8 eq.) were added and refluxed in dichloromethane for two days. The reaction mixture was filtered, concentrated under reduced pressure, and purified by flash column chromatography (Silica 60, dichloromethane / hexane) to produce 350 mg (29 %) of the azobenzene product as a vivid orange powder. ^{1}H NMR (500 MHz, $CDCl_3$, *E*-isomer): δ = 7.76 (d, *J* = 9.4 Hz, 4H), 4.42 (m, 4H), 1.43 (m, 4H). Appendix 1.

7.2.2 Bis(6-hydroxyhexyl) 4,4'-(diazene-1,2-diyl)(E)-bis(3,5-difluorobenzoate) (55)

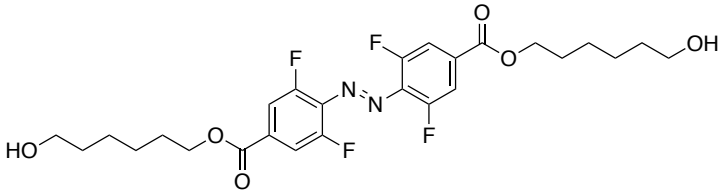

Failed attempt: To a 25 ml round-bottom flask, **54** (335 mg, 0.84 mmol, 1.0 eq.), 1,6-hexanediol (2.0 g, 16.8 mmol, 20 eq.), and potassium carbonate (13 mg, 0.09 mmol, 0.1 eq.) were added, followed by 6.0 ml of dimethylsulfoxide. The reaction mixture was stirred at 60 °C and 50 mbar for 20 hours, then extracted with ethyl acetate and water. It was noticed that hydrolysis of the ester moieties had competed with the transesterification reaction, as most of the product was insoluble in organic solvents and upon extraction moved into the aqueous phase. The product was thrashed.

Failed attempt: To a 25 ml round-bottom flask, **54** (191 mg, 0.48 mmol, 1.0 eq.), 1,6-hexanediol (1.2 g, 10 mmol, 20 eq.), and potassium carbonate (10 mg, 0.06 mmol, 0.1 eq.) were added, followed by 6.0 ml of dry dimethylsulfoxide. The reaction mixture was stirred at 60 °C and 50 mbar for 20 hours, then extracted with ethyl acetate and water. The same problem with hydrolysis was encountered, and the product was thrashed. A mistake in the experimental procedure published in literature [65] was pointed out by the authors; the amount of dry DMSO should actually be 10 % of the reported amount.

Successful attempt: To a 5 ml round-bottom flask, **54** (230 mg (0.58 mmol), 1,6-hexanediol (1.45 g, 12 mmol, 20 eq.), and potassium carbonate (12 mg, 0.09 mmol, 0.1 eq.) of potassium carbonate were added, followed by 0.5 ml of dry dimethylsulfoxide. The reaction mixture was stirred at 50 mbar for 9 hours of which the first 6 hours at 25 °C and the last 3 hours at 60 °C, then extracted with ethyl acetate and water. The organic phase was washed three times with water and once with brine, dried with magnesium sulfate, and concentrated to yield 253 of crude. Purified by flash column chromatography (Silica 60, 0–2 % methanol in ethyl acetate) to yield 44 mg (19 %) of recovered **54** and 128 mg (41 %) of the product **55**. ^{1}H NMR (500 MHz, $CDCl_3$): δ = 7.71 (d, *J* = 9.2 Hz, 4H), 4.34 (t, *J* = 6.9 Hz, 4H), 3.64 (t, *J* = 6.3 Hz, 4H), 1.79 (q, 4H), 1.65–1.30 (m, 12H). Appendix 2.

7.2.3 Bis(6-(acryloyloxy)hexyl) 4,4'-(diazene-1,2-diyl)(E)-bis(3,5-difluorobenzoate) (56)

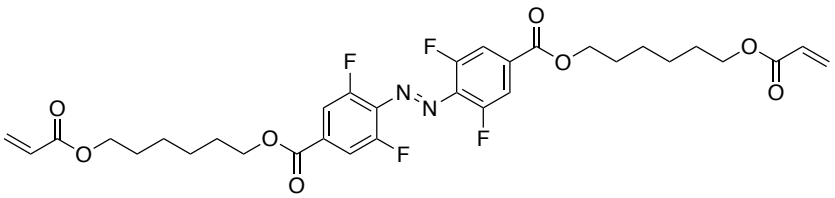

Into a 25 ml round-bottom flask, 130 mg (0.24 mmol) of **57** and 0.6 mg (0.005 mmol) of *N*,*N*-dimethylaminopyridine were added under argon. 15 ml of dry dichloromethane was added, followed by 0.33 ml (2.4 mmol) of dry triethylamine and 0.040 ml (0.48 mmol) of acryloyl chloride. The reaction mixture was stirred in room temperature under argon for 20 hours, extracted with water, washed twice with sodium bicarbonate and once with brine, dried with magnesium sulfate, and concentrated to yield 150 mg (90 %) of pure product **58** that was further purified by flash column chromatography (Silica 60, 0–10 % ethyl acetate in dichloromethane) to yield 100 mg of the product in high purity; the rest was lost due to spontaneous polymerization. ^{1}H NMR (500 MHz, $CDCl_3$): δ = 7.72 (d, *J* = 9.2 Hz, 4H), 6.39 (m, 2H), 6.11 (m, 2H), 5.81 (m, 2H), 4.36 (t, *J* = 6.6 Hz, 4H), 4.16 (t, *J* = 6.6 Hz, 4H), 1.75 (m, 8H), 1.47 (m, 8H). ^{13}C NMR (125 MHz, $CDCl_3$): δ = 166.4, 156.1, 154.2, 136.5, 133.7, 130.8, 128.6, 114.1, 66.2, 64.5, 28.6, 25.8. ^{19}F (470 Hz, $CDCl_3$): δ = 119.3 (d, *J* = 8.8 Hz, 4F). HR-MS (ESI+) m/z = 673.2149 (calcd. 673.2147 for $[C_{32}H_{34}F_4N_2O_8Na]^+$). Appendices 3, 4 and 5.

7.3 Diarylethene crosslinker

7.3.1 Methyl 3-(4,4,5,5-tetramethyl-1,3,2-dioxaborolan-2-yl)-benzoate (61)

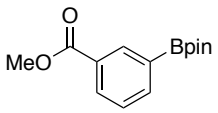

Compound **59** (1.0 g, 3.8 mmol, 1 eq.) and palladium bis(triphenylphosphine) chloride (187 mg, 0.27 mmol, 0.07 eq.) were dissolved in 50 ml of dry 1,4-dioxane. Anhydrous triethylamine (3.2 ml, 22.8 mmol, 6.0 eq.) and pinacolborane (1.7 ml, 11.4 mmol, 3.0 eq.) were added to the solution which was freeze-pump-thaw degassed twice, then heated under argon to 101 °C and stirred for 17 hours. The reaction mixture was then cooled to room temperature, filtered through Silica, diluted with ethyl acetate, washed twice with water, dried with magnesium sulfate and concentrated under reduced pressure. The crude product was purified by medium-pressure liquid chromatography (Silica 60, cyclohexane / ethyl acetate) to yield 141 mg (14.1 %) of **61** as a white solid. 465 mg of homocoupled side-product were also acquired. HR-MS (ESI+) *m/z* = 262.140 (calcd. 262.140 for $[C_{14}H_{20}O_4B]^+$).

7.3.2 Dimethyl 3,3'-(cyclopent-1-ene-1,2-diylbis(5-methylthiophene-4,2-diyl))dibenzoate (62)

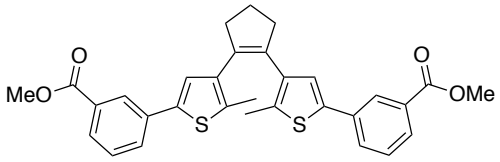

Failed attempt. Compound **61** (10 mg, 0.038 mmol, 2.0 eq.), **58** (6.3 mg, 0.019 mmol, 1.0 eq.), tetrakis(triphenylphosphine)palladium(0) (3.1 mg, 2.7 µmol, 0.07 eq.), and potassium carbonate (10.5 mg, 0.076 mmol, 4.0 eq.) were dissolved in 0.5 ml of toluene in a small vial and bubble-degassed for 5 minutes with argon. The mixture was then heated at 110 °C for 4 hours under argon, diluted with ethyl acetate, washed with water, and analyzed with TLC and UPLC. No product was formed.

Failed attempt. Compound **61** (10 mg, 0.038 mmol, 2.0 eq.), **58** (6.3 mg, 0.019 mmol, 1.0 eq.), bis(triphenylphosphine)palladium(0) chloride (1.9 mg, 2.7 µmol, 0.07 eq.), and potassium carbonate (10.5 mg, 0.076 mmol, 4.0 eq.) were dissolved in 0.5 ml of toluene in a small vial and bubble-degassed for 5 minutes with argon. The mixture was then heated at 110 °C for 4 hours under argon, diluted with ethyl acetate, washed with water, and analyzed with TLC and UPLC. No product was formed.

Failed attempt. Compound **61** (10 mg, 0.038 mmol, 2.0 eq.), **58** (6.3 mg, 0.019 mmol, 1.0 eq.), tetrakis(triphenylphosphine)palladium(0) (3.1 mg, 2.7 µmol, 0.07 eq.), and potassium carbonate (10.5 mg, 0.076 mmol, 4.0 eq.) were dissolved in 0.5 ml of 1:1 H2O/dioxane mixture in a small vial and bubble-degassed for 5 minutes with argon. The mixture was then heated at 110 °C for 4 hours under argon, diluted with ethyl acetate, washed with water, and analyzed with TLC and UPLC. No product was formed.

Failed attempt. Compound **61** (10 mg, 0.038 mmol, 2.0 eq.), **58** (6.3 mg, 0.019 mmol, 1.0 eq.), bis(triphenylphosphine)palladium(II) chloride (1.9 mg, 2.7 µmol, 0.07 eq.), and potassium carbonate (10.5 mg, 0.076 mmol, 4.0 eq.) were dissolved in 0.5 ml of 1:1 H2O/dioxane mixture in a small vial and bubble-degassed for 5 minutes with argon. The mixture was then heated at 110 °C for 4 hours under argon, diluted with ethyl acetate, washed with water, and analyzed with TLC and UPLC. No product was formed.

Successful attempt. 30 ml of anhydrous tetrahydrofuran was freeze-pump-thaw degassed and stored under argon. 15 ml of the degassed tetrahydrofuran was taken to another flask under argon, and **58** (500 mg, 1.5 mmol, 1.0 eq.) was dissolved and the solution cooled down to -78 °C. *sec*-Butyllithium (1.4 M in cyclohexane, 3.2 ml, 6.0 mmol, 3.0 eq.) was added dropwise and the solution was stirred for 25 minutes, turning brownish yellow. Triisopropylboronate (1.4 ml, 6.0 mmol, 4.0 eq.) was then added, and the resulting colorless suspension was stirred for 1 hour while gently warming to room temperature (solution **A**). Meanwhile, **59** (945 mg, 3.6 mmol, 2.4 eq.) and tetrakis(triphenylphosphine)palladium(0) (345 mg, 0.3 mmol, 0.2 eq.) were dissolved in the other

portion of degassed THF under argon. Aqueous sodium carbonate (2 M, 3.1 ml, 6.2 mmol), five droplets of ethylene glycol and **A** were added sequentially, and the resulting two-phase mixture was stirred at 65 °C for 3 hours, cooled down to room temperature, diluted with water, and extracted three times with ethyl acetate. The combined organic layers were washed with water, dried with magnesium sulfate, and concentrated under reduced pressure. The crude product was purified by medium-pressure liquid chromatography (Silica 60, ethyl acetate / cyclohexane) to afford **62** (388 mg, 49 %) as a white solid. ^{1}H NMR (500 MHz): δ = 8.17 (t, *J* = 1.6 Hz, 2H), 7.89 (dt, *J* = 7.8, 1.3 Hz, 2H), 7.66 (dt, *J* = 7.8, 1.5 Hz, 2H), 7.40 (t, *J* = 7.8 Hz, 2H), 7.12 (s, 2H), 3.92 (s, 6H), 2.86 (t, *J* = 7.4 Hz, 4H), 2.10 (p, *J* = 7.4 Hz, 2H), 2.00 (s, 6H). ^{13}C (125 Hz): δ = 166.9, 138.6, 136.9, 135.3, 134.8, 134.7, 130.7, 129.6, 128.9, 127.9, 126.3, 124.7, 58.3, 38.6, 26.9, 23.0, 14.5. HR-MS (ESI+) *m/z* = 529.150 (calcd. 529.150 for $[C_{31}H_{29}O_4S_2]^+$). Appendices 6 and 7.

7.3.3 Methyl 3-(4-(2-(5-chloro-2-methylthiophen-3-yl)cyclopent-1-en-1-yl)-5-methylthiophen-2-yl)benzoate (63)

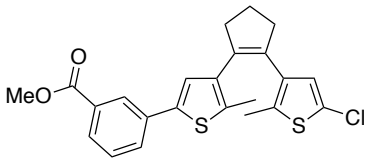

60 ml of anhydrous tetrahydrofuran was freeze-pump-thaw degassed and stored under argon. 30 ml of the tetrahydrofuran was taken to another flask under argon, and **58** (1.0 g, 3.0 mmol, 1.0 eq.) was dissolved and the solution cooled down to -78 °C. *n*-butyllithium (2.3 M in cyclohexane, 4.6 ml, 10.6 mmol, 3.5 eq.) was added dropwise and the solution was stirred for 25 minutes, turning red. Triisopropylboronate (2.8 ml, 12.0 mmol, 4.0 eq.) was then added, and the resulting colorless suspension was stirred for 1 hour while gently warming to room temperature (solution A). Meanwhile, **59** (1.89 g, 7.2 mmol, 2.4 eq.) and tetrakis(triphenylphosphine)palladium(0) (690 mg, 0.6 mmol, 0.2 eq.) were dissolved in the other portion of degassed THF under argon. Bubble-degassed aqueous sodium carbonate (2 M, 6.4 ml, 12.4 mmol), five droplets of ethylene glycol and A were added sequentially, and the resulting two-phase mixture was stirred at 65 °C for 20 hours, cooled down to room temperature, diluted with water, and extracted three times with ethyl acetate. The aqueous layer was noted to contain large amounts of hydrolyzed product (verified by UPLC). The combined organic layers were washed with water and brine, dried with magnesium sulfate, and concentrated under reduced pressure. The crude was purified by medium-pressure liquid chromatography (Silica 60, ethyl acetate / cyclohexane) to afford **63** in 532 mg (41.4 %) yield. ^{1}H NMR (500 MHz): δ = 8.16 (s, 1H), 7.88 (d, *J* = 8 Hz, 1H), 7.65 (d, *J* = 8 Hz, 1H), 7.40 (t, *J* = 7.7 Hz, 1H), 7.07 (s, 1H), 6.62 (s, 1H), 3.93 (s, 3H), 2.78 (m, 4H), 2.05 (p, *J* = 7.4 Hz, 2H), 1.98 (s, 3H), 1.87 (s, 3H). ^{13}C (125 Hz): δ = 167.0, 141.9, 138.7, 136.7, 135.3, 135.2, 134.8, 134.1, 133.3, 130.8, 129.7, 129.0, 128.0, 126.9, 126.3, 125.2, 124.6, 52.4, 38.6, 23.0, 14.6. HR-MS (ESI+) *m/z* = 428.07 (calcd. 428.07 for $[C_{23}H_{21}ClO_2S_2]^+$). Appendices 8 and 9.

7.3.4 3,3'-(Cyclopent-1-ene-1,2-diylbis(5-methylthiophene-4,2-diyl))dibenzoic acid (64)

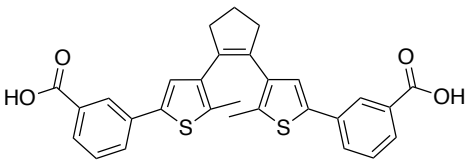

Compound **62** (350 mg, 0.66 mmol, 1.0 eq.) and potassium hydroxide (146 mg, 2.64 mmol, 4.0 eq.) were dissolved in a 1:1:0.1 mixture of tetrahydrofuran, water and methanol (12 ml) and stirred at 45 °C for 2 hours. The mixture was then heated to 65 °C and stirred for 1 hour. After the conversion was complete, the organic solvents were evaporated under reduced pressure and the aqueous phase was diluted with water and acidified with 1 M hydrochloric acid. The formed precipitate was extracted with ethyl acetate, washed with water and dried under vacuum to produce **64** in 310 mg (94 %) yield. HR-MS (ESI+) *m/z* = 501.121 (calcd. 501.119 for $[C_{29}H_{25}O_4S_2]^+$).

7.3.5 Bis(2-(acryloyloxy)ethyl) 3,3'-(cyclopent-1-ene-1,2-diylbis-(5-methylthiophene-4,2-diyl))dibenzoate (57)

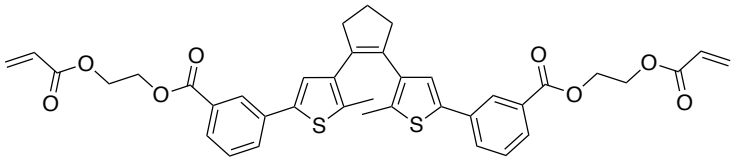

Compound **64** (128 mg, 0.26 mmol, 1.0 eq.) was suspended in dry dichloromethane (2 ml), and two droplets of dry *N*,*N*-dimethylformamide were added. The solution was then cooled down to +5 °C, and oxalyl chloride (0.070 ml, 103 mg, 0.78 mmol, 4.0 eq.) was added. The reaction was warmed slowly to room temperature and stirred for 1 hour after which no gas evolution was observed. The formed acyl chloride solution was then slowly added into a solution of 2-hydroxyethyl acrylate (0.064 ml, 70 mg, 0.60 mmol, 2.3 eq.), triethylamine (0.36 ml, 260 mg, 2.6 mmol, 10 eq.) and a grain of 4-dimethylaminopyridine in 2 ml of dry dichloromethane. Formation of hydrochloric acid and the subsequent precipitation of triethylammonium chloride was observed immediately. The reaction mixture was stirred overnight. After 15 hours, the mixture was diluted with dichloromethane, washed with water and sodium bicarbonate, dried with magnesium sulfate and concentrated under reduced pressure. The crude was further purified by medium-pressure liquid chromatography (Silica 60, ethyl acetate / cyclohexane) to yield 116 mg (65 %) of **57** as a colorless solid. ^{1}H NMR (300 MHz) δ = 8.18 (t, *J* = 1.6 Hz, 2H), 7.89 (dt, *J* = 7.8, 1.3 Hz, 2H), 7.68 (dt, *J* = 7.8, 1.5 Hz, 2H), 7.41 (t, *J* = 7.7 Hz, 2H), 7.14 (s, 2H), 6.46 (dd, *J* = 17.3, 1.5 Hz, 2H), 6.17 (dd, *J* = 17.3, 10.4 Hz, 2H), 5.87 (dd, *J* = 10.4, 1.5 Hz, 2H), 4.61–4.48 (m, 8H), 2.87 (t, *J* = 7.4 Hz, 4H), 2.10 (p, *J* = 7.4 Hz, 2H), 1.99 (s, 6H). ^{13}C NMR (125 MHz, $CDCl_3$): δ = 166.12, 165.93, 138.46, 135.27, 131.46, 126.35, 124.68,

62.77, 62.19, 38.57, 22.99, 14.49. HR-MS (ESI+): *m/z* = 697.202 (calcd. 697.192 for $[C_{39}H_{36}O_8S_2]^+$). Appendices 10 and 11.

7.4 Indigo crosslinker and side-chain

7.4.1 2-(2-bromoacetoxy)ethyl acrylate (67)

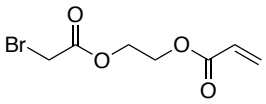

300 mg (2.58 mmol) of 2-hydroxyethyl acrylate **60** was dissolved in dry dichloromethane at room temperature under argon. 713 mg (5.16 mmol) of potassium carbonate was added, and 0.23 ml (2.58 mmol) of bromoacetyl bromide was added dropwise. The reaction mixture was stirred overnight under argon. After 16 hours TLC showed quantitative conversion. The reaction mixture was filtered, washed with water, saturated sodium carbonate and brine, dried with magnesium sulfate, and concentrated to yield 607 mg (99 %) of **67**. ^{1}H NMR (300 Hz) δ = 6.43 (d, *J* = 15.8 Hz, 1H), 6.13 (m, 1H), 5.87 (m, 1H), 4.40 (m, 4H), 3.85 (s, 2H). Appendix 12.

7.4.2 (*E*)-((2,2'-(3,3'-dioxo-[2,2'-biindolinylidene]-1,1'-diyl)bis-(acetyl))bis(oxy))bis(ethane-2,1-diyl) diacrylate (65)

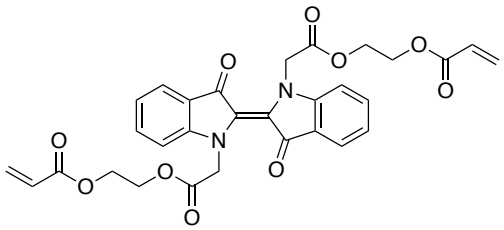

Failed attempt. Indigo (100 mg, 0.38 mmol, 1.0 eq.), **67** (325 mg, 1.53 mmol, 4.0 eq.), and cesium carbonate (248 mg, 0.76 mmol, 2.0 eq.) were suspended in 2 ml of fresh DMF under argon in room temperature and stirred for three days. No reaction occurred. The attempt to raise temperature lead to the formation of undesired side products only.

7.4.3 3-Bromopropyl 2-bromoacetate (69)

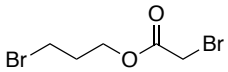

3-bromopropan-1-ol (1.0 g, 7.2 mmol, 1.0 eq.) and potassium carbonate (2.0 g, 14 mmol, 1.9 eq.) were dissolved in 50 ml of dry DCM under argon. Bromoacetyl bromide (0.63 ml, 7.2 mmol, 1.0 eq.) was added dropwise, and the reaction was stirred at room temperature for 1 hour. The reaction mixture was filtered, washed with H_2O and brine, dried

with magnesium sulfate, and concentrated under reduced pressure to yield 1.31 g (70 %) of product as a colorless oil. ^{1}H NMR (300 Hz) δ = 4.33 (t, *J* = 6.0 Hz, 2H), 3.84 (s, 2H), 3.48 (t, *J* = 6.5 Hz, 2H), 2.22 (p, *J* = 6.5 Hz, 2H). Appendix 13.

7.4.4 Bis(3-bromopropyl) 2,2'-(3,3'-dioxo-[2,2'-biindolinylidene]-1,1'-diyl)(*E*)-diacetate (70)

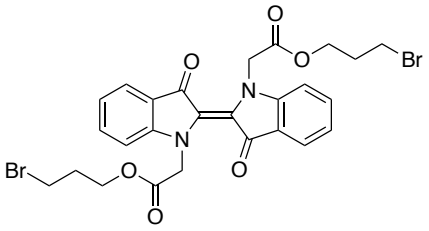

Indigo (200 mg, 0.76 mmol, 1.0 eq.), **69** (800 mg, 3.05 mmol, 4.0 eq.) and cesium carbonate (495 mg, 1.52 mmol, 2.0 eq.) were stirred in DMF (4 ml) at room temperature for 3 days. The reaction mixture was then diluted with ethyl acetate, washed twice with water and brine, dried with $MgSO_4$, and concentrated under reduced pressure. The crude product was purified by flash column chromatography (Silica 60, DCM) to produce a turquoise solid. The NMR spectrum was recorded, showing the following characteristic peaks of the product. ^{1}H NMR (300 MHz, $CDCl_3$): δ = 7.71 (2H), 7.55 (m, 2H), 7.04 (m, 4H), 4.78 (s, 4H). However, there was still **69** in the fraction, told by the integrals of the peaks at 4.32 (m, 14H), 3.48 (m, 16H) and 2.22 (m, 12H). A new purification by flash column chromatography (Silica 60, 20 % ethyl acetate / hexane) yielded **70** (41 mg, 9 %) as a pure product, confirmed by NMR data that was later lost. Appendix 14.

7.4.5 (*E*)-((2,2'-(3,3'-dioxo-[2,2'-biindolinylidene]-1,1'-diyl)bis-(acetyl))bis(oxy))bis(propane-3,1-diyl) diacrylate (71)

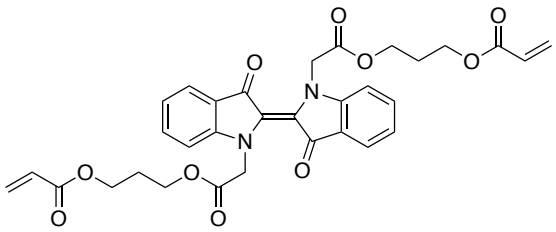

70 (41 mg, 0.066 mmol, 1.0 eq.), acrylic acid (18.0 mg, 0.25 mmol, 4.0 eq.) and potassium bicarbonate (20 mg, 0.20 mmol, 3.0 eq.) were dissolved in DMF (1 ml) and stirred under argon at room temperature for 20 hours. The reaction mixture was then diluted with ethyl acetate, washed four times with brine, dried with $MgSO_4$ and concentrated under reduced pressure. The crude product was purified by flash column chromatography (10 % ethyl acetate / dichloromethane) to yield the target molecule (45 mg, 99 %) as a turquoise solid. ^{1}H NMR (300 MHz, $CDCl_3$): δ = 7.73 (d, *J* = 7.6, 2H), 7.54 (m, 2H), 7.06 (m, 4H), 6.39 (m, 2H), 6.09 (m, 2H), 5.82 (m, 2H), 4.78 (s, 4H), 4.25 (m, 8H), 2.04 (p, *J* = 6.3, 4H). ^{13}C

NMR (125 MHz, $CDCl_3$): δ = 186.2, 169.1, 166.1, 153.6, 135.8, 131.1, 128.3, 124.5, 122.2, 121.9, 111.1, 62.1, 61.0, 51.3, 29.8. HR-MS (ESI+) *m/z* = 625.1722 (calcd. 625.1798 for $[C_{32}H_{30}N_2O_{10}Na]^+$). Appendices 15 and 16.

7.4.6 (E)-1-(4-methoxyphenyl)-[2,2'-biindolinylidene]-3,3'-dione (72)

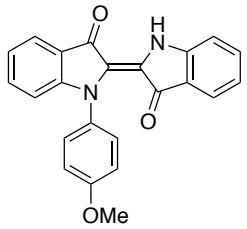

Toluene was bubble-degassed with argon for 30 minutes, after which indigo (500 mg, 1.9 mmol, 1.0 eq.), 4-iodoanisole (468 mg, 2.0 mmol, 1.1 eq.), copper (I) iodide (114 mg, 0.6 mmol, 0.32 eq.) and cesium carbonate (928 mg, 2.85 mmol, 1.5 eq.) were dissolved in it and stirred at 110 °C for 20 hours. The reaction mixture was then cooled to room temperature, diluted with dichloromethane, washed with ammonium chloride and brine, dried over magnesium sulfate and concentrated under reduced pressure. The crude mixture was filtered through Silica (ethyl acetate / dichloromethane) to yield 30.2 mg (4.3 %) of product as a green solid to be used in the next step without further purification as suggested in literature [21].

7.4.7 (*E*)-1-(2-iodoethyl)-1'-(4-methoxyphenyl)-[2,2'-biindolinylidene]-3,3'-dione (73)

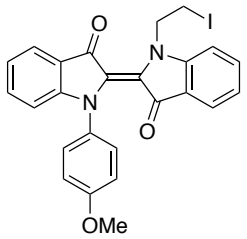

Failed attempt. **72** (30.2 mg, 0.082 mmol, 1.0 eq.), 1,2-diiodoethane (69.3 mg, 0.246 mmol, 3.0 eq.) and cesium carbonate (29.3 mg, 0.090 mmol, 1.1 eq.) were dissolved in N,N-dimethylformamide (1 ml) and stirred in 35 °C for 20 hours. The reaction mixture turned yellow-brown, and no indigo product was acquired.

7.4.8 (*E*)-1-(6-bromohexyl)-1'-(4-methoxyphenyl)-[2,2'-biindolinylidene]-3,3'-dione (74)

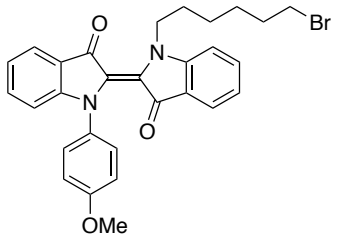

Failed attempt. **72** (16.7 mg, 0.045 mmol, 1.0 eq.), 1,6-dibromohexane (33.2 mg, 0.136 mmol, 3.0 eq.) and cesium carbonate (16.3 mg, 0.050 mmol, 1.1 eq.) were dissolved in 1 ml of DMF and stirred at room temperature overnight. After 20 hours, a color change from blue to green was observed. The reaction mixture was diluted with DCM, washed with brine, and solvent evaporated under reduced pressure. The precipitate was then dissolved in diethyl ether, washed three times with water, and concentrated under reduced pressure. The crude mixture was purified by flash column chromatography (0–5 % EtOAc / DCM) to yield no product.

7.5 DASA photoswitch dopant

7.5.1 *N*-butyl-4-hexylaniline (77)

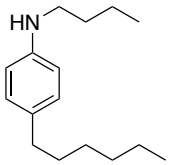

4-hexylaniline (1.2 ml, 6.1 mmol, 1.2 eq.) and butyraldehyde (0.46 ml, 5.1 mmol, 1 eq.) were dissolved in methanol (6 ml). Sodium cyanoborohydride (346 mg, 5.5 mmol, 1.1 eq.) and zinc chloride (400 mg, 2.9 mmol, 0.6 eq.) were dissolved in 6 ml of methanol in a separate vial and added dropwise to the reaction mixture which was stirred for 2 hours. Then aqueous Na_2CO_3 (2 M, 5 ml, 10 mmol) was added, leading to the formation of a white precipitate. The aqueous phase was extracted twice with Et_2O and the combined organic phase was then washed with H_2O and brine, dried with $MgSO_4$, and concentrated under reduced pressure. The crude was purified by flash column chromatography (Silica 60, 10 % ethyl acetate / hexane) to produce 1058 mg (89 %) of **77** as a pale yellow oil. ^{1}H NMR (500 MHz, $CDCl_3$): δ = 7.00 (d, J = 8.6 Hz, 2H), 6.57 (d, J = 4.6 Hz, 2H), 3.48 (br. s, 1H), 3.10 (t, J = 7.2 Hz, 2H), 2.51 (t, J = 8.0, 2H), 1.66–1.52 (m, 4H), 1.45 (m, 2H), 1.31 (m, 6H), 1.00–0.85 (m, 6H). Appendix 17.

7.5.2 5-(furan-2-ylmethylene)-1,3-dimethylpyrimidine-2,4,6(1H,3H,5H)-trione (48)

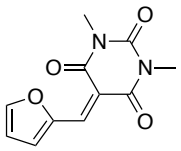

N,*N*'-dimethylbarbituric acid (1.56 g, 10 mmol, 1.0 eq.) and furfural (0.83 ml, 10 mmol, 1.0 eq.) were stirred in 40 ml of distilled water at room temperature for 2 hours. Vibrant yellow precipitate started forming immediately. After 2 hours the solids were filtered and dissolved in dichloromethane, washed with sodium bisulfite, sodium bicarbonate and brine, dried over magnesium sulfate, and concentrated under reduced pressure to yield 1.992 g (85.1 %) of pure **49** as a yellow powder. ^{1}H NMR (500 MHz, $CDCl_3$): δ = 8.62 (s, 1H), 8.42 (s, 1H), 7.84 (s, 1H), 6.73 (s, 1H), 3.39 (s, 6H). Appendix 18.

7.5.3 5-((2*Z*,4*E*)-5-(butyl(4-hexylphenyl)amino)-2-hydroxypenta-2,4-dien-1-ylidene)-1,3-dimethylpyrimidine-2,4,6(1*H*,3*H*,5*H*)-trione (80)

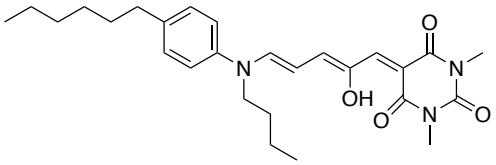

77 (540 mg, 2.3 mmol, 1 eq.) and **49** (538 mg, 2.3 mmol, 1 eq.) were stirred with 1 ml of dichloromethane at room temperature for 48 hours. Solvent was then evaporated under reduced pressure, dissolved in diethyl ether, filtered away 430 mg of pale blue solid (unreacted **49**) and concentrated under reduced pressure to yield the crude as an intense blue oil. The crude was further purified by flash column chromatography (Silica 60 deactivated with 2 % triethylamine / hexane, 50 % ethyl acetate / hexane) to yield the product as a purplish-blue solid in 69 mg (6.2 %) yield. A pure NMR spectrum proved impossible to acquire due to decomposition and thermal isomerization. Appendix 19.

7.6 Photochemical characterization

7.6.1 General methods

UV-Visible absorption spectra were recorded with an Agilent Cary 60 spectrophotometer equipped with an Ocean Optics Qpod 2e Peltier-thermostated cell holder whose temperature accuracy is 0.1 °C. Photoexcitation was conducted using a Prior Lumen 1600 light source containing multiple narrow-band LEDs at different wavelengths. Quartz absorption cuvettes with an optical path of 1.0 cm were used for all measurements.

Quantum yields were measured by irradiating the sample with an appropriate wavelength and simultaneously monitoring the absorption at a wavelength at which the change in absorbance upon isomerization is great. The irradiation was continued until a photostationary state had been reached.

Measured irradiation power inside the cuvette is shown in **Table 5** for the irradiation wavelengths. A Coherent LabMax thermal power meter and Thorlabs S170 optical power meter were utilized. The power could not be measured directly inside the cuvette, so it was measured before and after the cuvette holder and the power inside the cuvette was estimated to be the arithmetic average of these two. For example, the power of the 525 nm irradiation was measured to be 56.7 mW before and 35.3 mW after the cuvette holder, and thus the irradiation inside the cuvette was estimated to have a power of 45 ± 10 mW.

Table 5. *Irradiation power with different wavelengths.*

λ (nm)	365	405	500	525	550	660
P **(mW)**	67	287	53	45	179	154

The irradiation intensity in mol dm^{-3} s^{-1} was calculated with the formula

$$I_{in} = \frac{P\lambda}{hcN_A V}, \tag{28}$$

in which h is Planck's constant, c is the speed of light, N_A is Avogadro's constant, and V is the volume of the solution inside the cuvette. The volume was fixed as 2.0 ml for all samples.

7.6.2 Azobenzene crosslinker

The PSS composition of the azobenzene crosslinker was determined with the "PSS/*E*" method. The *Z* isomer does not absorb at ca. 350 and above ca. 520 nm, making it possible to deduce the *E* content in the PSS from the ratio of the PSS and E absorbances in those regions. The *E* content was determined to be 28 % in the PSS (**Fig. 42**). Thus, the pure *Z* spectrum was calculated using the equation

$$A_c = \frac{A_{PSS} - 0.28\, A_o}{0.72}. \tag{29}$$

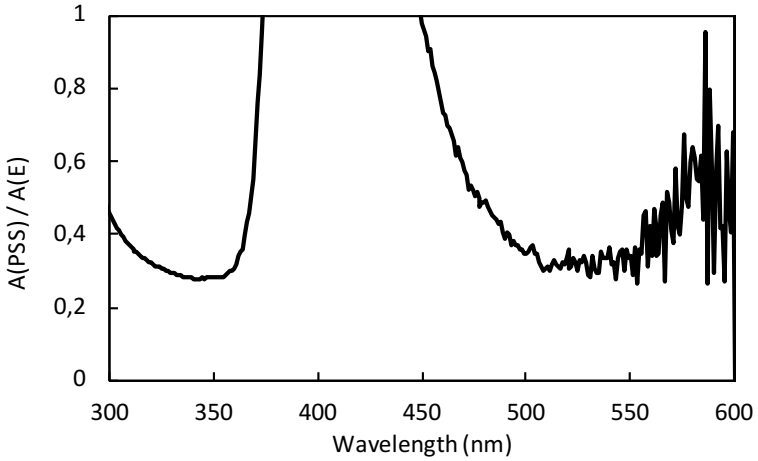

Figure 42. *The ratio of the PSS and pure E absorbances as a function of wavelength.*

Photoisomerization kinetics were studied by monitoring the absorbance at 330 nm and driving *E–Z* and *Z–E* isomerization reactions with 525 and 405 nm irradiation, respectively (**Fig. 43 a** and **c**). The quantum yields were then determined with the initial slope method (**Fig. 43 b** and **d** for *E–Z* and *Z–E*, respectively).

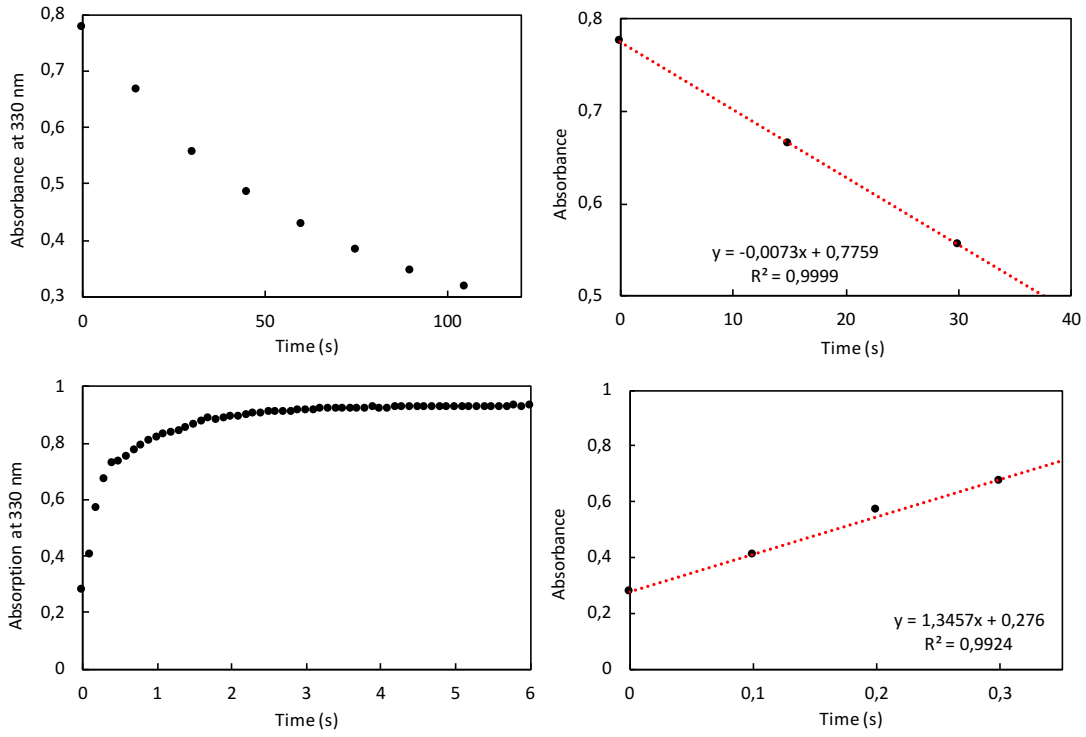

Figure 43. *a) Absorbance at 330 nm for the E–Z isomerization upon irradiation with 525 nm light and b) the respective linear fit of the initial slope. c) Absorbance at 330 nm for the Z–E isomerization upon irradiation with 405 nm light and d) the respective linear fit of the initial slope.*

From the initial slopes -0.0073 and 1.3457, the quantum yields were calculated with Eq. (18):

$$\phi_{E-Z} = \frac{0.0073\ \mathrm{s^{-1}} \times 6.626{\times}10^{-34}\ \mathrm{J\,s^{-1}} \times 2.998 \times 10^{8}\ \mathrm{m\,s^{-1}} \times 6.022 \times 10^{23}\ \mathrm{M^{-1}} \times 0.002\ \mathrm{dm^{3}}}{0.045\ \mathrm{W} \times 525 \times 10^{-9}\ \mathrm{m}\ \times (1{-}10^{-0.022}) \times 15\,440\ \mathrm{M^{-1}\,cm^{-1}} \times 1\ \mathrm{cm}} = 0.097$$

$$\phi_{Z-E} = \frac{1.3457\ \mathrm{s^{-1}} \times 6.626{\times}10^{-34}\ \mathrm{J\,s^{-1}} \times 2.998 \times 10^{8}\ \mathrm{m\,s^{-1}} \times 6.022 \times 10^{23}\ \mathrm{M^{-1}} \times 0.002\ \mathrm{dm^{3}}}{0.287\ \mathrm{W} \times 405 \times 10^{-9}\ \mathrm{m}\ \times (1{-}10^{-0.090}) \times 15\,440\ \mathrm{M^{-1}\,cm^{-1}} \times 1\ \mathrm{cm}} = 0.97$$

Thermal stability of the *Z*-isomer was studied at 60 °C. The solution was irradiated with 525 nm light and then let relax in dark. The spectrum was recorded every 30 min for 23 hours (**Fig. 44a**); longer measurement was not possible due to evaporation of the solvent. The absorbance at 320 nm was treated according to Eq. (27) to yield a linear dependence to time (**Fig. 44b**). From the slope, the thermal lifetime was calculated to be 137 988 s (38.3 h). It should be noted that the measurement was shorter than ideally but that the data fitted nevertheless very well to the linear model.

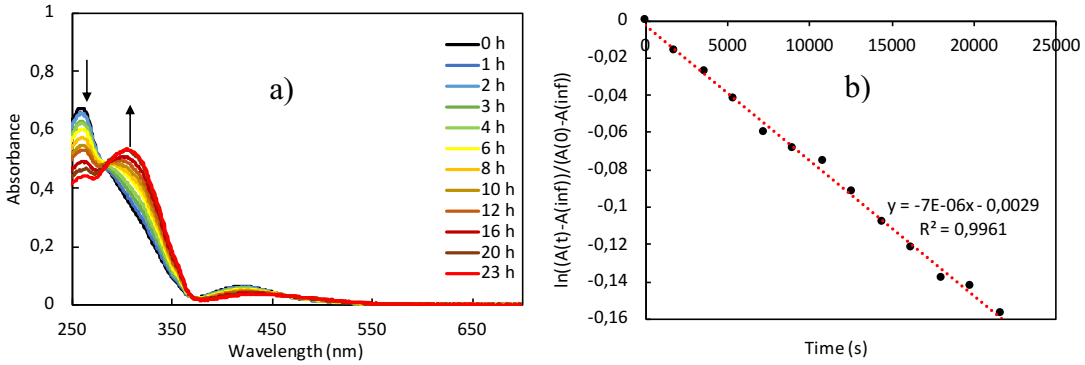

Figure 44. *Absorption spectra at 60 °C after relaxation times 0–23 h (left) and logarithmic representation of the thermal Z–E relaxation as a function of time and a linear fit (black dots and red dotted line, respectively; right). The arrows in a) indicate the changes upon thermal relaxation from Z to E.*

7.6.3 DAE crosslinker

The PSS composition was determined with ^{1}H NMR spectroscopy. A sample dissolved in $CDCl_3$ was irradiated in an NMR tube with 365 nm irradiation until the solution turned visibly purple. A small portion of the solution was then diluted with chloroform, and UV-Vis spectrum was measured for it. The NMR spectrum was recorded and from there the composition in the PSS was calculated by comparing the integrals of the signals at 8.18 and 8.20 ppm for open and closed isomer, respectively. The integral ratio was found to be 0.96:10 (see Appendix 20), meaning that 8.8 % of the compound was in closed and 91.2 % in open form. At the same time, the peak absorbance of the open form at 531 nm was 20.2 % of the absorbance at the isosbestic point (337 nm). In the PSS the respective absorbance value was 100.1 % of that in the isosbestic point. Thus, it can be calculated that in PSS, 44 % of molecules were in open form. The pure closed form spectrum can thus be derived from the measured pure open and PSS spectra with the equation

$$A_c = \frac{A_{PSS} - 0.56\,A_o}{0.44}\,. \qquad (30)$$

Kinetic studies were performed by monitoring the absorbance at 560 nm and driving the isomerization with 365 and 550 nm (**Fig. 45 a** and **c**, cyclization and cycloreversion, respectively). To calculate the isomerization quantum yield of cyclization, initial slope method was used. From the first five data points, a linear fit yielded a slope of 0.0698 s^{-1} (**Fig. 45b**). Now, Eq. (18) can be applied to yield

$$\phi_{o-c} = \frac{0.0698\ \mathrm{s^{-1}} \times 6.626{\times}10^{-34}\ \mathrm{J\,s^{-1}} \times 2.998 \times 10^{8}\ \mathrm{m\,s^{-1}} \times 6.022 \times 10^{23}\ \mathrm{M^{-1}} \times 0.002\ \mathrm{dm^{3}}}{0.067\ \mathrm{W} \times 365 \times 10^{-9}\ \mathrm{m} \times (1-10^{-0.01596}) \times 19\,647\ \mathrm{M^{-1}\,cm^{-1}} \times 1\ \mathrm{cm}} = 0.64.$$

For cycloreversion, it is possible to utilize Eq. (20) for the whole dataset. By plotting $\lg(10^{A(t)} - 1) - \lg(10^{A_0} - 1)$ as a function of time, a linear fit is acquired with the slope -0.0278 s^{-1} (**Fig. 45d**). Eq. (20) yields

$$\phi_{c-o} = \frac{0.0278\ \mathrm{s^{-1}} \times 6.626{\times}10^{-34}\ \mathrm{J\,s^{-1}} \times 2.998 \times 10^{8}\ \mathrm{m\,s^{-1}} \times 6.022 \times 10^{23}\ \mathrm{M^{-1}} \times 0.002\ \mathrm{dm^{3}}}{0.179\ \mathrm{W} \times 550 \times 10^{-9}\ \mathrm{m} \times 19\,647\ \mathrm{M^{-1}\,cm^{-1}} \times 1\ \mathrm{cm}} = 0.0034.$$

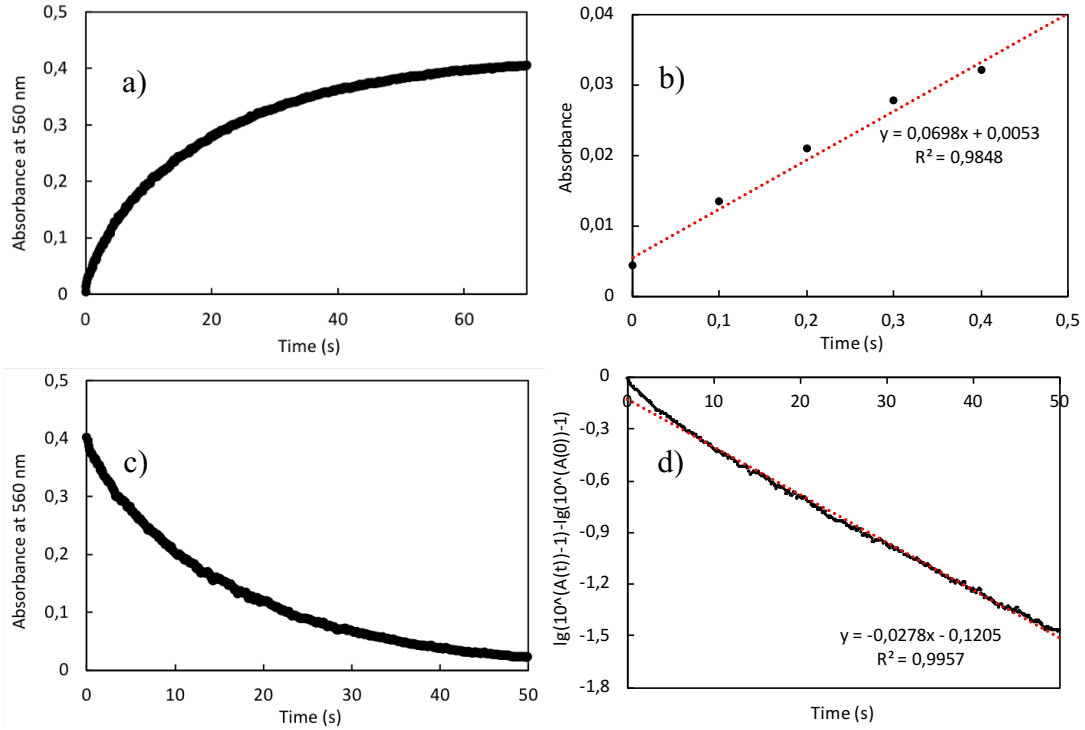

Figure 45. *a) Absorbance at 560 nm for the cyclization upon irradiation with 365 nm light and b) the respective linear fit of the initial slope. c) Absorbance at 560 nm for the cycloreversion upon irradiation with 550 nm light and d) the respective logarithmic representation with a linear fit.*

Thermal stability was monitored at 60 °C for 20 hours. No change in the absorption spectrum other than that resulting from the slow evaporation of the solvent was observed (**Fig. 46**).

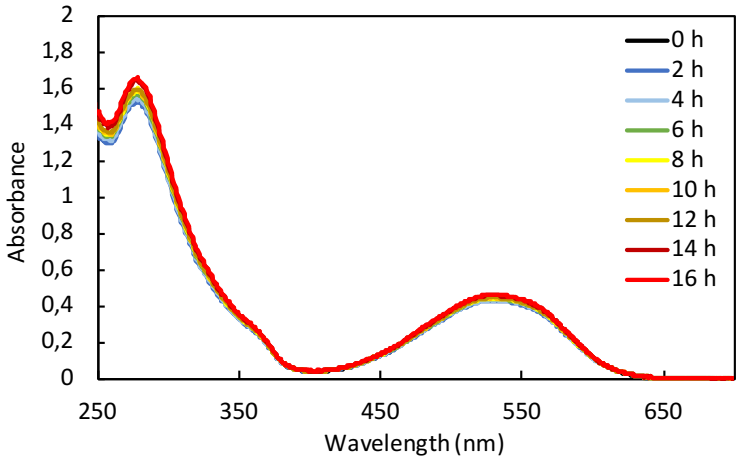

Figure 46. *The absorption spectra of the DAE crosslinker at 60 °C after relaxation times 0–16 h.*

7.6.4 Indigo crosslinker

The PSS composition was determined from the PSS and pure *E* spectra of the same sample via the "PSS/E-method". Because the *Z* isomer does not absorb above 650 nm whereas the absorption band of the *E* isomer extends to nearly 700 nm, the absorbance of the PSS mixture above 650 nm is attributed purely to *E*. Thus, when the ratio of the absorbances of PSS_{660} and *E* and PSS_{500} and *E* are plotted against wavelength (**Fig. 47**), the value of this function at ca. 660 nm yields the PSS ratios *Z*/*E* = 87:13 and 11:89 for the PSS upon irradiation with 660 and 500 nm light, respectively. Now, the pure *Z* spectrum can be derived from the measured pure *E* and PSS_{660} spectra with the equation

$$A_c = \frac{A_{PSS,660} - 0.13\,A_E}{0.87}. \tag{31}$$

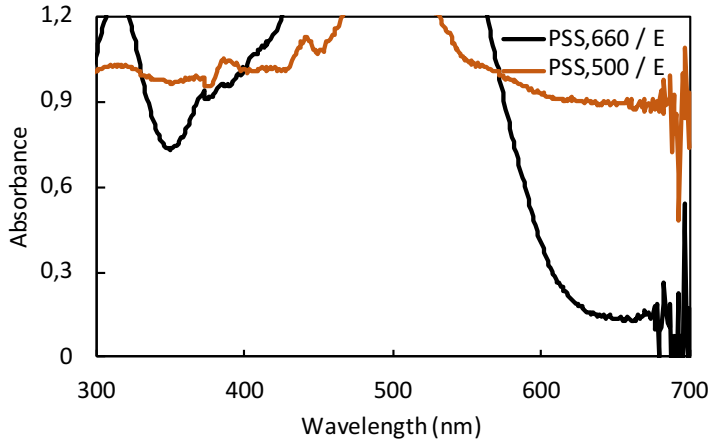

Figure 47. *The ratio of the photostationary state absorbances and the pure E-isomer absorbance as a function of wavelength.*

The quantum yields of *E–Z* and *Z–E* isomerization were calculated using the initial slope method. The kinetic absorbance data for the isomerization reactions and the initial slope fits are shown in **Fig. 48 a** and **b** for *E–Z* and **c** and **d** for *Z–E*. From the slopes (-0.2398 and 0.125, respectively) the quantum yields can now be calculated with Eq. (18):

$$\phi_{E-Z} = \frac{0.2398\ \mathrm{s^{-1}} \times 6.626{\times}10^{-34}\ \mathrm{J\ s^{-1}} \times 2.998 \times 10^{8}\ \mathrm{m\ s^{-1}} \times 6.022 \times 10^{23}\ \mathrm{M^{-1}} \times 0.002\ \mathrm{dm^{3}}}{0.154\ \mathrm{W} \times 660 \times 10^{-9}\ \mathrm{m} \times (1{-}10^{-0.1089}) \times 10\ 122\ \mathrm{M^{-1}\ cm^{-1}} \times 1\ \mathrm{cm}} = 0.37$$

$$\phi_{Z-E} = \frac{0.125\ \mathrm{s^{-1}} \times 6.626{\times}10^{-34}\ \mathrm{J\ s^{-1}} \times 2.998 \times 10^{8}\ \mathrm{m\ s^{-1}} \times 6.022 \times 10^{23}\ \mathrm{M^{-1}} \times 0.002\ \mathrm{dm^{3}}}{0.053\ \mathrm{W} \times 500 \times 10^{-9}\ \mathrm{m} \times (1{-}10^{-0.1198}) \times 10\ 167\ \mathrm{M^{-1}\ cm^{-1}} \times 1\ \mathrm{cm}} = 0.65$$

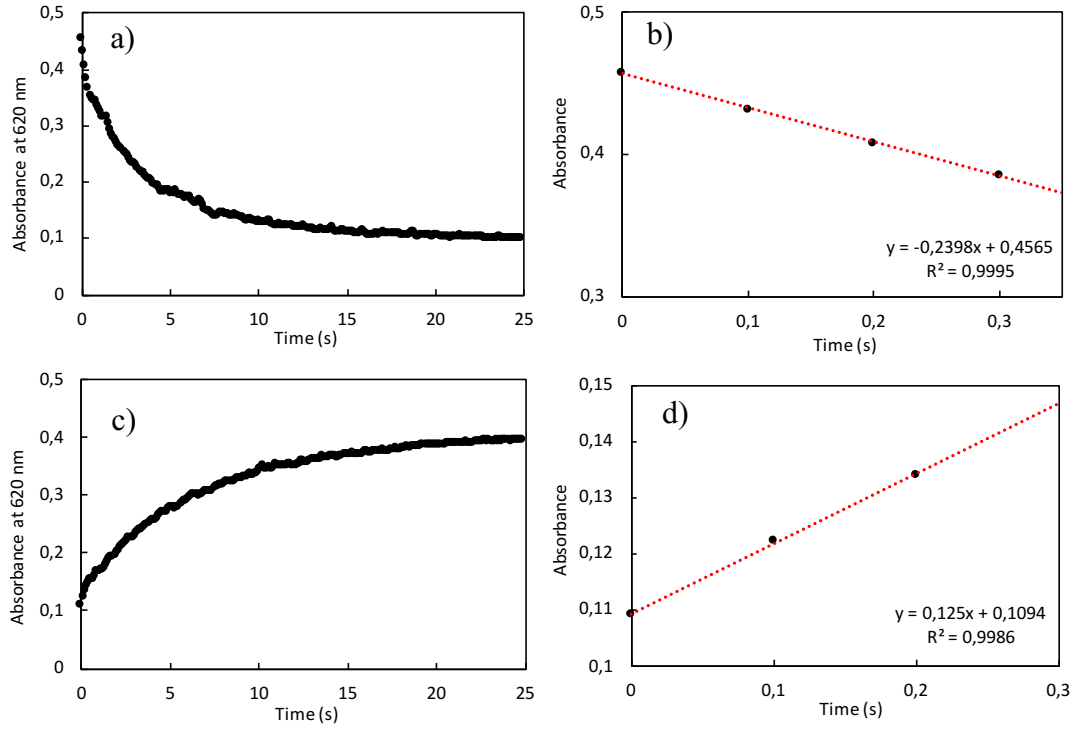

Figure 48. *a) Absorbance at 620 nm for the E–Z isomerization upon irradiation with 660 nm light and b) the respective linear fit of the initial slope. c) Absorbance at 620 nm for the Z–E isomerization upon irradiation with 500 nm light and d) the respective linear fit of the initial slope.*

Thermal stability of the *Z*-isomer was studied at 25 °C. By using the kinetic mode of the spectrometer, the absorbance at 620 nm was monitored in dark and treated with Eq. (27) to yield a linear representation as a function of time (**Fig. 49**). From the slope, the thermal lifetime was calculated to be 153 s (2.5 min).

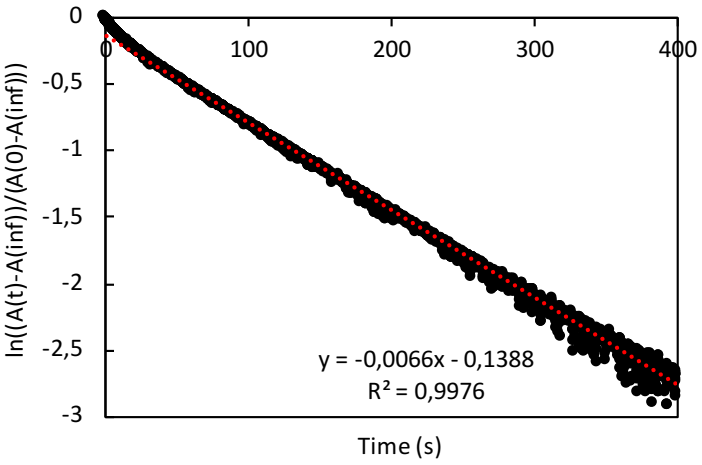

Figure 49. *Logarithmic representation of the thermal Z–E relaxation (black dots) as a function of time and a linear fit (red dotted line).*

7.6.5 DASA dopant

The quantum yield of the photocyclization reaction was determined by irradiating a freshly prepared DASA solution in acetonitrile with 550 nm light and monitoring the reaction by recording the spectrum with ca. 10 s intervals. As only the open triene form absorbs in the region, Eq. (21) can be utilized (**Fig. 50**). From the slope (-0.00810 s^{-1}), the quantum yield is determined as

$$\phi_{BA} = \frac{0.0081\ \mathrm{s^{-1}} \times\ 6.626{\times}10^{-34}\ \mathrm{J\ s^{-1}} \times 2.998 \times 10^{8}\ \mathrm{m\ s^{-1}} \times 6.022 \times 10^{23}\ \mathrm{M^{-1}} \times 0.002\ \mathrm{dm^{3}}}{0.179\ \mathrm{W} \times 550 \times 10^{-9}\ \mathrm{m} \times 19\,647\ \mathrm{M^{-1}\ cm^{-1}} \times 1\ \mathrm{cm}} = 0.0010.$$

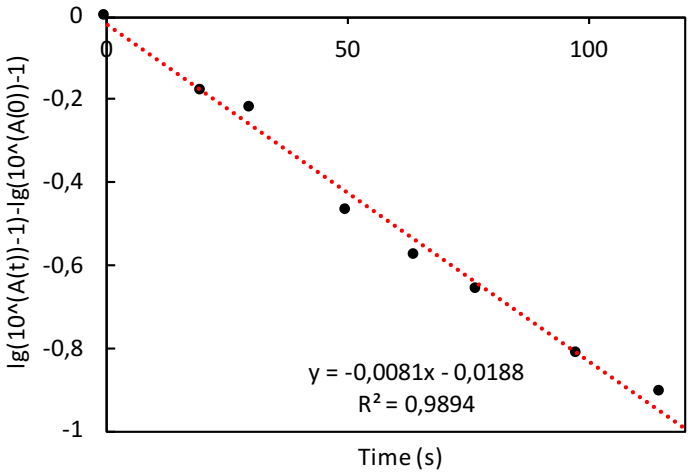

Figure 50. *The linear representation of the absorbance at 580 nm for the irradiation with 550 nm light and a linear fit.*

The thermal lifetime was studied by irradiating the switch with 550 nm until completely in the cyclic form, and then recording the spectra at 1–10 min intervals at 25 °C after ceasing the irradiation. The absorbance at 580 nm was treated with Eq. (27) to yield the

linear representation in **Fig. 51**. From the slope, the thermal lifetime was calculated to be 909 s (15.2 min).

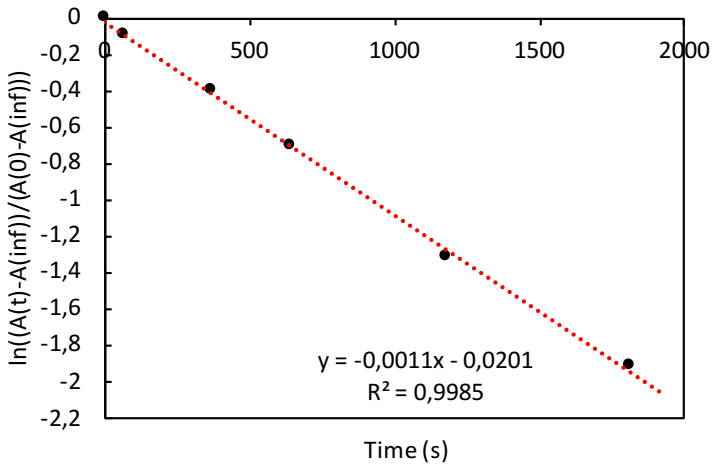

Figure 51. *Logarithmic representation of the thermal cyclic–open relaxation (black dots) as a function of time and a linear fit (red dotted line).*

REFERENCES

[1] H. Bouas-Laurent, H. Dürr, Organic photochromism (IUPAC Technical Report), Pure Appl. Chem. 73 (2001) 639–665. doi:10.1351/pac200173040639.

[2] L. Gerhard, K. Edelmann, J. Homberg, M. Valášek, S.G. Bahoosh, M. Lukas, F. Pauly, M. Mayor, W. Wulfhekel, An electrically actuated molecular toggle switch, Nat. Commun. 8 (2017) 14672. http://dx.doi.org/10.1038/ncomms14672.

[3] P.C. Knipe, S. Thompson, A.D. Hamilton, Ion-mediated conformational switches, Chem. Sci. 6 (2015) 1630–1639. doi:10.1039/c4sc03525a.

[4] J. Zhang, Q. Zou, H. Tian, Photochromic materials: More than meets the eye, Adv. Mater. 25 (2013) 378–399. doi:10.1002/adma.201201521.

[5] B.M. Neilson, C.W. Bielawski, Illuminating photoswitchable catalysis, ACS Catal. 3 (2013) 1874–1885. doi:10.1021/cs4003673.

[6] W.A. Velema, W. Szymanski, B.L. Feringa, Photopharmacology: Beyond proof of principle, J. Am. Chem. Soc. 136 (2014) 2178–2191. doi:10.1021/ja413063e.

[7] M. Semeraro, S. Silvi, A. Credi, Artificial molecular machines driven by light, Front. Biosci. 13 (2008) 1036–1049.

[8] M. Irie, Diarylethenes for Memories and Switches, Chem. Rev. 100 (2000) 1685–1716. doi:10.1021/cr980069d.

[9] T. Ikeda, O. Tsutsumi, Optical switching and image storage by means of azobenzene liquid-crystal films, Science (80-.). 268 (1995) 1873–1875.

[10] P. Zacharias, M.C. Gather, A. Kohnen, N. Rehmann, K. Meerholz, Photoprogrammable organic light-emitting diodes., Angew. Chem. Int. Ed. Engl. 48 (2009) 4038–4041. doi:10.1002/anie.200805969.

[11] I. Willner, S. Rubin, Control of the Structure and Functions of Biomaterials by Light, Angew. Chemie (International Ed. English). 35 (1996) 367–385. doi:10.1002/anie.199603671.

[12] H. Zeng, P. Wasylczyk, D.S. Wiersma, A. Priimagi, Light Robots: Bridging the Gap between Microrobotics and Photomechanics in Soft Materials, Adv. Mater. 1703554 (2017) 1–9. doi:10.1002/adma.201703554.

[13] Y. Hu, Z. Li, T. Lan, W. Chen, Photoactuators for Direct Optical-to-Mechanical Energy Conversion: From Nanocomponent Assembly to Macroscopic

Deformation, Adv. Mater. 28 (2016) 10548–10556. doi:10.1002/adma.201602685.

[14] Z. Mahimwalla, K.G. Yager, J.I. Mamiya, A. Shishido, A. Priimagi, C.J. Barrett, Azobenzene photomechanics: Prospects and potential applications, 2012. doi:10.1007/s00289-012-0792-0.

[15] M.M. Russew, S. Hecht, Photoswitches: From molecules to materials, Adv. Mater. 22 (2010) 3348–3360. doi:10.1002/adma.200904102.

[16] M. Irie, T. Fukaminato, K. Matsuda, S. Kobatake, Photochromism of diarylethene molecules and crystals: Memories, switches, and actuators, Chem. Rev. 114 (2014) 12174–12277. doi:10.1021/cr500249p.

[17] C. Ash, M. Dubec, K. Donne, T. Bashford, Effect of wavelength and beam width on penetration in light-tissue interaction using computational methods, Lasers Med. Sci. 32 (2017) 1909–1918. doi:10.1007/s10103-017-2317-4.

[18] H. Rau, Photoisomerization of Azobenzenes, Photochem. Photophysics. 1 (1989) 119–141. doi:10.1039/c0cp02588g.

[19] M. Hanazawa, R. Sumiya, Y. Horikawa, M. Irie, Thermally Irreversible Photochromic Systems. Reversible Photocyclization of 1,2-Bis(2-methyl benzo[b]thiophen-3-yl)perfluorocycloalkene Derivatives, J. Chem. Soc. Chem. Commun. (1992) 206–207.

[20] B.S. Lukyanov, M.B. Lukyanova, Spiropyrans: synthesis, properties, and application, Chem. Heterocycl. Compd. 41 (2005) 281–311. doi:10.1007/s10593-005-0148-x.

[21] C.Y. Huang, A. Bonasera, L. Hristov, Y. Garmshausen, B.M. Schmidt, D. Jacquemin, S. Hecht, N,N′-Disubstituted Indigos as Readily Available Red-Light Photoswitches with Tunable Thermal Half-Lives, J. Am. Chem. Soc. 139 (2017) 15205–15211. doi:10.1021/jacs.7b08726.

[22] S. Helmy, F.A. Leibfarth, S. Oh, J.E. Poelma, C.J. Hawker, J.R. De Alaniz, Photoswitching using visible light: A new class of organic photochromic molecules, J. Am. Chem. Soc. 136 (2014) 8169–8172. doi:10.1021/ja503016b.

[23] L.A. Tatum, X. Su, I. Aprahamian, Simple hydrazone building blocks for complicated functional materials, Acc. Chem. Res. 47 (2014) 2141–2149. doi:10.1021/ar500111f.

[24] H. Qian, S. Pramanik, I. Aprahamian, Photochromic Hydrazone Switches with Extremely Long Thermal Half-Lives, J. Am. Chem. Soc. 139 (2017) 9140–9143. doi:10.1021/jacs.7b04993.

[25] C. Knie, M. Utecht, F. Zhao, H. Kulla, S. Kovalenko, A.M. Brouwer, P. Saalfrank,

S. Hecht, D. Bléger, ortho-Fluoroazobenzenes: Visible Light Switches with Very Long-Lived Z Isomers, Chem. Eur. J. 20 (2014) 16492–16501.

[26] Z. Ahmed, A. Siiskonen, M. Virkki, A. Priimagi, Controlling azobenzene photoswitching through combined ortho-fluorination and -amination, Chem. Commun. 53 (2017) 12520–12523. doi:10.1039/C7CC07308A.

[27] IUPAC, Quantum Yield, in: A.D. McNaught, A. Wilkinson (Eds.), Compend. Chem. Terminol., 2nd ed., Blackwell Scientific Publications, Oxford, 1997: p. 4991. doi:10.1351/goldbook.Q04991.

[28] M.M. Lerch, W. Szymański, B.L. Feringa, The (photo)chemistry of Stenhouse photoswitches: Guiding principles and system design, Chem. Soc. Rev. 47 (2018) 1910–1937. doi:10.1039/c7cs00772h.

[29] A. Priimägi, Polymer-azobenzene complexes: from supramolecular concepts to efficient photoresponsive polymers, 2009.

[30] D. Bléger, J. Schwarz, A.M. Brouwer, S. Hecht, o-Fluoroazobenzenes as Readily Synthesized Photoswitches Offering Nearly Quantitative Two-Way Isomerization with Visible Light, J. Am. Chem. Soc. 134 (2012) 20597–20600. doi:10.1021/ja310323y.

[31] C. Knie, M. Utecht, F. Zhao, H. Kulla, S. Kovalenko, A.M. Brouwer, P. Saalfrank, S. Hecht, D. Bléger, Ortho-Fluoroazobenzenes: Visible Light Switches with Very Long-Lived Z Isomers, Chem. - A Eur. J. 20 (2014) 16492–16501. doi:10.1002/chem.201404649.

[32] M. Irie, M. Mohri, Thermally irreversible photochromic systems. Reversible photocyclization diarylethene derivatives, J. Org. Chem. 53 (1988) 803–808. doi:10.1039/C39920000206.

[33] R.M. Kellogg, M.B. Groen, H. Wynberg, Photochemically Induced Cyclization of Some Furyl-and Thienylethenes, J. Org. Chem. 32 (1967) 3093–3100. doi:10.1021/jo01285a035.

[34] T. Yamaguchi, K. Uchida, M. Irie, Asymmetric photocyclization of diarylethene derivatives, J. Am. Chem. Soc. 119 (1997) 6066–6071. doi:10.1021/ja970200j.

[35] L.N. Lucas, J.J.D. De Jong, J.H. Van Esch, R.M. Kellogg, B.L. Feringa, Syntheses of dithienylcyclopentene optical molecular switches, European J. Org. Chem. (2003) 155–166. doi:10.1002/1099-0690(200301)2003:1<155::AID-EJOC155>3.0.CO;2-S.

[36] G. Hohlneicher, M. Muller, M. Demmer, J. Lex, J.H. Penn, L. Gan, P.D. Loesel, 1,2-Diphenylcycloalkenes: electronic and geometric structures in the gas phase,

solution, and solid state, J. Am. Chem. Soc. 110 (1988) 4483–4494. doi:10.1021/ja00222a001.

[37] S. Stolik, J.A. Delgado, A. Pérez, L. Anasagasti, Measurement of the penetration depths of red and near infrared light in human ″ex vivo″ tissues, J. Photochem. Photobiol. B Biol. 57 (2000) 90–93. doi:10.1016/S1011-1344(00)00082-8.

[38] J. Pina, D. Sarmento, M. Accoto, P.L. Gentili, L. Vaccaro, A. Galvão, J.S. Seixas de Melo, Excited-State Proton Transfer in Indigo, J. Phys. Chem. B. 121 (2017) 2308–2318. doi:10.1021/acs.jpcb.6b11020.

[39] G.M. Wyman, Spectroscopic Studies on Dyes. III. The Structure of Indanthrones, J. Am. Chem. Soc. 78 (1956) 4599–4604. doi:10.1021/ja01599a023.

[40] G.M. Wyman, A.F. Zenhausern, Spectroscopic Studies on Dyes. V. Derivatives of cis-Indigo, J. Org. Chem. 30 (1965) 2348–2352. doi:10.1021/jo01018a055.

[41] E.D. Głowacki, G. Voss, K. Demirak, M. Havlicek, N. Sünger, A.C. Okur, U. Monkowius, J. Gąsiorowski, L. Leonat, N.S. Sariciftci, A facile protection-deprotection route for obtaining indigo pigments as thin films and their applications in organic bulk heterojunctions, Chem. Commun. 49 (2013) 6063–6065. doi:10.1039/c3cc42889c.

[42] Y. Matsumoto, H. Tanaka, A simple preparative method of N-arylindigos and substitution effects in UV/Visible absorption, Heterocycles. 60 (2003) 1805–1810.

[43] J. Stenhouse, Über die oele, die bei der einwirkung der Schwefelsäure auf verschiedene vegetabilien entshehen, Justus Liebig's Ann. Der Chemie. 74 (1850) 278–279.

[44] K. Honda, H. Komizu, M. Kawasaki, Reverse photochromism of Stenhouse salts, Chem. Commun. (1982) 253–254. doi:10.1039/c39820000253.

[45] G. Piancatelli, A. Scettri, S. Barbadoro, A useful preparation of 4-substituted 5-hydroxy-3-oxocyclopentene, Tetrahedron Lett. 17 (1976) 3555–3558. doi:https://doi.org/10.1016/S0040-4039(00)71357-8.

[46] G. Piancatelli, A. Scettri, Heterocyclic steroids—III: The synthetic utility of a 2-furyl steroid, Tetrahedron. 33 (1977) 69–72. doi:https://doi.org/10.1016/0040-4020(77)80434-1.

[47] J.R. Hemmer, S.O. Poelma, N. Treat, Z.A. Page, N.D. Dolinski, Y.J. Diaz, W. Tomlinson, K.D. Clark, J.P. Hooper, C. Hawker, J. Read De Alaniz, Tunable Visible and Near Infrared Photoswitches, J. Am. Chem. Soc. 138 (2016) 13960–13966. doi:10.1021/jacs.6b07434.

[48] H. Decker, T. von Fellenberg, Zur Begründung der Oxoniumtheorie, Justus

Liebig's Ann. Der Chemie. 364 (1909) 1–44.

[49] E. Fischer, Y. Hirshberg, Formation of coloured forms of spirans by low-temperature irradiation, J. Chem. Soc. (1952) 4522–4524.

[50] R. Klajn, Spiropyran-based dynamic materials, Chem. Soc. Rev. 43 (2014) 148–184. doi:10.1039/c3cs60181a.

[51] S. Swansburg, E. Buncel, R.P. Lemieux, Thermal racemization of substituted indolinobenzospiropyrans: Evidence of competing polar and nonpolar mechanisms, J. Am. Chem. Soc. 122 (2000) 6594–6600.

[52] R.S. Stoll, S. Hecht, Artificial light-gated catalyst systems, Angew. Chemie - Int. Ed. 49 (2010) 5054–5075. doi:10.1002/anie.201000146.

[53] M. V. Peters, R.S. Stoll, A. Kühn, S. Hecht, Photoswitching of basicity, Angew. Chemie - Int. Ed. 47 (2008) 5968–5972. doi:10.1002/anie.200802050.

[54] A. Ueno, K. Takahashi, T. Osa, Photocontrol of catalytic activity of capped cyclodextrin, J. Chem. Soc. Chem. Commun. (1981) 94–96. doi:10.1039/C39810000094.

[55] D. Sud, T.B. Norsten, N.R. Branda, Photoswitching of stereoselectivity in catalysis using a copper dithienylethene complex, Angew. Chemie Int. Ed. 44 (2005) 2019–2021.

[56] D. Wilson, N.R. Branda, Turning "On" and "Off" a Pyridoxal 5′-Phosphate Mimic Using Light, Angew. Chemie. 124 (2012) 5527–5530. doi:10.1002/ange.201201447.

[57] W.J. Deal, B.F. Erlanger, D. Nachmansohn, Photoregulation of Biological Activity By Photochromic Reagents, Iii. Photoregulation of Bioelectricity By Acetylcholine Receptor Inhibitors, Proc. Natl. Acad. Sci. 64 (1969) 1230–1234. doi:10.1073/pnas.64.4.1230.

[58] J. Bieth, S.M. Vratsanos, N. Wassermann, B.F. Erlanger, Photoregulation of Biological Activity By Photochromic Reagents, II. Inhibitors of acetylcholinesterase, Proc. Natl. Acad. Sci. 64 (1969) 1103–1106.

[59] W.A. Velema, J.P. Van Der Berg, M.J. Hansen, W. Szymanski, A.J.M. Driessen, B.L. Feringa, Optical control of antibacterial activity, Nat. Chem. 5 (2013) 924.

[60] R.S. Kularatne, H. Kim, J.M. Boothby, T.H. Ware, Liquid crystal elastomer actuators: Synthesis, alignment, and applications, J. Polym. Sci. Part B Polym. Phys. 55 (2017) 395–411. doi:10.1002/polb.24287.

[61] S. Chandrasekhar, Liquid crystals, 2nd ed., Cambridge University Press, New

York, 1992.

[62] H. Yu, Recent advances in photoresponsive liquid- crystalline polymers containing azobenzene chromophores, J. Mater. Chem. C. 2 (2014) 3047–3054. doi:10.1039/c3tc31991a.

[63] H. Zeng, M. Lahikainen, O.M. Wani, A. Berdin, Liquid Crystal Polymer Networks and Elastomers for Light - Fueled Robotics Photoactuation : A New Paradigm for Soft Micro-robotics, in: Photoactive Funct. Soft Mater., 2019: pp. 197–226.

[64] E. Takács, L. Wojnárovits, Comparison of the reactivity of acrylate and methacrylate monomers, Radiat. Phys. Chem. 46 (1995) 1007–1010. doi:https://doi.org/10.1016/0969-806X(95)00310-T.

[65] K. Kumar, C. Knie, D. Bléger, M.A. Peletier, H. Friedrich, S. Hecht, D.J. Broer, M.G. Debije, A.P.H.J. Schenning, A chaotic self-oscillating sunlight-driven polymer actuator, Nat. Commun. 7 (2016) 1–8. doi:10.1038/ncomms11975.

[66] C.E. Hoyle, C.N. Bowman, Thiol-ene click chemistry, Angew. Chemie - Int. Ed. 49 (2010) 1540–1573. doi:10.1002/anie.200903924.

[67] J.I. Mamiya, A. Kuriyama, N. Yokota, M. Yamada, T. Ikeda, Photomobile polymer materials: Photoresponsive behavior of cross-linked liquid-crystalline polymers with mesomorphic diarylethenes, Chem. - A Eur. J. 21 (2015) 3174–3177. doi:10.1002/chem.201406299.

[68] R. Klajn, P.J. Wesson, K.J.M. Bishop, B.A. Grzybowski, Writing self-erasing images using metastable nanoparticle “inks,” Angew. Chemie - Int. Ed. 48 (2009) 7035–7039. doi:10.1002/anie.200901119.

[69] F. Stellacci, C. Bertarelli, F. Toscano, M.C. Gallazzi, G. Zerbi, Diarylethene-based photochromic rewritable optical memories: on the possibility of reading in the mid-infrared, Chem. Phys. Lett. 302 (1999) 563–570.

[70] G. Pariani, R. Castagna, G. Dassa, S. Hermes, C. Vailati, A. Bianco, C. Bertarelli, Diarylethene-based photochromic polyurethanes for multistate optical memories, J. Mater. Chem. 21 (2011) 13223–13231.

[71] M. Häckel, L. Kador, D. Kropp, H.W. Schmidt, Polymer blends with azobenzene-containing block copolymers as stable rewritable volume holographic media, Adv. Mater. 19 (2007) 227–231. doi:10.1002/adma.200601458.

[72] E. Merino, Synthesis of azobenzenes: the coloured pieces of molecular materials, Chem. Soc. Rev. 40 (2011) 3835. doi:10.1039/c0cs00183j.

[73] P. Griess, Bemerkungen zu der Abhandlung der HH. Weselsky und Benedikt „Ueber einige Azoverbindungen”, Berichte Der Dtsch. Chem. Gesellschaft. 12

(1879) 426–428. doi:10.1002/cber.187901201117.

[74] A. Baeyer, Nitrosobenzol und Nitrosonaphtalin, Chem. Ber. 7 (1874) 1638.

[75] L. Wallach, O., Belli, Über die Umwandlung von Azoxybenzol in Oxyazobenzol, Chem. Ber. 13 (1880) 525–527.

[76] I. Szele, H. Zollinger, Azo coupling reactions structures and mechanisms, in: Prep. Org. Chem., Springer, 1983: pp. 1–66.

[77] E.S. Bacon, D.H. Richardson, The Reduction of Nitro-compounds by Aldehydes in Ethyl-alcoholic Potassium Hydroxide Solution, J. Chem. Soc. 7 (1932) 884–888.

[78] E. Bamberger, F. Tschirner, Zur Oxydation aromatischer Basen, Berichte Der Dtsch. Chem. Gesellschaft. 32 (1899) 342–355. doi:10.1002/cber.18990320159.

[79] I. Shimao, S. Oae, The Wallach Rearrangement of Some 4,4′-Disubstituted Azoxybenzenes, Bull. Chem. Soc. Jpn. 56 (1983) 643–644. doi:10.1246/bcsj.56.643.

[80] Y.K. Lim, K.S. Lee, C.G. Cho, Novel route to azobenzenes via Pd-catalyzed coupling reactions of aryl hydrazides with aryl halides, followed by direct oxidations, Org. Lett. 5 (2003) 979–982. doi:10.1021/ol027311u.

[81] S. Dixon, Elimination reaction of fluoroolefins with organolithium compounds, J. Org. Chem. 21 (1956) 400–403. doi:10.1021/jo01110a005.

[82] G. Szalõki, J.L. Pozzo, Synthesis of symmetrical and nonsymmetrical bisthienylcyclopentenes, Chem. - A Eur. J. 19 (2013) 11124–11132. doi:10.1002/chem.201301645.

[83] S. Hiroto, K. Suzuki, H. Kamiya, H. Shinokubo, Synthetic protocol for diarylethenes through Suzuki-Miyaura coupling, Chem. Commun. 47 (2011) 7149–7151. doi:10.1039/c1cc12020d.

[84] J.E. Mc Murry, M.P. Fleming, New Method for the Reductive Coupling of Carbonyls to Olefins. Synthesis of β-Carotene, J. Am. Chem. Soc. 96 (1974) 4708–4709. doi:10.1021/ja00821a076.

[85] M.M.K. and M.A.K. and V.A. Migulin, McMurry reaction in the synthesis of photochromic dihetarylethenes, Russ. Chem. Rev. 78 (2009) 329. http://stacks.iop.org/0036-021X/78/i=4/a=R04.

[86] G. Sevez, J.L. Pozzo, Toward multi-addressable molecular systems: Efficient synthesis and photochromic performance of unsymmetrical bisthienylethenes, Dye. Pigment. 89 (2011) 246–253. doi:10.1016/j.dyepig.2010.03.018.

[87] M. Kose, Novel sulfoxide-introducing reaction and photochromic reactions of ethenylsulfinyl derivatives of dithienylethenes, J. Photochem. Photobiol. A Chem. 165 (2004) 97–102. doi:10.1016/j.jphotochem.2004.03.003.

[88] A. Baeyer, Synthese des Isatins und des Indigblaus, Berichte Der Dtsch. Chem. Gesellschaft. 11 (1878) 1228–1229.

[89] H. Zollinger, Zollinger, Color chemistry: Syntheses, Properties, and Applications, John Wiley & Sons, Germany, 2003.

[90] S.K. Manna, S. Mazumdar, Tuning the substrate specificity by engineering the active site of cytochrome P450cam: A rational approach, Dalt. Trans. 39 (2010) 3115–3123. doi:10.1039/b922606k.

[91] P.Y.S. Lam, C.G. Clark, S. Saubern, J. Adams, M.P. Winters, D.M.T. Chan, A. Combs, New aryl/heteroaryl C-N bond cross-coupling reactions via arylboronic acid/cupric acetate arylation, Tetrahedron Lett. 39 (1998) 2941–2944. doi:10.1016/S0040-4039(98)00504-8.

[92] J.C. Vantourout, H.N. Miras, A. Isidro-Llobet, S. Sproules, A.J.B. Watson, Spectroscopic Studies of the Chan-Lam Amination: A Mechanism-Inspired Solution to Boronic Ester Reactivity, J. Am. Chem. Soc. 139 (2017) 4769–4779. doi:10.1021/jacs.6b12800.

[93] D. Kumar, V. Arun, M. Pilania, M.K. Mehra, S.B. Khandagale, Diaryliodonium salts: Emerging reagents for arylations and heterocycles synthesis, Chem. Biol. Interface. 6 (2016) 270–281.

[94] M.M. Heravi, Z. Kheilkordi, V. Zadsirjan, M. Heydari, M. Malmir, Buchwald-Hartwig reaction: An overview, J. Organomet. Chem. 861 (2018) 17–104. doi:10.1016/j.jorganchem.2018.02.023.

[95] J. Yongwen, M. Dawei, Modern Ullmann–Goldberg Chemistry: Arylation of N-Nucleophiles with Aryl Halides, Copper-Mediated Cross-Coupling React. (2013). doi:doi:10.1002/9781118690659.ch1.

[96] E. Knoevenagel, Condensation von Malonsäure mit aromatischen Aldehyden durch Ammoniak und Amine, Berichte Der Dtsch. Chem. Gesellschaft. 31 (1898) 2596–2619.

[97] M. Lahikainen, H. Zeng, A. Priimagi, Reconfigurable photoactuator through synergistic use of photochemical and photothermal effects, Nat. Commun. 9 (2018) 4148. doi:10.1038/s41467-018-06647-7.

[98] S. Iamsaard, E. Anger, S.J. Aßhoff, A. Depauw, S.P. Fletcher, N. Katsonis, Fluorinated Azobenzenes for Shape-Persistent Liquid Crystal Polymer Networks,

Angew. Chemie - Int. Ed. 55 (2016) 9908–9912. doi:10.1002/anie.201603579.

[99] M. Kathan, P. Kovaricek, C. Jurissek, A. Senf, A. Dallmann, A.F. Thunemann, S. Hecht, Control of Imine Exchange Kinetics with Photoswitches to Modulate Self-Healing in Polysiloxane Networks by Light Illumination., Angew. Chem. Int. Ed. Engl. 55 (2016) 13882–13886. doi:10.1002/anie.201605311.

[100] IUPAC, Glossary of Terms Used in Photochemistry, 3rd ed., 2006.

[101] G. Zimmerman, L.-Y. Chow, U.-J. Paik, The Photochemical Isomerization of Azobenzene1, J. Am. Chem. Soc. 80 (1958) 3528–3531. doi:10.1021/ja01547a010.

[102] E. Griese, Photochromic properties of nonsymmetrically functionalized dithienylethenes, Humboldt University of Berlin, 2017.

[103] M. Herder, B.M. Schmidt, L. Grubert, M. Pätzel, J. Schwarz, S. Hecht, Improving the Fatigue Resistance of Diarylethene Switches, J. Am. Chem. Soc. 137 (2015) 2738–2747. doi:10.1021/ja513027s.

APPENDIX 1. ^{1}H NMR SPECTRUM OF COMPOUND 54

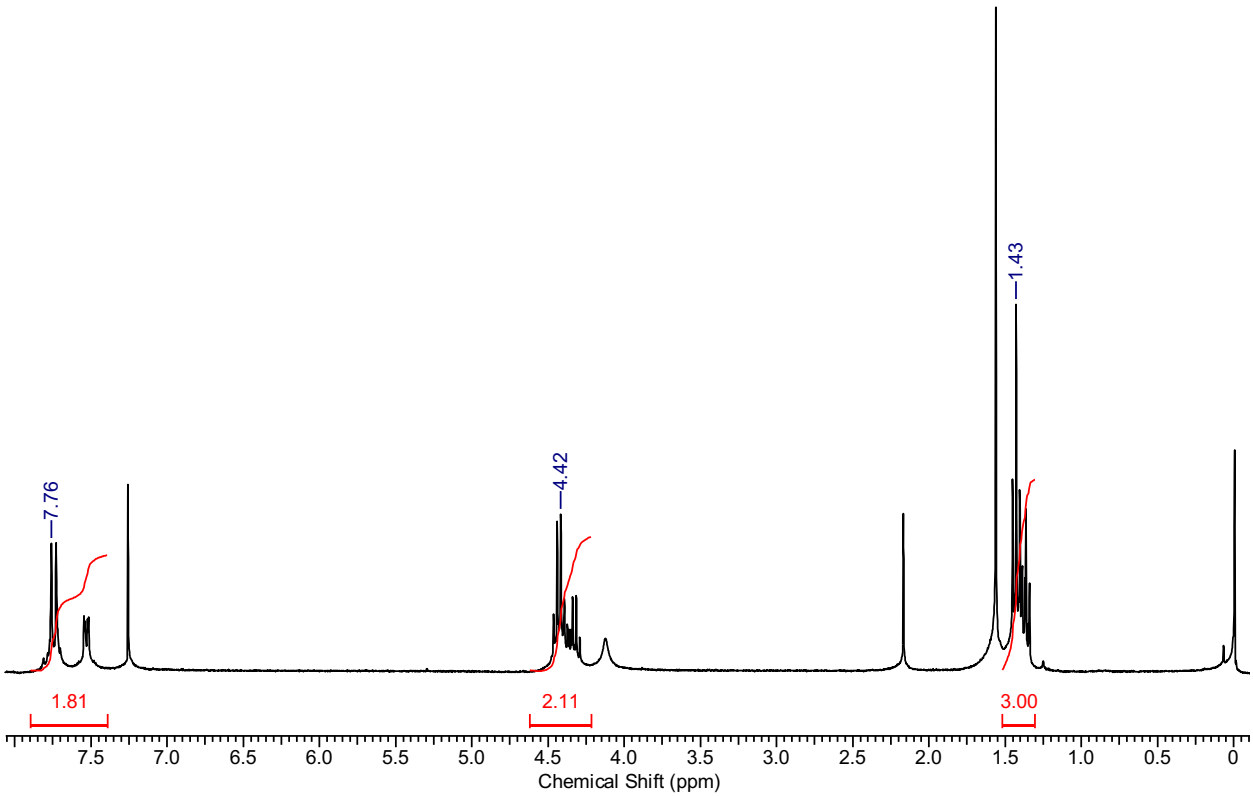

APPENDIX 2. ^{1}H NMR SPECTRUM OF COMPOUND 55

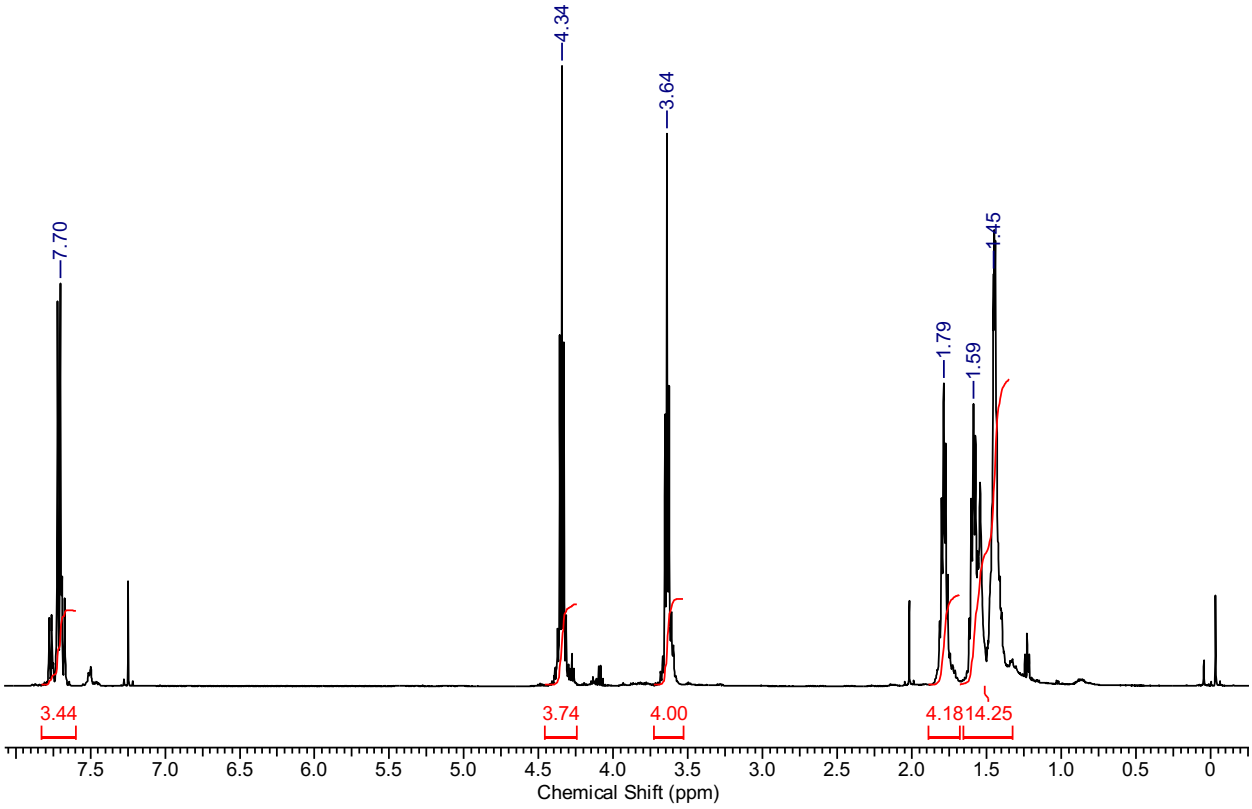

APPENDIX 3. ^{1}H NMR SPECTRUM OF COMPOUND 56

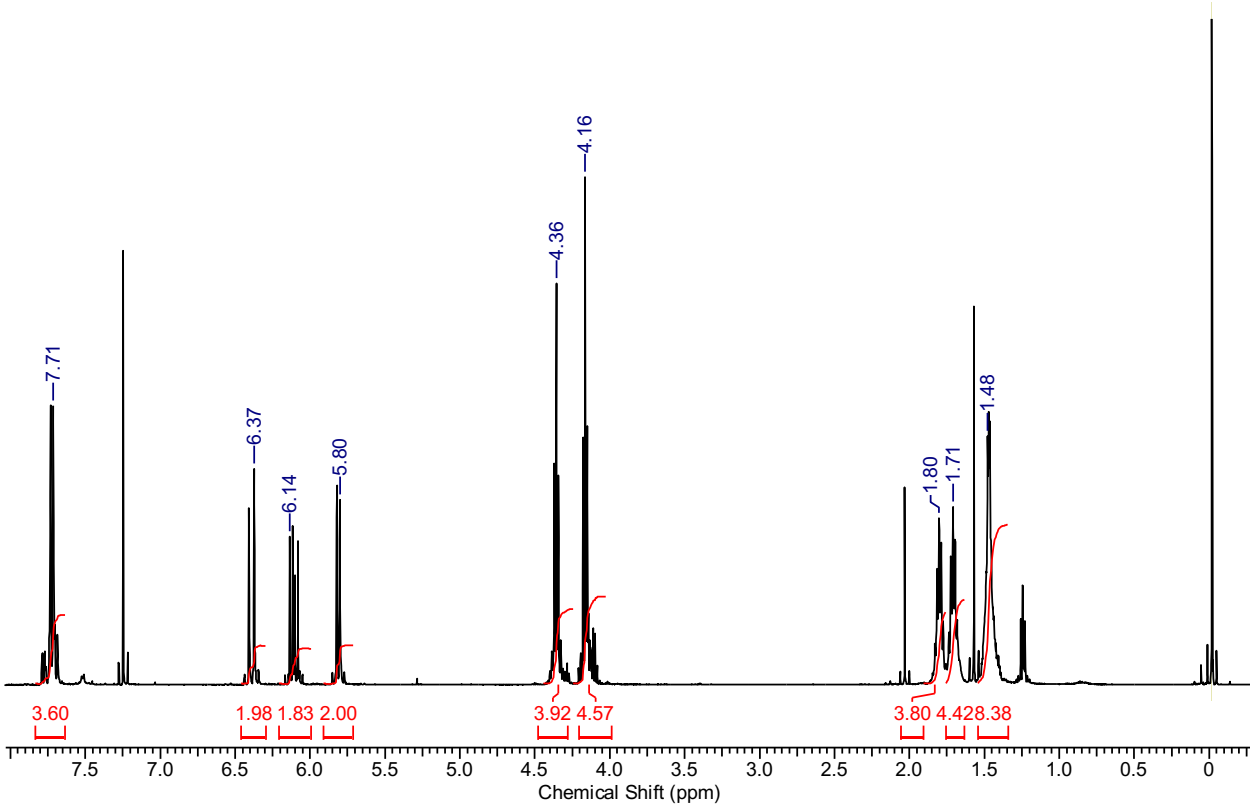

APPENDIX 4. ^{13}C NMR SPECTRUM OF COMPOUND 56

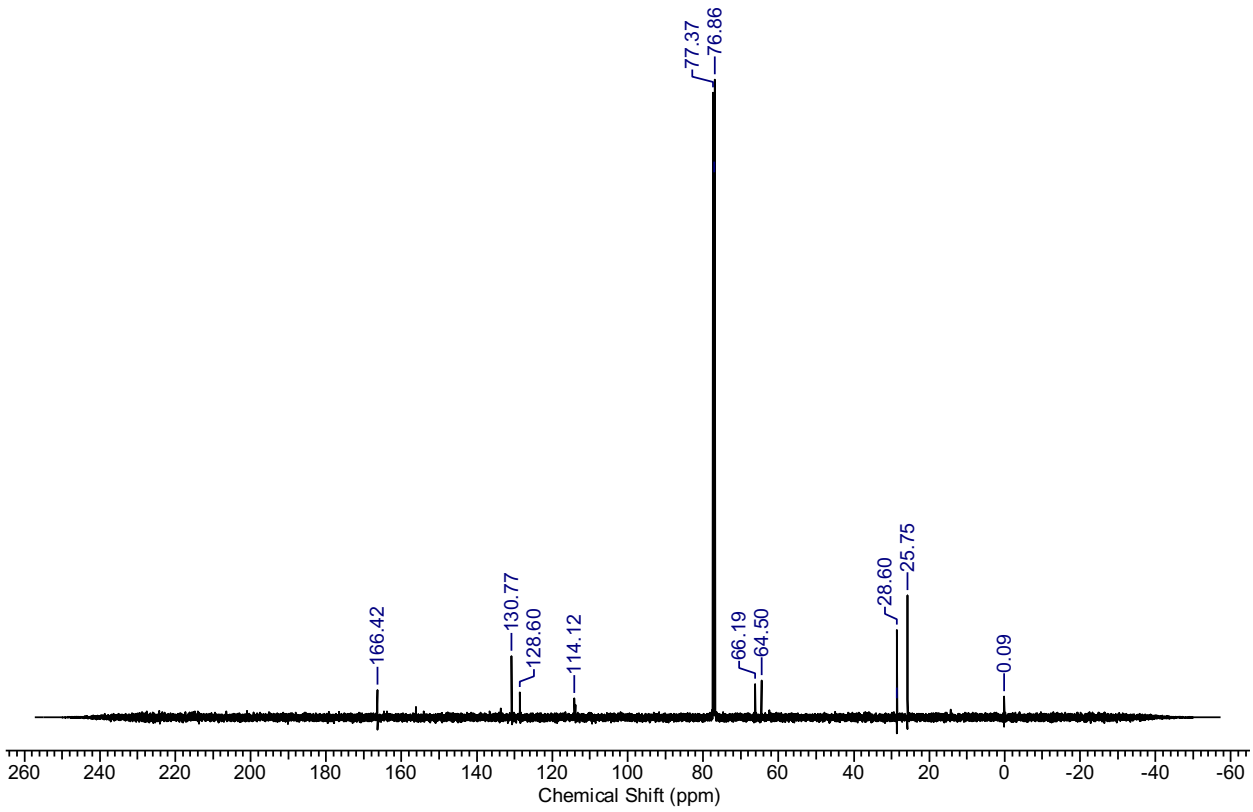

APPENDIX 5. ^{19}F NMR SPECTRUM OF COMPOUND 56

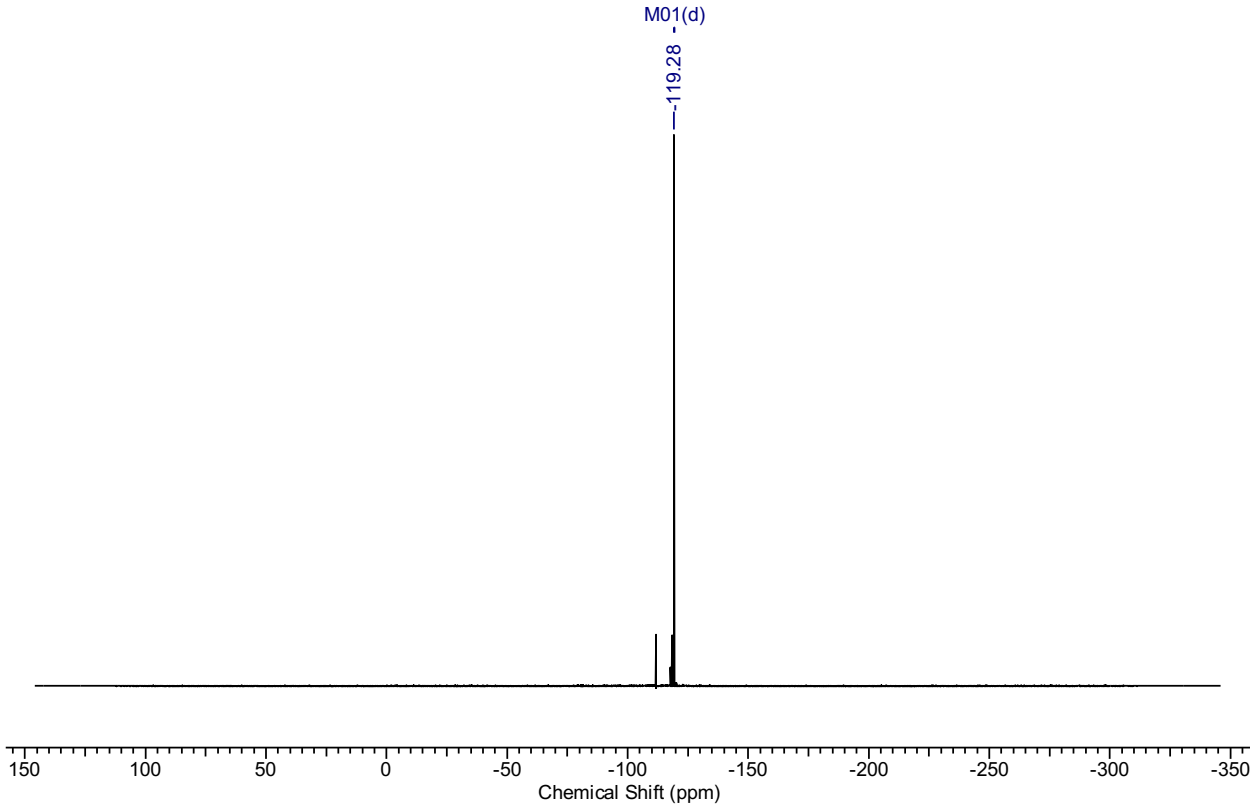

APPENDIX 6. ^{1}H NMR SPECTRUM OF COMPOUND 62

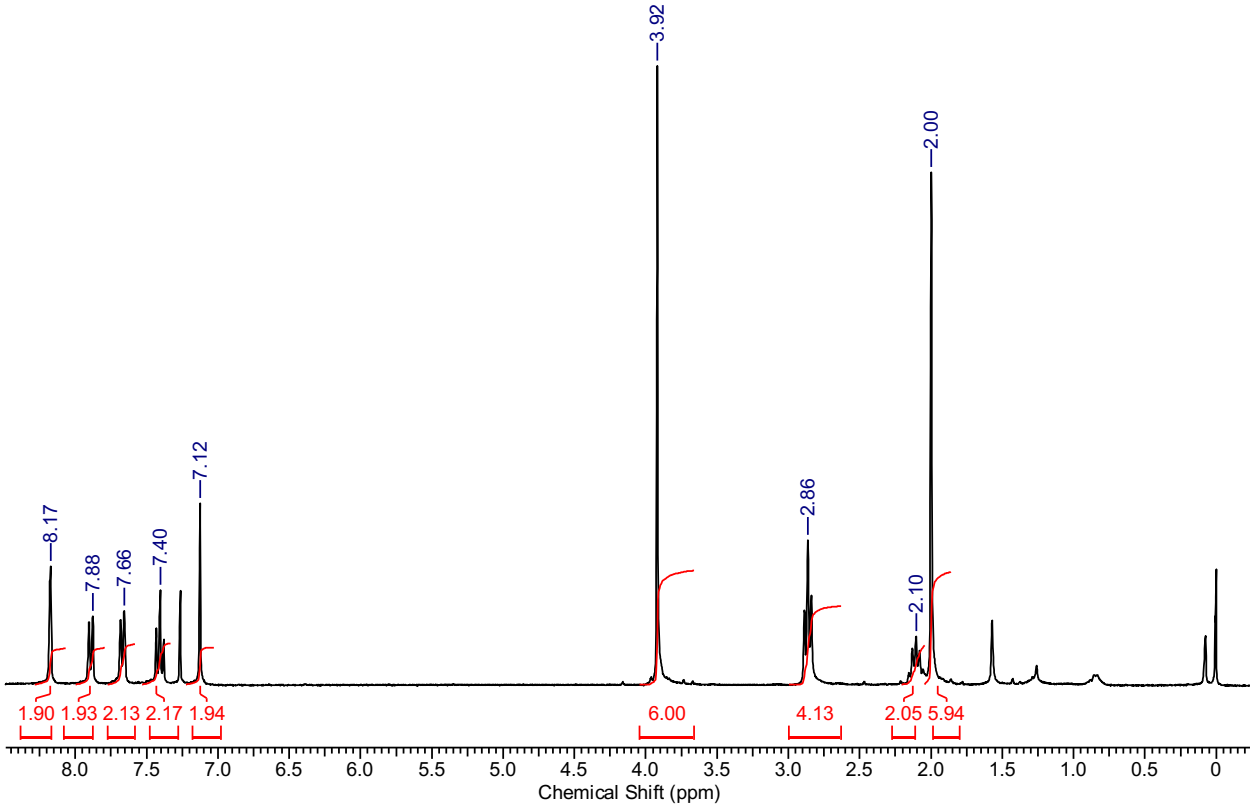

APPENDIX 7. ^{13}C NMR SPECTRUM OF COMPOUND 62

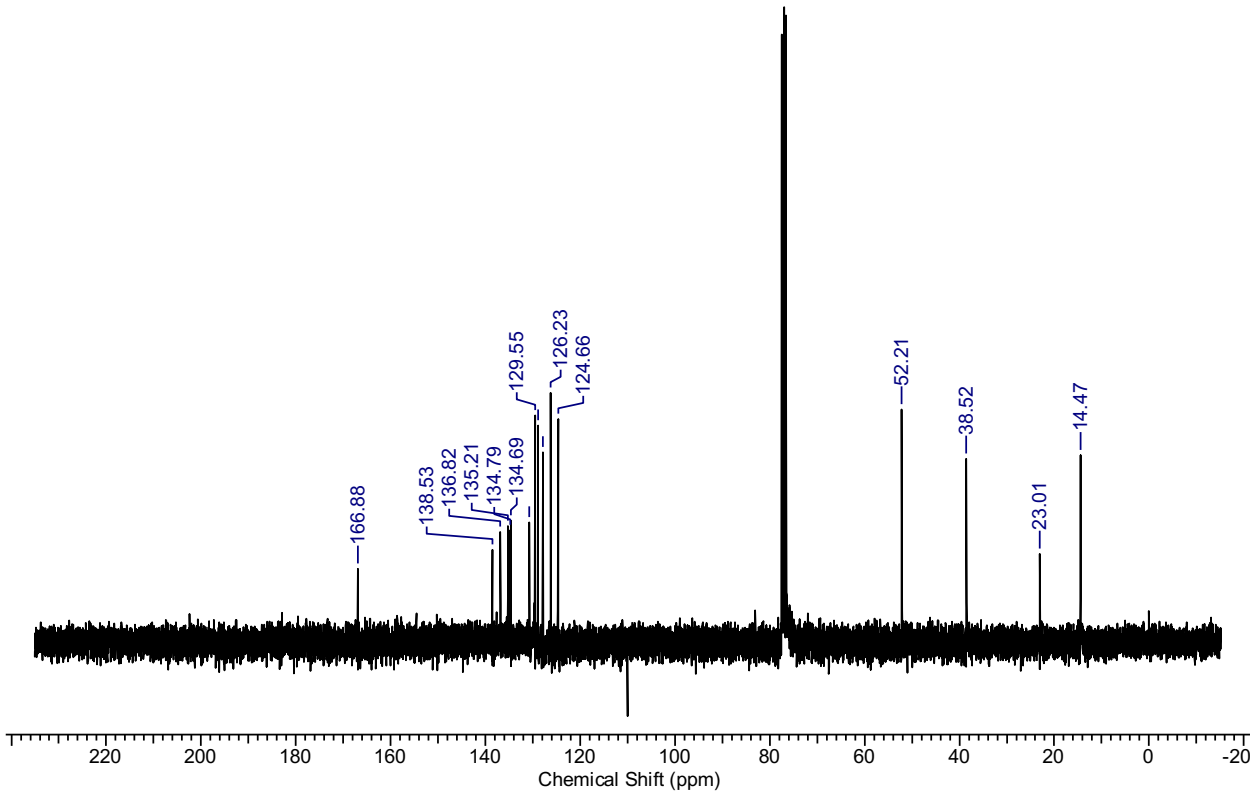

APPENDIX 8. ^{1}H NMR SPECTRUM OF COMPOUND 63

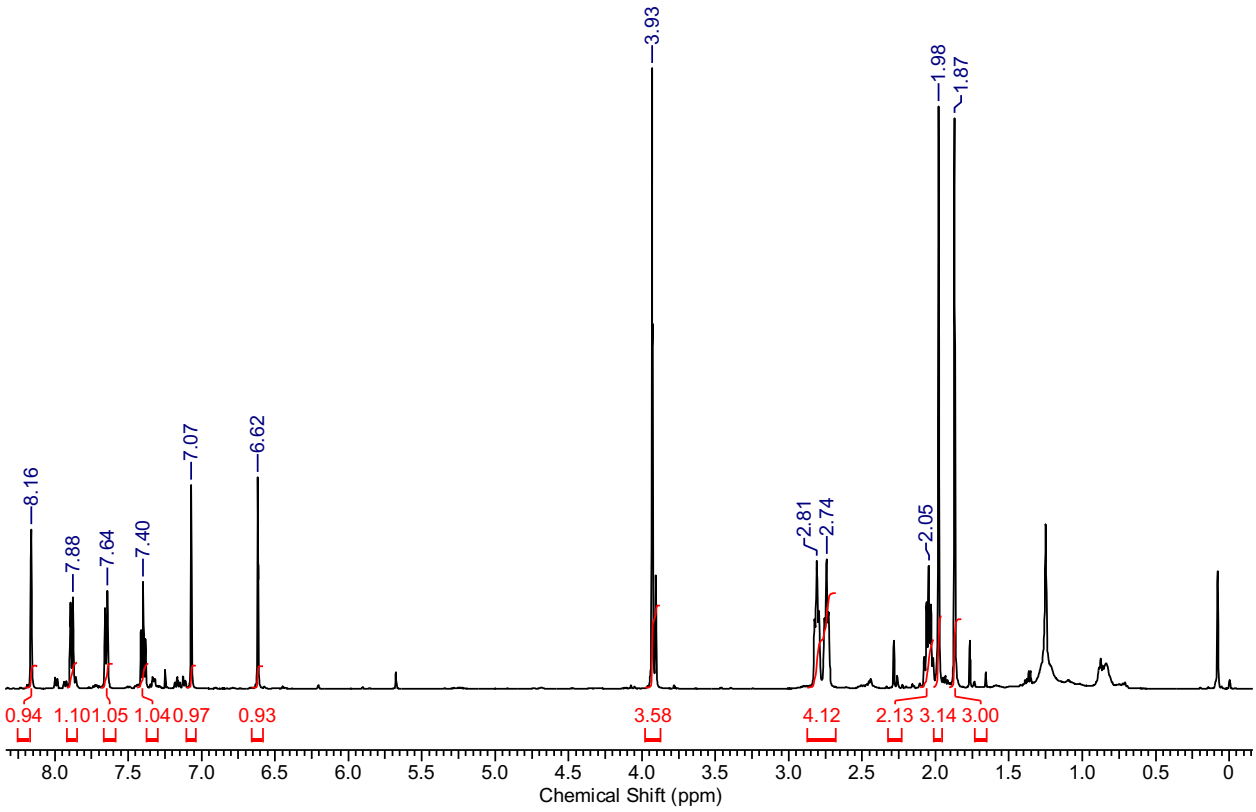

APPENDIX 9. ^{13}C NMR SPECTRUM OF COMPOUND 63

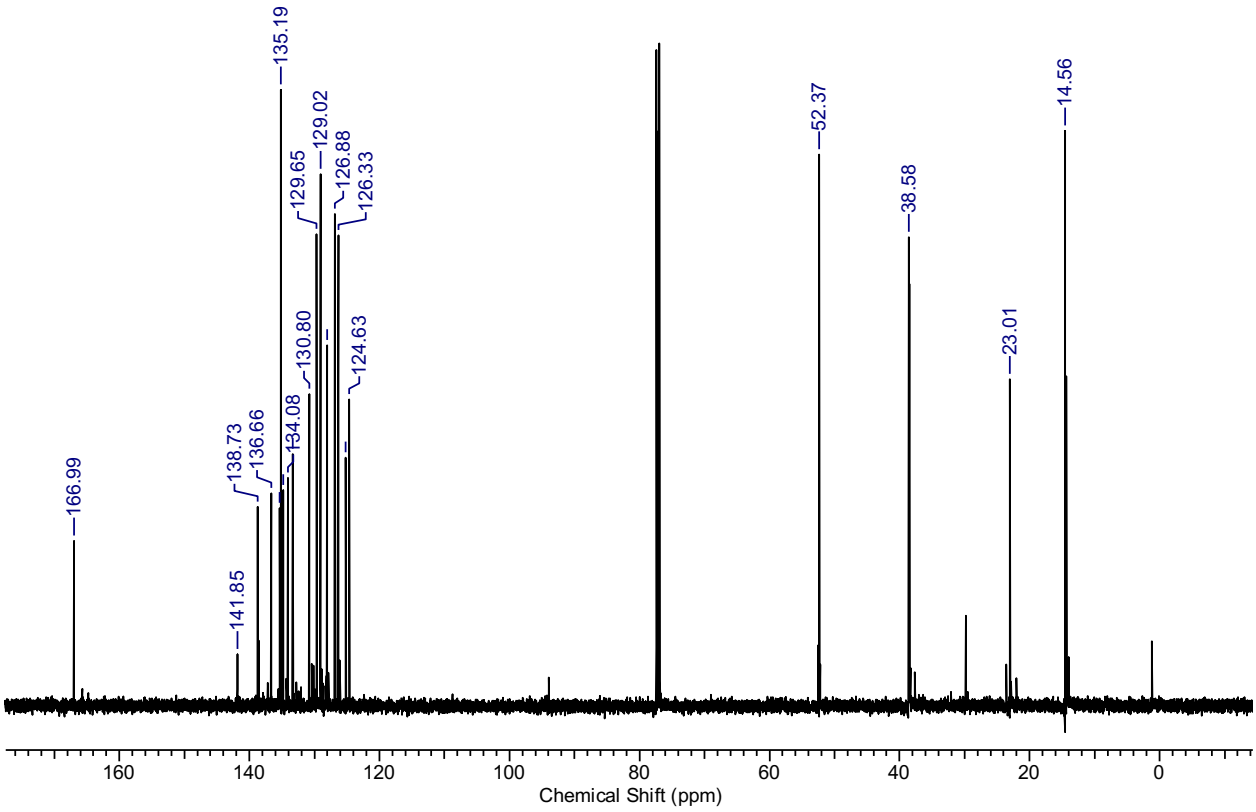

APPENDIX 10. ^{1}H NMR SPECTRUM OF COMPOUND 57

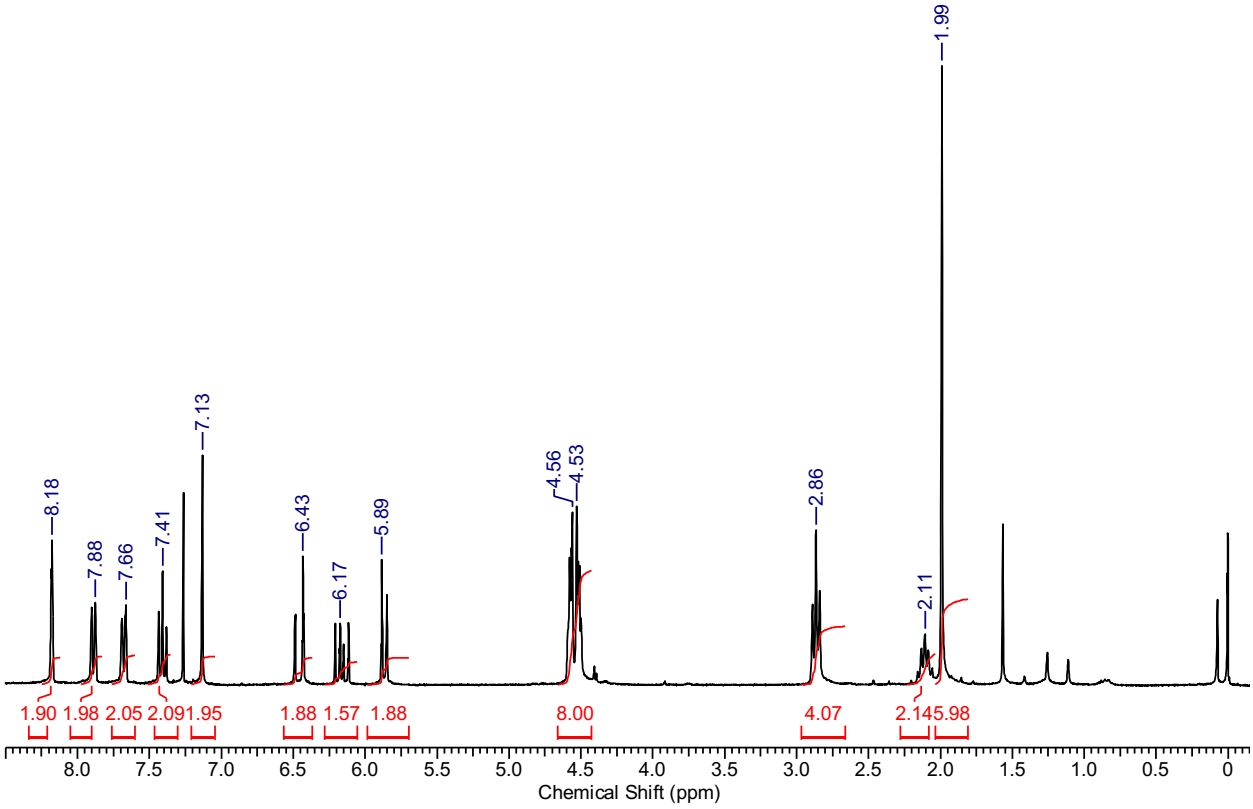

APPENDIX 11. ^{13}C NMR SPECTRUM OF COMPOUND 57

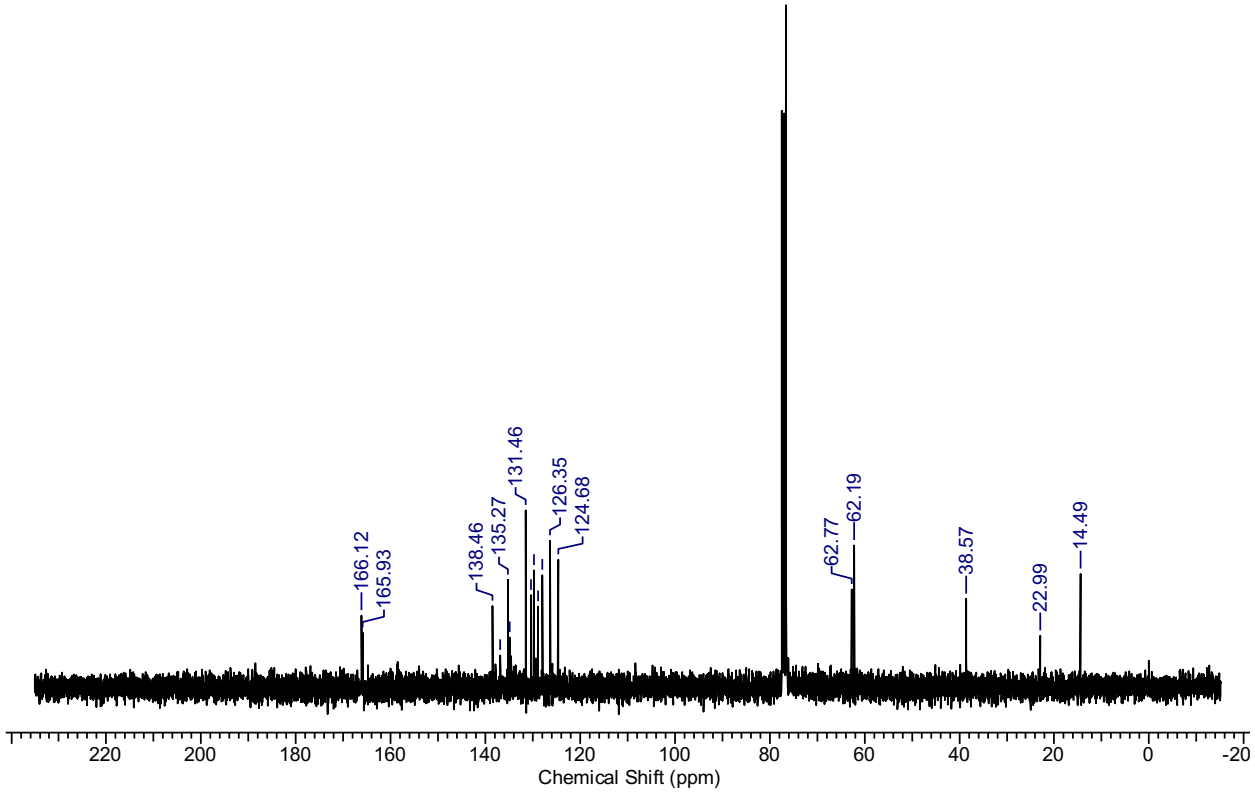

APPENDIX 12. ^{1}H NMR SPECTRUM OF COMPOUND 67

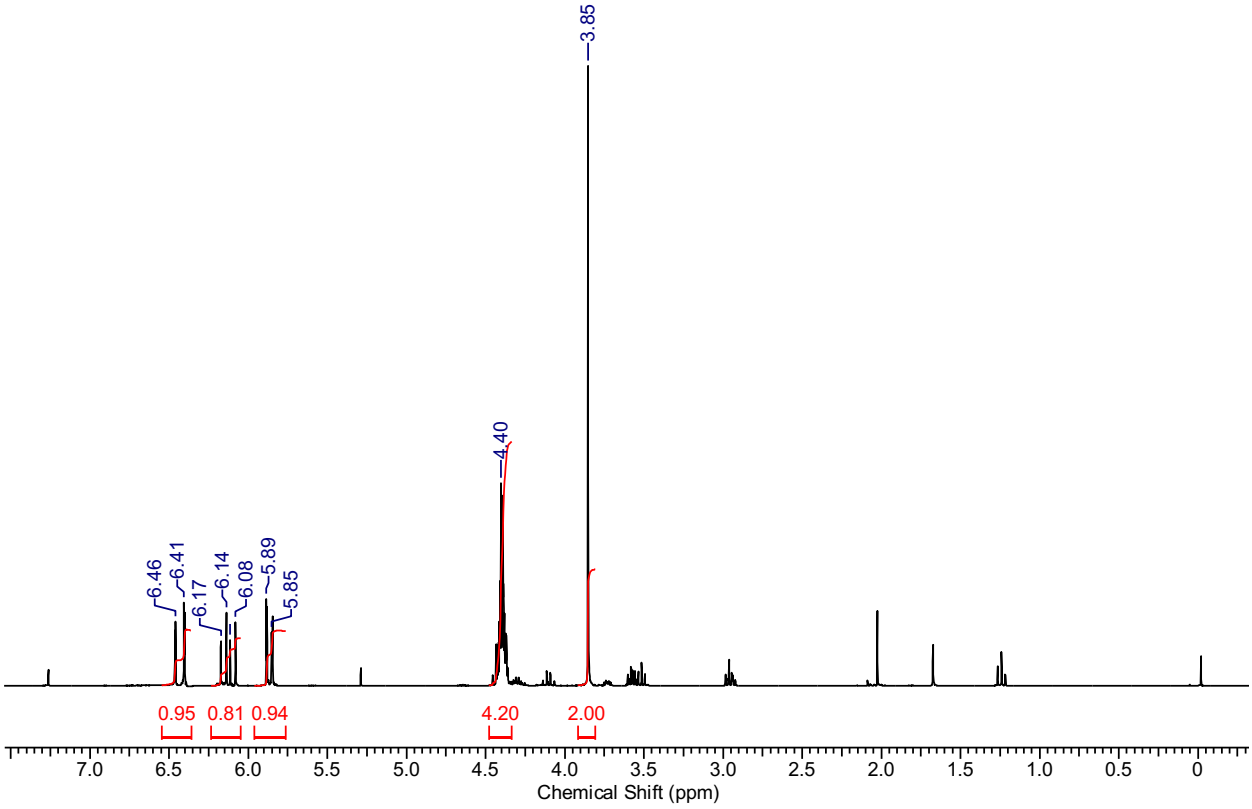

APPENDIX 13. ^{1}H NMR SPECTRUM OF COMPOUND 69

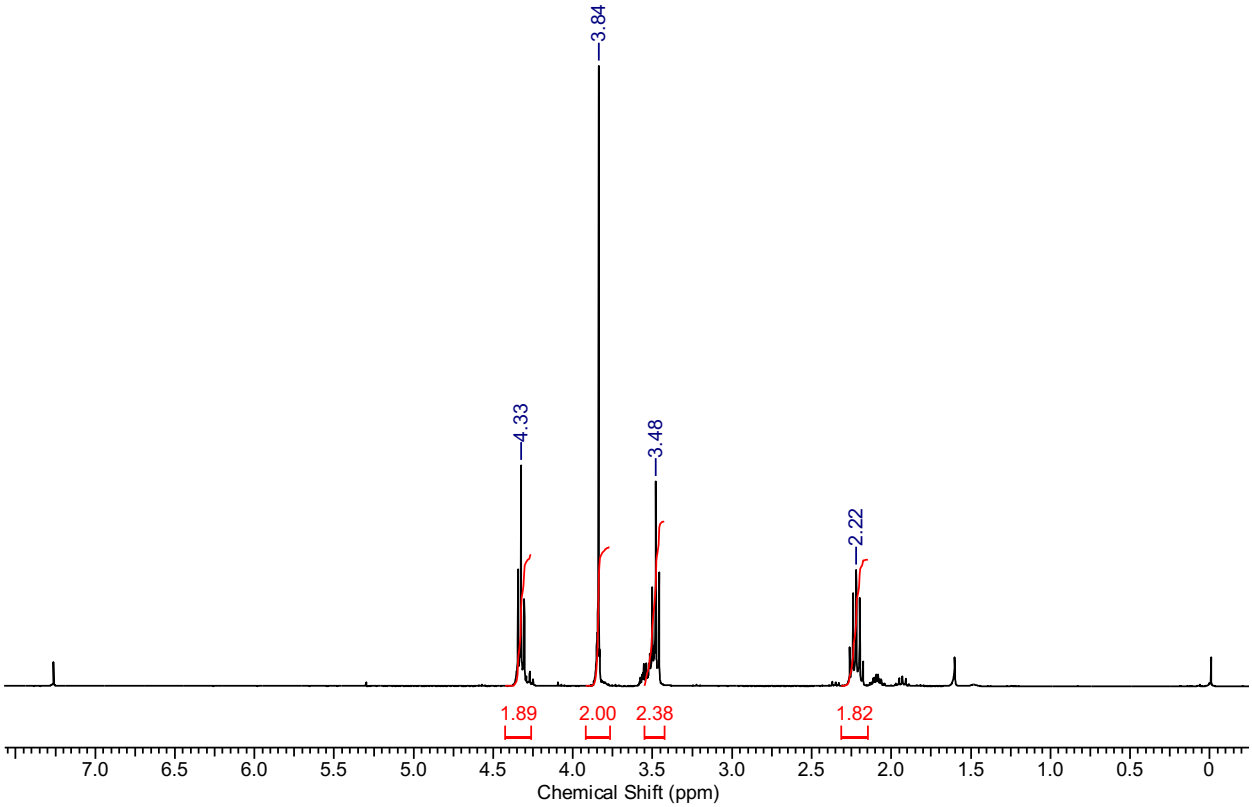

APPENDIX 14. ^{1}H NMR SPECTRUM OF COMPOUND 70

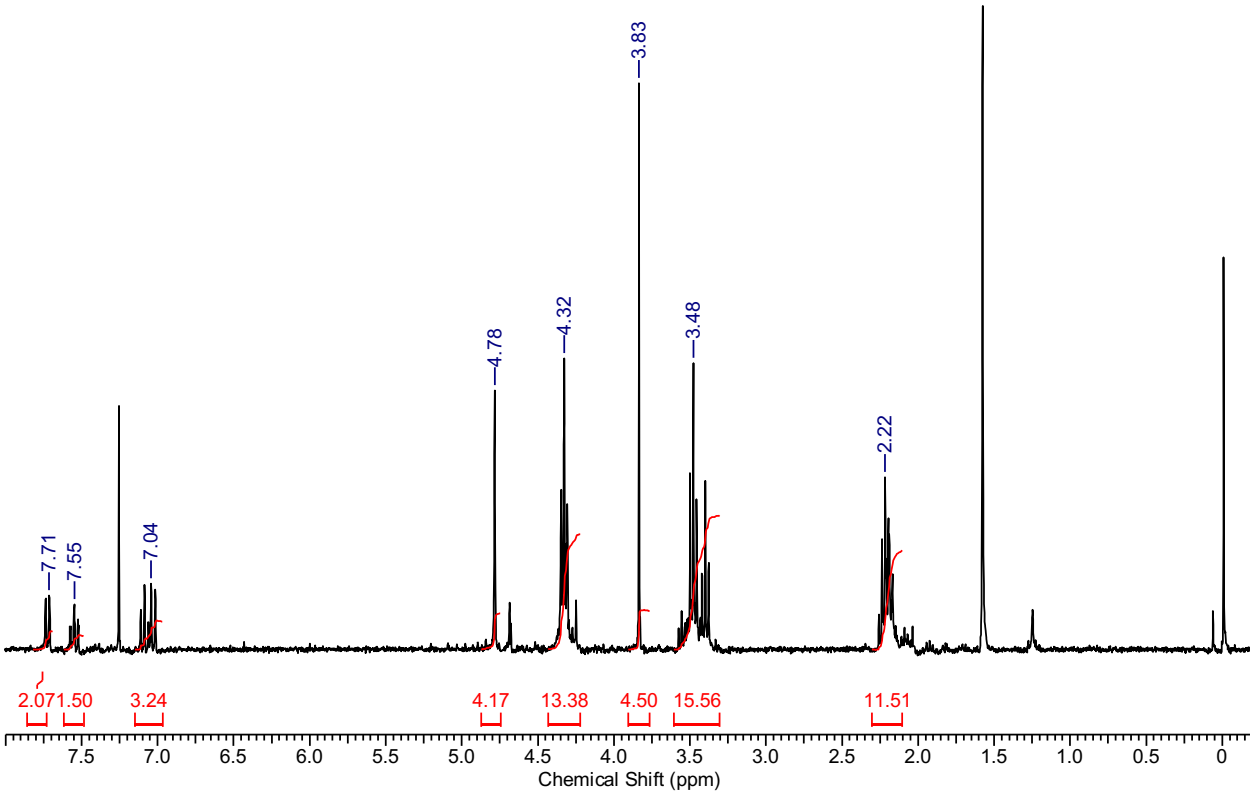

APPENDIX 15. ^{1}H NMR SPECTRUM OF COMPOUND 71

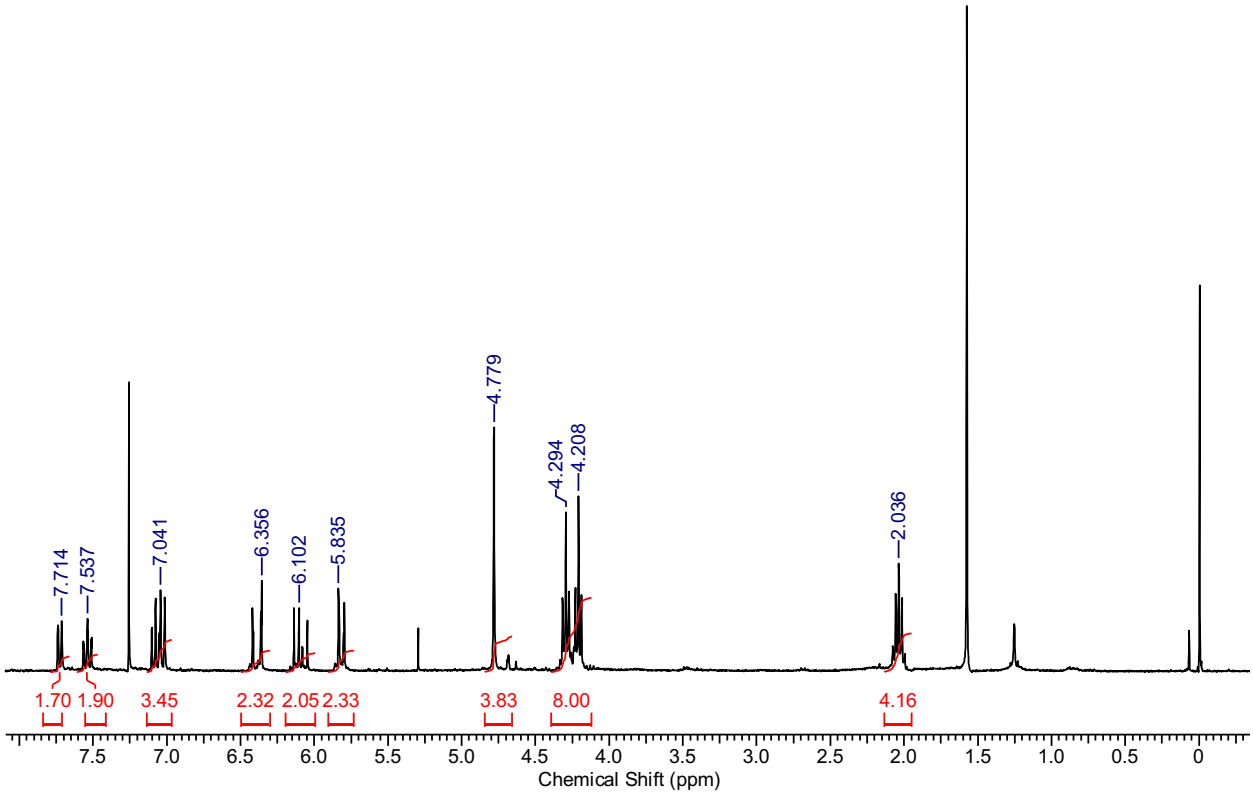

APPENDIX 16. ^{13}C NMR SPECTRUM OF COMPOUND 71

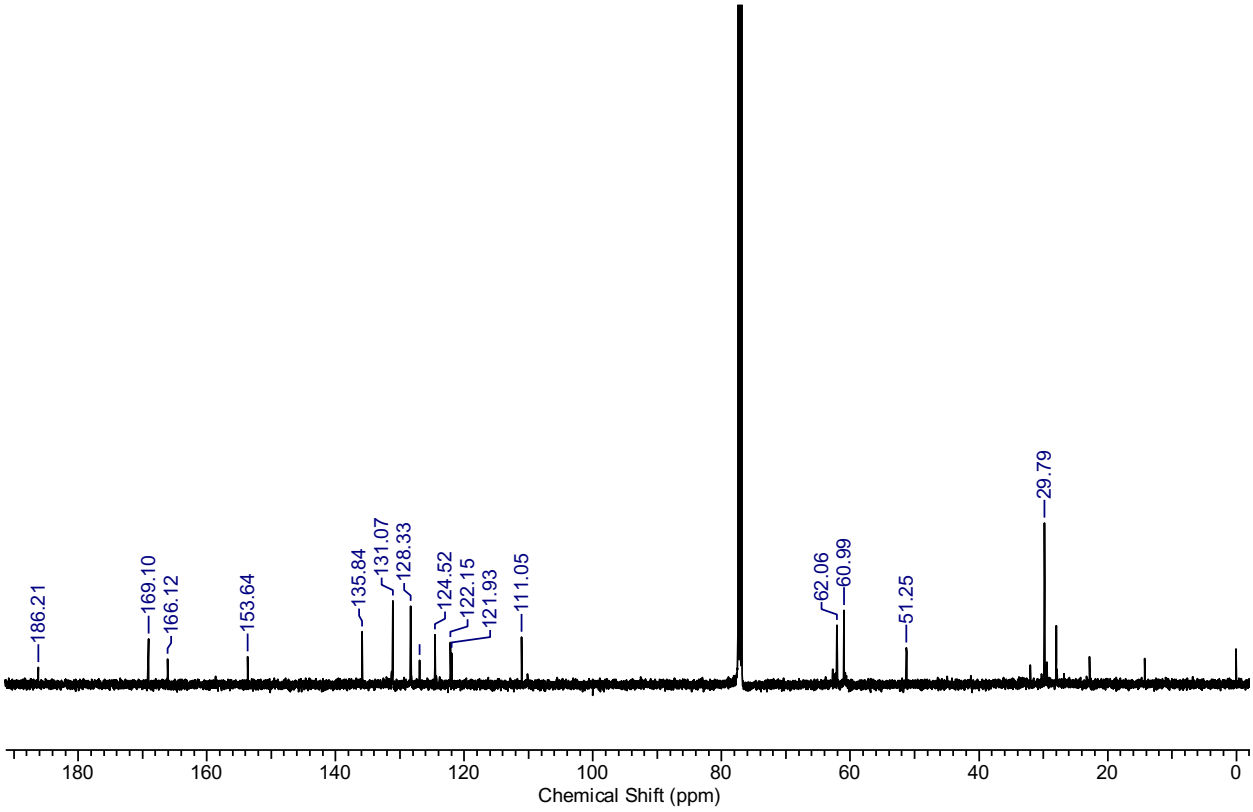

APPENDIX 17. ^{1}H NMR SPECTRUM OF COMPOUND 77

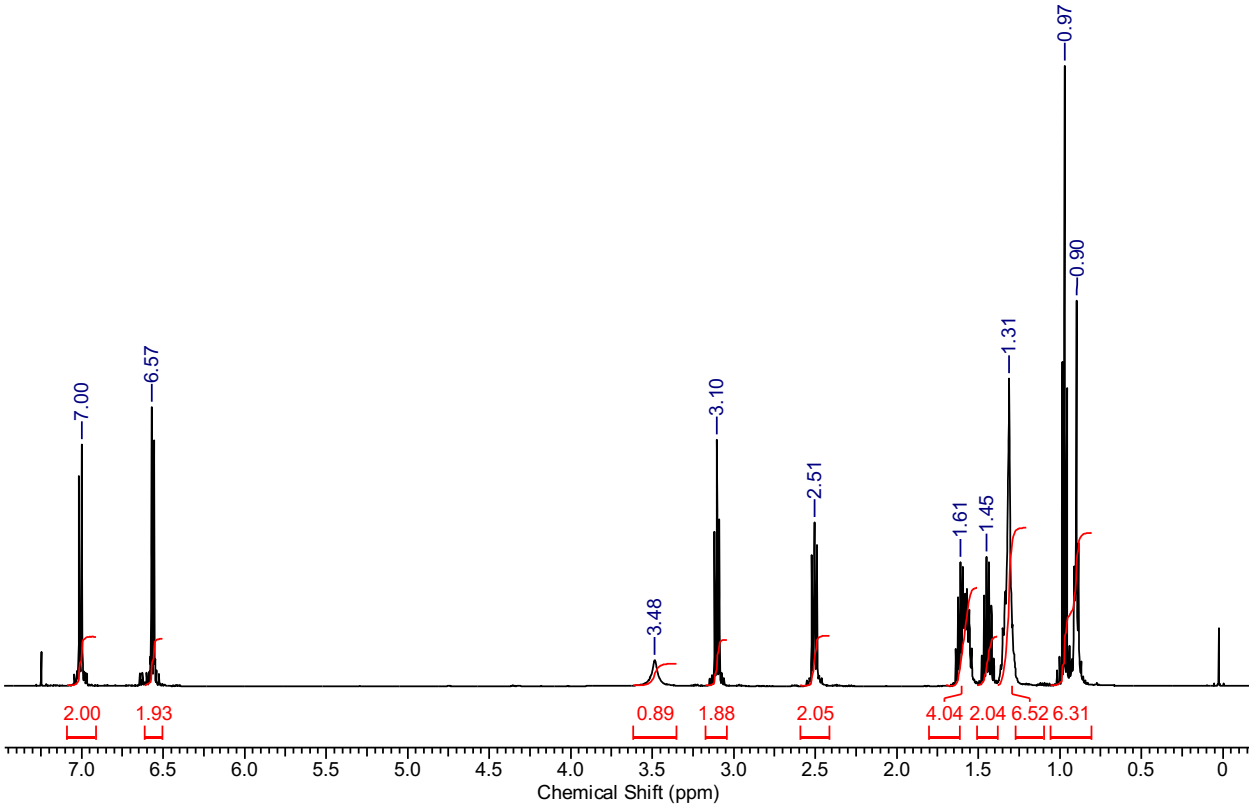

APPENDIX 18. ^{1}H NMR SPECTRUM OF COMPOUND 48

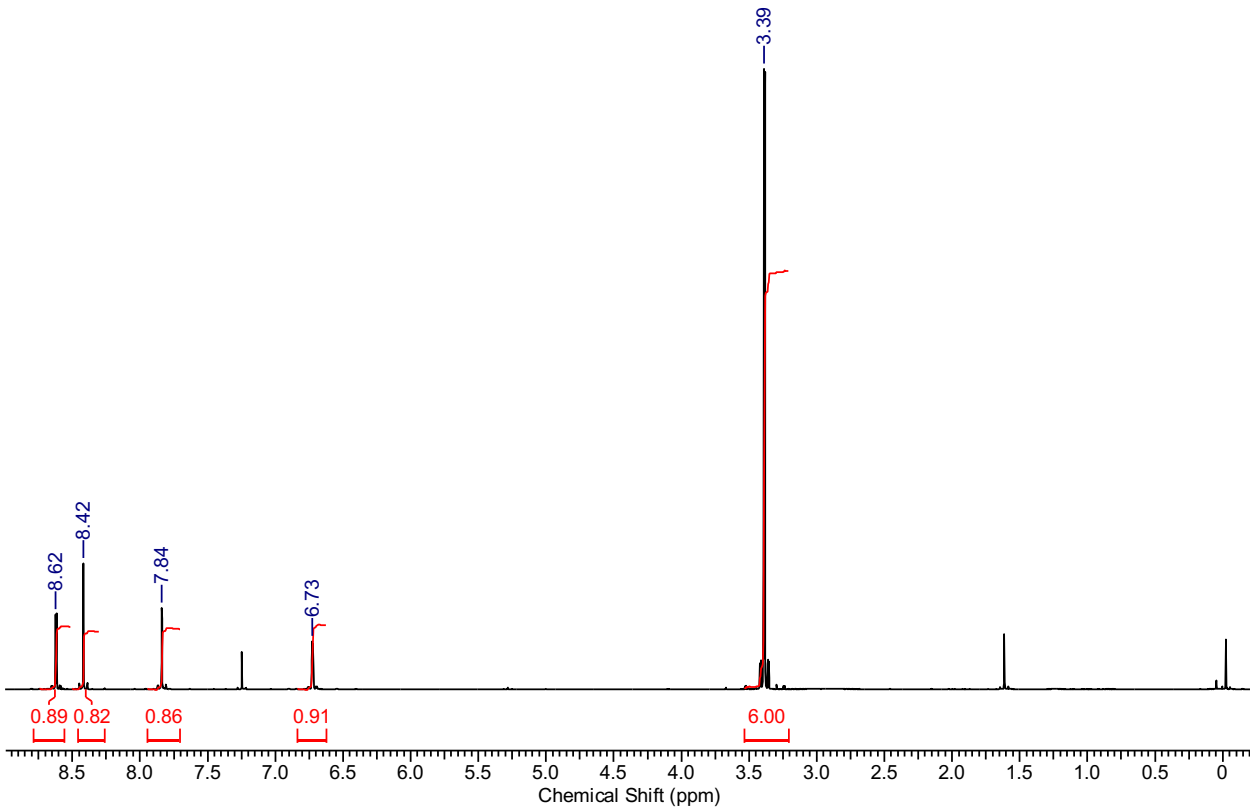

APPENDIX 19. ^{1}H NMR SPECTRUM OF COMPOUND 78

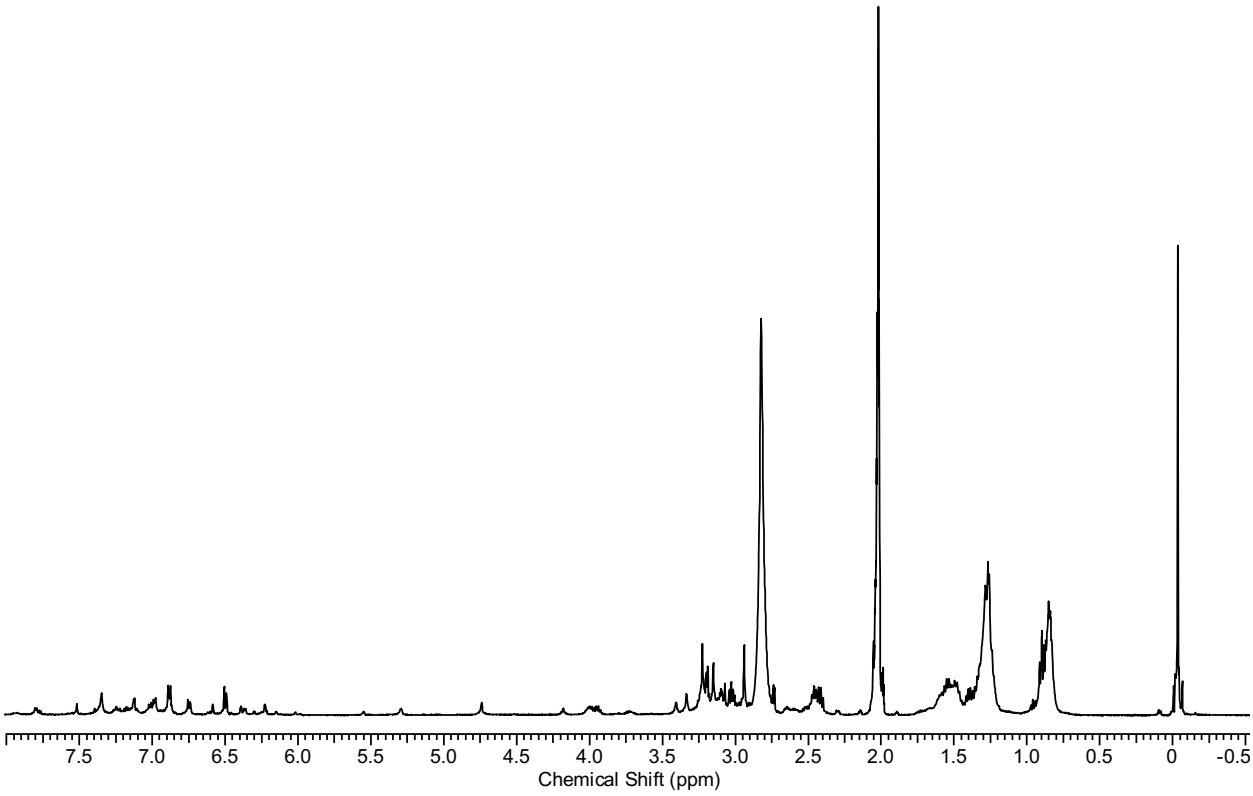

APPENDIX 20. DIARYLETHENE PSS COMPOSITION FROM ^{1}H NMR SPECTRUM OF COMPOUND 57